

PRECIPITATION HARDENING IN

MAGNESIUM ALLOYS

P.A. Nuttall, B.Sc., A.I.M.

Thesis submitted to the University of Nottingham
for the degree of Doctor of Philosophy, October 1973

CONTENTS

<u>INTRODUCTION</u>	1
Chapter 1: <u>PRECIPITATION FROM SUPERSATURATED SOLID SOLUTIONS</u>	 3
1.1 Formation of Precipitates	3
1.2 Formation of G.P. Zones	7
1.3 Formation of Transition Precipitates	9
Nucleation by G.P. zones or clusters	12
Precipitate nucleation on grain boundaries	16
Precipitation on dislocations	17
Precipitation on stacking faults	19
Precipitation around insoluble particles	20
Effect of trace elements on precipitate nucleation	21
Summary	23
Chapter 2: <u>PRECIPITATION FROM C.P.H. MAGNESIUM SOLID SOLUTION</u>	 24
2.1 Magnesium Thorium Alloys	24
Effect of zinc additions to Mg-Th alloys	28
Effect of manganese additions to Mg-Th alloys	29
2.2 Magnesium Rare Earth Alloys	29
2.3 Magnesium-Zinc	32
2.4 Magnesium-Aluminium	34
2.5 Magnesium-Silver	35
2.6 Magnesium-Zirconium	36
2.7 Magnesium-Manganese	37
2.8 Magnesium Tin and Magnesium Lead	38
Summary	39

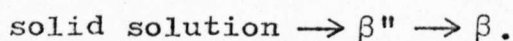
Chapter 3:	<u>EXPERIMENTAL DETAILS</u>	40
3.1	Preparation of Alloys	40
3.2	Solution Treatment Procedures	41
3.3	Ageing Environments	42
3.4	Resistivity Measurements	42
	Kelvin double bridge circuit	43
	Potentiometric circuit	45
3.5	Electron Microscopy	47
	Preparation of thin foils	47
	Calibration of the electron microscope	48
3.6	Creep Testing	49
Chapter 4:	<u>THE Mg-Th SYSTEM: EFFECT OF ZIRCONIUM ADDITIONS</u>	50
4.1	The β' hex Phase	51
4.2	The β and β' cubic Phases	55
4.3	Discussion	56
	Summary	62
Chapter 5:	<u>THE Mg-Th SYSTEM: EFFECT OF Mn, Zn AND Ag ADDITIONS</u>	64
5.1	Trace Additions of Zn, Ag and Mn	64
5.2	Precipitation in the Mg-Th-Mn System	67
5.3	Precipitation in the Mg-Th-Zn System	68
5.4	Discussion	70

Chapter 6:	<u>THE Mg-Nd SYSTEM: EFFECT OF ZINC ADDITIONS ON MICROSTRUCTURE</u>	73
6.1	Preliminary Investigations	73
6.2	Low Temperature Processes	74
6.3	Medium Temperature Processes	75
6.4	High Temperature Processes	78
6.5	Discussion	81
Chapter 7:	<u>THE Mg-Nd SYSTEM: EFFECT OF ZINC ON MECHANICAL PROPERTIES</u>	88
7.1	Room Temperature Proof Stress	88
7.2	Creep Testing	89
7.3	Microstructure of the Alloys	91
	Binary Mg 2.8% Nd alloy	92
	Mg 2.8% Nd 0.25% Zn alloy	92
	Mg 2.8% Nd 0.7% Zn alloy	92
	Mg 2.8% Nd 1.3% Zn alloy	93
7.4	Discussion	94
Chapter 8:	<u>GENERAL SUMMARY AND CONCLUSIONS</u>	98
Appendix I:	<u>CRYSTALLOGRAPHY OF THE HEXAGONAL CLOSE-PACKED SYSTEM</u>	102
Appendix II:	<u>ALLOY COMPOSITIONS</u>	105
	<u>ACKNOWLEDGEMENTS</u>	106
	<u>REFERENCES</u>	107

SYNOPSIS

Structural and kinetic aspects of precipitation in the systems Mg-Th and Mg-Nd, with various ternary additions, have been studied, using electron microscopy and electrical resistivity techniques.

The sequence of precipitation in the Mg-Th alloy is



Small additions of manganese and silver have little affect on the precipitation process but additions of zirconium and zinc alter the process significantly. The β'' reaction is completely suppressed by an addition of 0.3% zinc and a phase not present in the binary system, β' Mg_2Th , is formed as two polymorphs in the zirconium containing alloy.

The sequence of precipitation in the Mg-Nd system is completely changed by the zinc addition. Alloys containing Mg 2.8% Nd 1.3% Zn have the following precipitation sequence



The low temperature reaction has not been elucidated but it occurs with an activation energy approximating to that of vacancy migration in magnesium, and may possibly be

associated with short range order.

The structures of these various alloys have been correlated with their creep and mechanical properties. In particular, the creep properties of the Mg-Nd-Zn alloy have been shown to be superior to those of the binary Mg-Nd alloy and the improvement has been attributed to the γ'' phase restricting dislocation motion on the $\{10\bar{1}1\}$ planes.

INTRODUCTION

In contrast to the extensive knowledge of strengthening by second phase particles in b.c.c. and f.c.c. materials [1] comparatively little is known about the mechanisms of precipitation and dispersion hardening in h.c.p. materials. Of the common hexagonal metals, titanium, magnesium and zinc are all used as the basis of alloys for diverse applications. Magnesium, however, is of particular interest because of its very low specific gravity (approximately one-quarter that of steel and two-thirds that of aluminium). Many components previously made of denser materials can therefore be produced in magnesium alloys with a substantial saving in weight. The earlier disadvantages of magnesium alloys, such as large grain size and poor corrosion resistance, have largely been overcome and magnesium is now the basis of a large number of commercial alloys which are used in both the cast and wrought condition. Development of these alloys has mainly been on an empirical basis and a knowledge of the underlying factors concerned in the strengthening effects of these additions is not known for many of the alloy systems.

This thesis examines in detail the effect of various ternary additions on the structural ageing characteristics of the systems Mg-Th and Mg-Nd. These alloys, particularly

Mg-Th, have been shown to have attractive high temperature tensile and creep properties. High-purity binary alloys have been previously studied and shown to be of the age-hardening type; in both cases a sequence of transition precipitates has been established. The commercial alloys, however, are more complex in that they contain a variety of other elements. The effect of these impurity and ternary addition elements on both the precipitation characteristics and the mechanical properties of Mg-Th and Mg-Nd alloys has been studied.

The first chapter deals with precipitation in a general sense and is followed by a chapter devoted to a review of the literature on precipitation in magnesium alloys, as they are of particular relevance to this thesis.

CHAPTER 1

PRECIPITATION FROM SUPERSATURATED SOLID SOLUTIONS

1.1 Formation of Precipitates

The requirement for an alloy to be capable of precipitation hardening is that it should show a decreasing solid solubility with decrease in temperature. If such an alloy is held at a temperature above the solvus temperature, where it exists as a single phase, and is quenched rapidly from that temperature, a metastable, supersaturated solid solution will be formed. The tendency will be for this metastable situation to revert to the condition of lowest energy, that of a saturated solid solution containing the equilibrium phase. The driving force for such a reaction is the reduction in volume free energy of the system. However, opposing this change is the energy associated with the surface of the particle formed and the strain energy due to the volumetric misfit between the precipitate and matrix. These can take relatively large values and lead to extremely high activation energies for the solid solution to decompose directly to the equilibrium precipitate. To counteract this effect transition phases are often involved in the precipitation process. These have

interfaces which are either coherent or partially coherent with the parent matrix and therefore their surface energies are small. Consequently these transition phases form because the precipitation process follows the path of minimum activation energy rather than maximum free energy loss. These transition phases are normally classified into Guinier-Preston (G.P.) zones and transition precipitates. The former are solute rich zones fully coherent with the matrix and have a crystal structure which is identical or closely related to that of the matrix. Transition precipitates may only be partially coherent with the matrix and usually have a crystal structure quite distinct from that of the matrix. The dividing line between these two types of phase is not sharp and, in fact, G.P. zones could be regarded as being a special case of transition precipitate.

The nature of the interface between matrix and precipitate is governed by the lattice misfit. A coherent interface between two crystals means that the crystals are in contact such that the plane of atoms constituting the interface has an atomic arrangement, disregarding chemical species of the atoms, which is common to both crystal structures. Any slight misfit between matrix and precipitate is accommodated by elastic strains. When this misfit becomes too large to be accommodated by elastic strains alone, structural

dislocations are formed at the precipitate-matrix interface. This creates an interface known as quasi-coherent. An interface where these dislocations become so numerous that they can no longer be individually recognised is known as non-coherent. A completely non-coherent interface is usual with equilibrium precipitates, however, this does not preclude the possibility that the equilibrium precipitate, or transition precipitates, may form on a certain specific plane or grow in a characteristic crystallographic direction to reduce the misfit, and hence the surface energy, between the matrix and precipitate.

Nabarro [2] has shown that the strains in matrix and precipitate govern the shape of the precipitate and its habit plane. He showed that the strain energy increases in the sequence plate > needle > sphere. Thus in a system where the atomic volume of matrix and precipitate are almost identical the precipitate would be expected to form as a sphere, conversely, a large atomic misfit would favour a plate-shaped precipitate. Thus in Al-Ag alloys where the misfit is small G.P. zones take the form of spheres, whereas in Al-Cu where the misfit is $\sim 10\%$ the zones are disc-shaped.

Peak strengthening in any alloy is usually associated with one or more transition precipitates and is governed by the interactions between the precipitates and glide dislocations. Hence, as well as the nature of the

interface, the morphology, size and distribution of the precipitate particles will have a profound effect on the properties. Nicholson, Kelly and Nutting [3] proposed three distinct types of precipitate-dislocation interaction, namely:

- (i) chemical hardening, where a dislocation passes through a solute rich zone and shears the zone increasing the number of solute-solvent bonds;
- (ii) internal strain hardening, caused by the strain field around a particle due to the atomic mismatch between matrix and precipitate, opposing the motion of dislocations;
- (iii) dispersion hardening, non deformable particles oppose the movement of dislocations, the dislocation must either loop around the particle or cross slip past it, causing a back stress impeding further dislocation movement. The stress needed to move the dislocations will increase as the interparticle distance decreases.

Alloys can be heat treated to produce metastable precipitates which lead to useful strength increments. Because of the considerations discussed above, the magnitude of this strength increment will depend on the size, number and distribution of precipitate and this, in turn, will depend on such factors as dislocation

density, concentration of vacancies and small amounts of other elements. These factors will be discussed in greater detail in later sections.

1.2 Formation of G.P. Zones

It has been shown [4] that the structural model of G.P. zones in Al-Cu alloys proposed by Guinier necessitates a diffusion coefficient at least 10^7 times higher than that calculated by extrapolation of high temperature diffusion data. This apparent anomaly can be explained [5,6] by assuming that the vacancy concentration immediately following the quench is not the equilibrium concentration at the quench temperature but the value in equilibrium at the solution treatment temperature. This gives a value for the room temperature diffusion coefficient which is in good agreement with experimental data. It also explains why the rate of zone formation is dependent on quenching rate, homogenisation temperature, reversion and step quenching, all of which affect the vacancy concentration. Other theories have been proposed [7,8,9] but none have explained the dependence of rate of zone formation on the above factors and the so called "excess vacancy mechanism" is generally accepted.

In pure aluminium these excess vacancies are eliminated at sinks after ageing at 20°C for approximately

thirty minutes, but in a dilute Al-Cu alloy [10], after an initially rapid rate of clustering, a slower rate was found to persist for several weeks. Assuming that the initial "fast reaction" is due to movement of quenched-in vacancies, the existence of a "slow reaction" suggests that a non-equilibrium concentration of vacancies persists in the presence of an abundance of vacancy sinks such as dislocation loops, dislocation lines and grain boundaries. Hart [11] suggested that vacancy-solute clusters are formed due to the existence of a binding energy between vacancies and solute atoms. It was proposed that clusters trap vacancies and migrate through the lattice and that zones grow by absorbing smaller clusters and single copper atoms. A modification of this theory [12] considers that zones remain static but act as controlled emitters and absorbers of vacancies. These zones have a characteristic binding energy with vacancies E_B . If E_B is small, as for example in Al-Ag and Al-Zn, the zones are poor sinks for vacancies and hence no slow reaction is present. However, if E_B is large, as is the case in Al-Cu and Al-Mg-Si, then the zones will contain large numbers of vacancies and a slow reaction will persist for some time. A further refinement of Hart's theory [13] suggests that solute vacancy atom complexes migrate to zones, deposit their solute atoms and then the vacancy is driven back into the matrix by a concentration gradient. Experimental evidence

has recently been claimed to support the latter theory [14]. It is difficult to distinguish between the various hypotheses but there is evidence for high vacancy concentrations present in zones [15,16].

1.3 Formation of Transition Precipitates

True homogeneous nucleation in alloy systems is rare. G.P. zones are examples but homogeneous nucleation of the equilibrium or transition phase is known only in the systems Cu-Co [17], Ni-Al [18] and Al-Li [19]. In all these cases the precipitated phase has an identical structure to the parent matrix and a misfit between precipitate and matrix of $< 2\%$. This leads to a small surface energy and allows precipitation to occur with reasonable undercooling. Turnbull and Servi [17] studied the system Cu-Co and found that small particles of cobalt precipitate with a misfit of -2% at undercooling ranges between 60 and 90°C , depending on solute concentration. The results were interpreted in terms of classical nucleation theory and they predicted an interfacial energy of approximately 200 mJ/m^2 , in good agreement with the theoretically derived value of 235 mJ/m^2 .

The concentration of nuclei of critical size C_k is given by [20]

$$C_k = \frac{N_s}{\hat{c}} \exp - \left(\frac{\Delta G_k}{kT} \right) \quad (1.1)$$

where

N_s is the density of potential nucleation sites

\hat{c} is the composition of the nucleus

ΔG_k is the activation energy for formation of the initial nucleus.

The steady state nucleation rate (J_k) is proportional to C_k and therefore

$$\frac{J_k^{\text{het}}}{J_k^{\text{hom}}} \cong \frac{N_s^{\text{het}}}{N_s^{\text{hom}}} \exp - \left(\frac{\Delta G_k^{\text{het}} - \Delta G_k^{\text{hom}}}{kT} \right). \quad (1.2)$$

Since $\Delta G_k^{\text{het}} < \Delta G_k^{\text{hom}}$ the exponent is always greater than unity and only the restricted number of sites available prevents the complete dominance of heterogeneous nucleation.

Typical values of $\frac{N_s^{\text{hom}}}{N_s^{\text{het}}}$ are shown on page 11 for various crystal defects [21].

Defect density	Grain boundary		Grain edge		Dislocation density	Vacancy concentration
	Grain size	Grain size	Grain size	Grain size		
	0.5 mm	0.05mm	0.5 mm	0.05 mm	10^7	10^{-6}
					10^{10}	10^{-4}
					cm cm^{-3}	cm cm^{-3}
$N_s^{\text{het}}/N_s^{\text{hom}}$	\dots	10^{-6}	10^{-5}	10^{-13}	10^{-8}	10^{-5}
						10^{-6}
						10^{-4}

TABLE I

Typical site density ratios for different defects relative to homogeneous nucleation [21]

The table shows that the highest value of the ratio is $10^{-4} - 10^{-5}$. Thus for a typical nucleation rate of 10^{12} nuclei/cm³/sec it is necessary for $\Delta G_{\text{het}} < 0.6 \Delta G_{\text{hom}}$ if heterogeneous nucleation is to be of equal importance to homogeneous. This is well satisfied in most systems and heterogeneous nucleation is often decisive. The components of ΔG_k are shown below.

$$\Delta G_k = \Delta G_{\text{vol}} + \Delta G_{\text{surf}} + \Delta G_{\text{strain}}$$

The reduction in ΔG_{het} over ΔG_{hom} is due to the reduction of either or both of the surface or strain energies caused by the interaction of the defects with the precipitate nucleus.

The effect of several of these imperfections on the precipitation process will now be discussed at greater length.

Nucleation by G.P. zones or clusters

Until recently the very fine dispersions of θ' in Al-Cu, Mg Zn₂ in Al-Zn-Mg and β in Cu-Be were thought to be typical examples of homogeneous nucleation in solids. However, work suggested [22] that this distribution was very sensitive to quench rate, and periods of ageing at low temperatures prior to the normal heat treatment. Lorimer [23] has suggested the term "homogeneously

distributed" to describe this type of precipitation and two theories have been proposed to explain the phenomenon.

Nicholson and co-workers [24,25,26] have made a detailed study of this type of precipitation in Al-Zn-Mg, Al-Ge and Al-Cu alloys. Nicholson considers that when the temperature falls below T_{GP} , the G.P. zone solvus temperature, during the quench, zones are rapidly nucleated; these zones will grow during the quench and during an ageing treatment at any temperature $T_1 < T_{GP}$. The growth will occur by a coarsening reaction and at any time during this initial ageing period a size distribution of zones will be present. On up-quenching to a temperature above T_{GP} , the zones will begin to revert. However, there will be a hysteresis effect and during this time the alloy will contain a number of solute rich regions, some of which will be larger than the critical size d_c necessary for the transformation to a precipitate. The longer the pre-ageing time and the higher the pre-ageing temperature (assuming $T_1 < T_{GP}$) the more zones will exceed d_c and therefore the finer will be the subsequent precipitate dispersion. Obviously a high value of the second ageing temperature (T_2) will necessitate a larger critical size d_c and this would lead to a coarser precipitate dispersion as fewer zones would attain the critical size necessary for transformation to a precipitate. The theory proposes that at longer ageing times $T < T_{GP}$.

isothermal transformation to precipitate takes place. This would explain the effect of pre-ageing treatment and also provide an explanation of the precipitate free zones (p.f.z.) found adjacent to the grain boundaries in many alloy systems. After the quench a vacancy profile will be formed due to a loss of vacancies near the grain boundary. The diffusivity in the regions immediately adjacent to the grain boundaries will be lower than in the grain and hence the average size of the G.P. zones will be smaller in this region. The boundary of the p.f.z. will thus occur where the critical size d_c exceeds the maximum zone size d_m . As the holding time at $T_1 < T_{GP}$ increases the p.f.z. will become narrower due to the increase in the mean size of the G.P. zones.

An alternative model for precipitate nucleation has been suggested by Pashley and co-workers [27,28,29]. They introduce a temperature T_c above which nucleation of clusters will not occur when excess vacancies are absent. No mention is made of zones but small clusters of solute atoms are assumed to form during storage or low temperature ageing, leading to a reduction of supersaturation in the region around the cluster. On up-quenching, the supersaturation is further reduced and the size at which a cluster is stable is increased, therefore causing some clusters to grow at the expense of others. The temperature T_c has been shown [25] to be simply the highest temperature

possible for the nucleation of G.P. zones, i.e.,

$$T_c = T_{GP} - \Delta T,$$

where ΔT is a small undercooling necessary for nucleation of G.P. zones.

Both these theories are able to explain the formation of precipitate free zones, the effects of prior low temperature ageing and double ageing experiments. However, the results obtained for Al-Si and Al-Ge alloys are difficult to explain by the former theory. Both the alloy systems exhibit similar precipitation sequences, forming elemental silicon and germanium respectively as a diamond cubic structure. This dispersion is refined by a pre-ageing treatment at low temperatures. Lorimer and Nicholson [26] claim that zones form in these alloys and that the mechanism of precipitation is as described; but Koster [30] has carried out work on the Al-Ge system and claims no transition phases or zones are formed. Al-Si [31] alloys have also been extensively studied, using sensitive electrical resistivity measurements, and no trace of zone formation has been found. It is difficult, therefore, to see how the results claimed in the Al-Si and Al-Ge systems can be explained assuming, as seems likely, that zones do not form in these alloys. A likely explanation would seem to be nucleation from some type of vacancy defect.

Precipitate nucleation on grain boundaries

Precipitation on grain boundaries is the best known example of heterogeneous nucleation and can be observed in many alloy systems at relatively low magnifications. Nucleation is greatly assisted at these sites by a reduction in both the surface and strain energies for precipitation and, in practice, many grain boundary precipitates nucleate with an orientation relationship with one of the adjoining grains, hence resulting in an even lower value of ΔG_k^{het} .

Work by Unwin and Nicholson [32] has suggested that the rate of precipitation at a grain boundary is a function of the misorientation. They conclude that nucleation behaviour can be divided into two types:

- (i) very low angle grain boundaries of misorientation $< 2^\circ$ and high angle boundaries with misorientation near a coincident site relationship;
- (ii) low angle boundaries with misorientations between 2° and 10° and random high angle boundaries.

Type (i) boundaries show a very large nucleation rate compared with type (ii), suggesting that the number of sites on the first is small.

Precipitation on dislocations

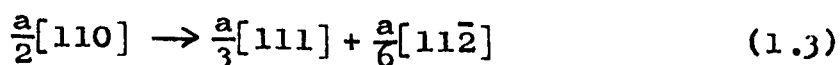
Dislocation lines can be generated by quenching stresses, cold work prior to ageing and the retention of an excess of vacancies. The activation energy for precipitation at a dislocation is reduced because any misfit between precipitate and matrix can be accommodated, either partially or wholly, by the dislocation. Examples of systems which have been seen to exhibit dislocation nucleated precipitates are numerous and include examples from h.c.p. [33], b.c.c. [34] and f.c.c. [35] systems. Cahn [36] has proposed a theoretical model for the nucleation of a non-coherent cylindrical precipitate on a dislocation line. He assumes the misfit balances the strain free energy and hence nucleation is facilitated. In fact, Cahn shows that precipitation on dislocations is greater than homogeneous precipitation by a factor of 10^{78} . However, this theory does not have anything to say about the nucleation of particles with complex strain fields.

It has been found that with precipitates with definite habit planes not all the habits are observed on any one dislocation line. This effect arises because a dislocation can best accommodate the lattice misfit of a precipitate if the misfit vector of the precipitate is parallel to the Burgers vector of the dislocation.

Conversely, precipitation will not occur if the misfit vector is perpendicular to the Burgers vector of the dislocation. An example of this is illustrated by θ' precipitation in Al-Cu alloys. The precipitate forms as plates on $\{100\}$ and therefore the three misfit directions lie in $\langle 100 \rangle$. For a glide dislocation of Burgers vector $\frac{a}{2}[110]$, the misfit along $[100]$ and $[010]$ will be accommodated whilst the misfit along $[001]$ will not.

Dislocation nucleated precipitates can be the major mode of decomposition of an alloy as dislocation densities of the order of 10^{10} to 10^{11} cm^{-2} can be produced by cold work between quenching and ageing. A problem arises in that the density of dislocations tends not to be uniformly distributed and can form into cellular networks and sub-grain boundaries. The resulting precipitate structure will also be non-uniform and the mechanical properties of the materials can be poor.

A special case of precipitation on dislocations has been found in austenitic stainless steels [37,38,39]. Silcock and Tunstall [40] showed that stacking faults of the extrinsic type were present and that they formed by the reaction



Various carbides precipitate on the Frank partial and this partial then expands through the lattice by climb on (111) .

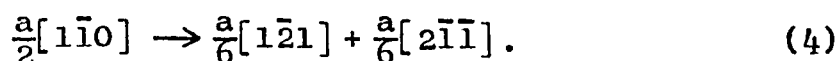
The climb of the Frank partial is assisted by vacancies generated at the precipitate interface due to the large atomic misfit (20-25%) between the carbide and the matrix. The dislocation eventually by-passes the particle completely by an Orowan-type mechanism, leaving a region of extrinsic stacking fault as it moves, and eventually is available to nucleate further particles of carbide. It can be seen from the description that the presence of the stacking fault is incidental to the mechanism of precipitation. The term repeated nucleation on dislocations has been suggested for this type of precipitation [21].

Precipitation on stacking faults

In considering stacking fault precipitation we are considering heterogeneous precipitation which occurs on an extended dislocation by virtue of the presence of the stacking fault rather than because of the presence of the necessary bounding dislocations.

When a glissile dislocation in a f.c.c. lattice splits into a pair of partial dislocations, a layer of h.c.p. lattice is formed between the partials. Suzuki [41], suggested that, because of the difference in structure, the equilibrium concentration of solute in the faulted layer may differ from that of the surrounding matrix. He

suggested that solute may segregate to the fault, which may extend due to the change in stacking fault energy. Segregation of solute to the fault could lead to nucleation of precipitate if the matrix and precipitate have related crystal structures. An example of this mechanism has been found in Al-Ag alloys [42,43] where the precipitate is γ' (Ag_2Al) which has a hexagonal structure. Helical dislocations degenerate on ageing into long, narrow stacking faults. A number of discrete nuclei form on each dislocation, possibly at jogs, at points where the dislocation cuts a (111) plane. The dislocation can then dissociate to give an intrinsic stacking fault



Since the structure of the fault is identical to that of the precipitate, then a thin layer of γ' can precipitate by enrichment of the fault with silver atoms. Continued ageing leads to growth of this γ' . Similar results have been found in Cu-Si [44] and Al-Cu-Li [45] alloys.

Precipitation around insoluble particles

In most commercial alloys, particles will remain undissolved during solution-treatment and these may have an effect on the nucleation of precipitates. Due to the

difference in the thermal expansion coefficients of matrix and precipitate, localised stresses are induced during quenching, which may lead to the generation of dislocations around the particle. Nucleation on these dislocations then occurs by the mechanisms previously discussed. An example of this is the nucleation of niobium carbide in niobium containing steels [46].

Another method by which an insoluble particle can affect the precipitation process is by means of a particle lowering the surface free energy for precipitation in a rather similar way to a grain boundary. The site will not be as favourable as a grain boundary if the interface is coherent or semi-coherent, but if the interface is non-coherent the site will perhaps be more favourable due to the presence of a high solute concentration.

Effect of trace elements on precipitate nucleation

Several workers have studied the effect of cadmium, indium and tin [47,48,49] on the precipitation process in Al-Cu alloys. These additions influence the normal precipitation process in Al-Cu in two separate ways, they reduce the rate of formation of G.P. zones, and they assist the formation of the θ' phase at the expense of θ'' at higher ageing temperatures.

Studies in an Al-Cu - .024% Sn alloy [49]

have shown that the rate of clustering in the ternary alloy is slower than that of the binary by a factor of 10^4 . Silcock has proposed the existence of a binding energy between the ternary atom and a vacancy and, depending on the value of this binding energy relative to that of the zone forming atom with a vacancy, many of the excess vacancies will be bound up with the ternary atoms and therefore will be unable to assist the formation of G.P. zones.

Silcock, Heal and Hardy [47] observed that θ' precipitation in Al-Cu containing small additions of indium was accompanied by diffraction effects unrelated to the θ' or aluminium matrix diffraction spots. These anomalous reflections were explained by the absorption of indium atoms at the interface between θ' and the matrix. This atom positioning resulted in a closer match between θ' and the matrix. An additional effect involving vacancy solute atom complexes has also been proposed [50,51] based on electron microscope and electrical resistivity observations. It was suggested that θ' nucleates by the agglomeration of these clusters and growth of the precipitate is controlled by the movement of complexes to it.

Another effect of trace elements additions can be to change the free energy relationships in an alloy so that a different phase precipitates. It has been shown [52]

that an addition of 0.45% silver to a range of Al-Cu-Mg alloys induces precipitation of the T phase; the phases normally present are G.P. zones and the S' (Al₂ Cu Mg) phase.

Although trace element additions have been widely studied, only limited success has been achieved in predicting their behaviour. In some cases the trace element effect appears to be unique to a particular alloy system, whereas in others the same element may stimulate nucleation of precipitates in several alloy systems.

Summary

A full understanding of the nucleation phenomenon in precipitation hardening alloys requires a detailed knowledge of the following factors in addition to those predicted by classical nucleation theory:

- (i) vacancy concentration immediately after quenching;
- (ii) lattice imperfections;
- (iii) role of impurity and trace element additions;
- (iv) volume change associated with phase change;
- (v) nature of stresses between matrix and precipitate.

Factors (ii) to (v) influence the interfacial energy between matrix and nucleus which is probably the most important factor controlling nucleation.

CHAPTER 2

PRECIPITATION FROM C.P.H. MAGNESIUM SOLID SOLUTION

This chapter is devoted to a review of the literature, to date, on precipitation from hexagonal magnesium solid solutions. The Mg-Li alloys are of b.c.c. structure and will therefore not be considered. As the Mg-Th and Mg-Nd systems are of particular relevance to this thesis they will be discussed first.

2.1 Magnesium Thorium Alloys

Interest in Mg-Th alloys has been due to the fact that they have extremely good elevated temperature strength and creep resistance [53]. These properties are improved by the addition of small amounts of zirconium [54], which act as a grain refiner. The precipitation processes in Mg-Th-Zr alloys are thought to be the same as those in binary Mg-Th alloys as no intermetallics of zirconium with thorium or magnesium are thought to form.

Sturkey [55] studied a 3.0% Th 0.7% Zr alloy, using reflection electron diffraction and X-ray techniques. He reported an equilibrium phase with a face centred cubic structure of $a_0 = 1.437$ nm, in good agreement with previous work and from X-ray intensity

data assumed it to be iso-structural with $Mn_{23}Th_6$, i.e. $Mg_{23}Th_6$ and not Mg_5Th as previously reported [56]. In addition, Sturkey presented evidence for the existence of a transition phase of the f.c.c. Cu_2Mg Laves phase type, with $a_0 = 0.857$ nm. He suggested that the most favourable orientation relationship for the phase would be $(111) Mg_2Th \parallel (0001) Mg$.

Kent and Kelly [57] studied a binary Mg 0.5% Th alloy and detected a phase not previously reported. At low ageing temperatures (200 - 220°C) plate shaped precipitates were observed on the $\{10\bar{1}0\}$ matrix planes. Electron diffraction patterns showed streaking midway between matrix spots indicating that the plates were thin normal to the $\{10\bar{1}0\}$ and the phase was ordered, with a structure strongly resembling that of the matrix.

Resistivity work [58] suggested that the precipitation was a two stage process at temperature ranges 140 - 240°C and 270 - 380°C. The lower temperature range was examined using electron microscopy and micrographs purporting to be of circular G.P. zones were reported. These, however, were almost certainly confused with contamination on the foil surface.

Mushovic and Stoloff [59,60] identified the precipitate reported by Kent and Kelly as an ordered, hexagonal Mg_3Cd (DO_{19}) type precipitate forming on the matrix $\{10\bar{1}0\}$ planes. It was claimed that on prolonged

ageing at 325°C the DO_{19} structure transformed into the f.c.c. Laves phase reported by Sturkey and that this latter phase precipitated on $\{10\bar{1}0\}$ and not $\{0001\}$, as predicted by Sturkey. The diffraction evidence presented, however, is not convincing and can be explained in terms of reflections from an epitaxial film of magnesium oxide.

Evidence for a low temperature reaction was found by Crook [61] who, using resistivity techniques on a Mg 3.0% Th alloy, detected a resistivity fall of 4 - 6% at ageing temperatures < 150°C. No electron diffraction evidence, however, was found for G.P. zone formation and it was concluded that the precipitation sequence in the binary alloy was



No trace of the cubic β' $Mg_2 Th$ phase reported by Sturkey and Mushovic and Stoloff was found. This precipitation sequence has since been confirmed in the binary alloy [62].

In a recent paper Stratford [63], using a ternary 3.0% Th .7% Zr alloy, proposed a precipitation sequence as follows:

- (i) β'' ordered DO_{19} super-lattice on $\{10\bar{1}0\}$ planes.

The composition of these plates was claimed to be $Mg Th_3$, and not $Mg_3 Th$, as previously inferred [59 - 61].

- (ii) a hexagonal phase which forms from β'' by an in situ transformation. The lattice parameters were reported to be $a = 1.066$ nm, $c = 0.828$ nm, $c/a = .78$, with an orientation relationship of

$$\begin{aligned} (0\bar{1}\bar{1}2) \text{ precipitate} & \parallel (\bar{1}102) \text{ Mg} \\ (11\bar{2}1) \text{ precipitate} & \parallel (10\bar{1}3) \text{ Mg}. \end{aligned}$$

- (iii) Transformation to two stable forms of Mg_2Th

- (a) hexagonal structure which forms as discs parallel to (0001) Mg with the orientation relationship

$$\begin{aligned} (2\bar{1}\bar{1}0) \text{ Mg}_2\text{Th} & \parallel (10\bar{1}0) \text{ Mg} \\ (\bar{1}\bar{1}23) \text{ Mg}_2\text{Th} & \parallel (1\bar{1}01) \text{ Mg}; \end{aligned}$$

- (b) cubic structure taking the form of ribbons parallel to $\{10\bar{1}0\}$ planes with the relationship

$$\begin{aligned} (131) \text{ Mg}_2\text{Th} & \parallel (10\bar{1}0) \text{ Mg} \\ (310) \text{ Mg}_2\text{Th} & \parallel (0001) \text{ Mg}. \end{aligned}$$

- (iv) $\beta \text{ Mg}_3\text{Th}_8$ forming only at grain boundaries after periods of up to 16 hours at 330°C .

Two polymorphs of Mg_2Th are known to exist [64] but the above work of Stratford was the first time the hexagonal polymorph had been observed in the precipitation sequence.

Pike [65] has also examined both a binary and ternary alloy and has shown that the stage (ii) precipitation

proposed by Stratford is not in fact a separate phase; the diffraction patterns can be interpreted in terms of relrod intersections from the β'' phase.

In conclusion it can be said that, although the precipitation sequence in the binary Mg-Th system is agreed to be a two stage process, the precipitation sequence in the alloy with zirconium appears more complex. The effect of zirconium is not, as previously thought, simply that of a grain refiner but must have some effect on the precipitation process.

Effect of zinc additions to Mg-Th alloys

Small additions of zinc have been found to result in marked structural changes: β'' formation is completely suppressed and at high ageing temperatures β precipitation is accompanied by the formation of additional structural defects. These defects were found to be intrinsic stacking faults bounded by $\frac{1}{3}\langle 10\bar{1}0 \rangle$ partial dislocations. An extensive study of such faults [66] suggest that they result from the segregation of both thorium and zinc atoms to the dislocations.

Effect of manganese additions to Mg-Th alloys

Stratford and Beckley [62] studied a 2.0% Th 1.0% Mn alloy and found only one transition phase. This was a hexagonal precipitate $a = .556 \text{ nm}$ ($\sqrt{3}a \text{ Mg}$), $c = 3.16 \text{ nm}$ ($6 \times c \text{ Mg}$) taking the form of discs on (0001) matrix planes with an orientation relationship.

$$(0001) \text{ Mg} \parallel (0001) \text{ ppt}$$

$$\{11\bar{2}0\} \text{ Mg} \parallel \{10\bar{1}0\} \text{ ppt}.$$

This precipitate was extremely stable, large amounts being present at ageing times of up to 1200 hours at 325°C . The alloy eventually transforms to a mixture of Mg_3Th_8 and Mn_3Th_8 .

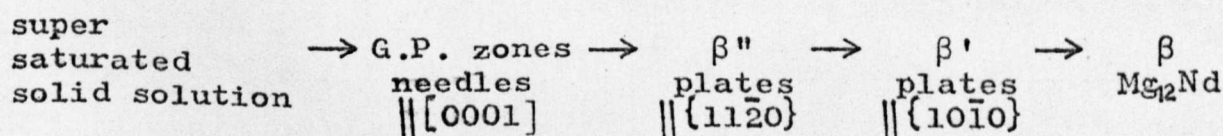
2.2 Magnesium Rare Earth Alloys

Rare earth metals are added to magnesium in the form of mischmetal, which contains approximately 75% Ce, 25% La, 18% Nd and 7% Pr, or didymium which contains approximately 60% Nd and 40% Pr. A series of commercial alloys are available which have useful properties at service temperatures up to 250°C . The response to age hardening increases as the neodymium content of the rare earth mixture increases [67] showing that this element is largely responsible for the properties

of this type of alloy. This is attributed to the fact that neodymium has a higher solid solubility in magnesium than other rare earths [68].

The equilibrium phase in these alloys has been studied by X-ray powder diffraction techniques. Early results showed the precipitates to be of two forms denoted β and x , the β being body centred cubic with $a = 1.458$ nm and the x a low symmetry phase [69]. Later workers confirmed these results [70,71]. Later X-ray diffraction studies [72] showed that the above results and those of previous workers could be interpreted as arising from a single equilibrium phase with a body centred tetragonal ThMn_{12} structure, lattice parameters $a = 1.031$ nm, $c = 0.593$ nm. This structure has since been confirmed by other workers [73,74,75,65].

Recently [75] an extensive study has been made on the system Mg-Nd using electron microscopy and electrical resistivity techniques. The ageing sequence was concluded to be



The β'' phase was found to be of DO_{19} structure similar to β'' in Mg-Th and therefore with probable composition Mg_3Nd .

The parameters of β'' were: $a\beta'' = 2a_{\text{Mg}}$ $c\beta'' = c_{\text{Mg}}$
 $a\beta'' \parallel a_{\text{Mg}}$ $c\beta'' \parallel c_{\text{Mg}}$.

The β' phase was found to nucleate extensively on dislocations and had a hexagonal structure

$$a = 0.52 \text{ nm} \quad c = 1.30 \text{ nm}.$$

Activation energies for the precipitation of the various phases were determined and found to be 74, 153, 146 and 145 kJ/mol for the stages G.P. zone β'' , β' and β respectively. The value for G.P. zone formation is close to the activation energy for the migration of vacancies in magnesium and the remainder of the values are comparable with the value of 134 kJ/mol, which is the activation energy for self diffusion in magnesium.

Ternary additions to the magnesium rare earth alloys have been studied by various workers. Increases in properties over binary alloys have been claimed for small additions of zirconium, zinc and manganese; the effect of manganese being attributed to a delay in the coarsening of the equilibrium precipitate [76]. A 2 - 3% addition of silver to a Mg 3.0% Nd .7% Zr alloy results in a room temperature strength increment of 50% [77]. The effect of this addition on the precipitation sequence, however, has not yet been reported in the literature.

2.3 Magnesium-Zinc

Sturkey and Clark [78] studied Mg-Zn alloys in the range 4% - 8% zinc. Electron diffraction studies showed the presence of a transition phase in the form of rods perpendicular to the basal plane and with a $MgZn_2$ type Laves phase structure. In a later study Clark [79] found that the strengthening caused by the above transition phase, designated $MgZn'$, was due to dislocations bowing between precipitates by the Orowan mechanism. The introduction of dislocations by cold work prior to ageing resulted in a refinement of the precipitate dispersion but no change in the strengthening mechanism. This hardening mechanism is in contrast to that proposed by Chun and Byrne [80]; in their opinion strengthening in Mg-Zn alloys is mainly due to the cutting of the transition $MgZn'$ precipitates. Sturkey and Clark [78,79] found no evidence for any G.P. zone reaction in their studies but Murikami [81], using a Laue X-ray method, reported that in a single crystal aged at 70°C plate like G.P. zones were formed on the $\{10\bar{1}1\}$ planes. His evidence, however, is far from convincing. More recently, Japanese workers [82 - 85] have shown that the resistivity behaviour in alloys aged at temperature $< 100^\circ C$ is extremely complex; this again was assumed to be due to G.P. zone formation. This low temperature reaction was

shown to be strongly dependent on solution treatment temperature [86] and the presence of a 'slow reaction' was detected. On the evidence available at the present time, it would seem that some type of low temperature reaction is occurring in this system. However, no convincing diffraction evidence has been presented and nothing has been seen with the electron microscope.

Much of the work on the Mg-Zn system is due to Gallot and colleagues [87 - 90] who have extensively studied a 6% Zn alloy using X-ray techniques. After prolonged ageing at 50°C [89] no diffraction evidence of G.P. zones was found. The transition phase previously reported by Sturkey and Clark was shown to exist in two forms, designated β_1' and β_2'

(i) β_1' needles perpendicular to $\{0001\}$ Mg.

$$[11\bar{2}0] \beta_1' \parallel [0001] \text{ Mg}$$

$$[0001] \beta_1' \parallel [11\bar{2}0] \text{ Mg}$$

(ii) β_2' plates parallel to $\{0001\}$

$$\{0001\} \beta_2' \parallel \{0001\} \text{ Mg}$$

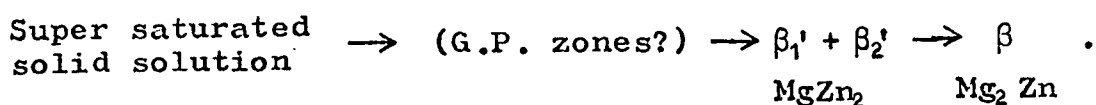
$$\langle 11\bar{2}0 \rangle \beta_2' \parallel \langle 10\bar{1}0 \rangle \text{ Mg.}$$

Both have the Laves phase MgZn_2 structure and both types of β' transform on further ageing to the equilibrium precipitate, which is triclinic of composition Mg_2Zn_3 [89].

Hall [90] carried out an investigation using double ageing, direct quenching techniques and attempted to explain

his results on the basis of nucleation from G.P. zones [26]. The dispersion of precipitates was refined by a double ageing technique but the degree of refinement was a factor of 10 only as opposed to 10^3 in the case of aluminium alloys.

In conclusion it can be said that the existence of G.P. zones in Mg-Zn alloys is still in question but the remainder of the precipitation sequence is well established



2.4 Magnesium-Aluminium

Clark [25,92,93] showed that a Mg 9% Al alloy age-hardens by continuous precipitation of plates of the equilibrium precipitate Mg₁₇Al₁₂ on the basal plane of the magnesium matrix. No evidence for the formation of G.P. zones or a transition lattice of Mg₁₇Al₁₂ was found. Cellular or discontinuous precipitation occurs competitively with general or continuous precipitation at all ageing temperatures but general precipitation is greatly enhanced by the introduction of cold work in the interval between quenching and ageing. The dislocations introduced act as nuclei for Mg₁₇Al₁₂ precipitates which Clark observed to be extensively dislocation nucleated

in all samples. It was concluded by Clark that the poor age hardening response in this alloy was due to the precipitation of an incoherent phase with a large interparticle spacing. However, recent work [94] has shown the possibility of a further precipitate in this system. Small particles < 5.0 nm diameter were formed in the early stages of ageing at low temperatures. The structure of this phase was not determined but diffraction evidence suggests that the particles are a transition phase denoted β' not G.P. zones. The β phase was found on subsequent ageing to precipitate with the relationship

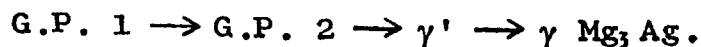
$$(0\bar{1}1) \beta \parallel (0001) \text{Mg} \quad (211) \beta \parallel (10\bar{1}0) \text{Mg}$$

and occasionally

$$(0\bar{1}1) \beta \parallel (0001) \text{Mg} \quad (100) \beta \parallel (10\bar{1}0) \text{Mg}.$$

2.5 Magnesium-Silver

The system Mg-Ag has been extensively studied by Nagashima [95 - 98] using X-ray diffraction techniques. The ageing sequence deduced was



G.P. 1 zones were formed as plates parallel to $\{10\bar{1}1\}$ Mg and were found to exist only at temperatures below 60°C. These zones grow to a maximum size of 13.0 nm in diameter.

The G.P. 2 phase co-exists with the G.P. 1 zones at low temperatures but on ageing at temperatures above 60°C only the G.P. 2 phase is found, indicating an extremely low G.P. 1 solvus temperature. The G.P. 2 phase consists of a complex ordered arrangement of atoms in the shape of an oblate spheroid, becoming later a plate with the major axes parallel to the matrix basal plane. On ageing at temperatures between 150°C and 200°C the transition phase γ' , whose structure has not been determined, precipitates on either the matrix (0001) or $\{11\bar{2}0\}$ planes. On prolonged ageing at temperatures in excess of 200°C the equilibrium γ Mg, Ag phase forms.

2.6 Magnesium-Zirconium

Interest in the system Mg-Zr has been stimulated by the possibility of the alloys being used as a canning material in nuclear reactors. A typical composition is 0.5% Zr; the alloy has a high creep ductility, is resistant to grain growth and has a low capture cross section to thermal neutrons, making it an ideal alloy for canning materials. No compounds form between zirconium and magnesium and strengthening is due to precipitation of ϵ ZrH_2 [99,100,101]. This hydride forms as plates parallel to (0001) Mg, the edges of the plates lying parallel to $\langle 11\bar{2}0 \rangle$ [102,103]. The hydride forms as

a result of water vapour or hydrogen being present in the furnace atmosphere during heat treatment. A further study by Harris and Partridge [104] showed that grain boundaries and dislocations act as preferential sites for nucleation of the ϵ hydride. Improved properties have been shown [62] to occur in alloys given a prolonged homogenisation prior to heat treatment resulting in a more uniform dispersion of the ϵ ZrH_2 .

2.7 Magnesium-Manganese

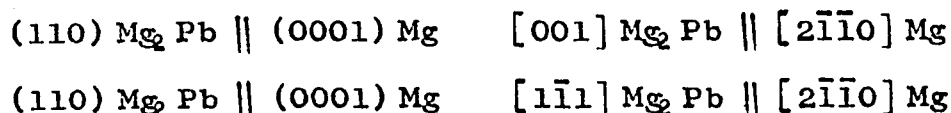
The system Mg-Mn precipitates α Mn, which forms as plates lying perpendicular to the matrix basal plane. The orientation relationship was found to be

$$\begin{aligned} \{111\} \alpha & \parallel \{0001\} \text{Mg} \\ \{1\bar{1}0\} \alpha & \parallel \{10\bar{1}0\} \text{Mg}. \end{aligned}$$

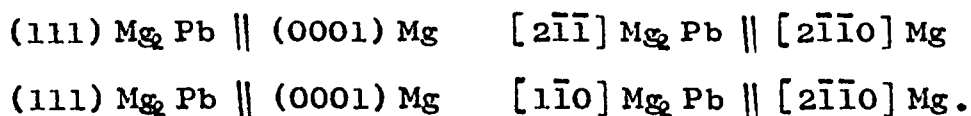
Work has been carried out on the increase of critically resolved shear stress due to the presence of these incoherent particles which are effectively orientated to block basal slip. The strength increment due to the presence of these particles was found to be due to the cutting of α Mn particles by dislocations.

2.8 Magnesium Tin and Magnesium Lead

The systems Mg-Pb and Mg-Sn are very similar as both precipitate the compound Mg_2X where X is tin or lead. In both alloy systems the structure of the compound is cubic with an anti- CaF_2 structure. The system Mg-Pb hardens by precipitation of plates of Mg_2Pb lying parallel to the basal plane with the orientation relationship [107,108]



at ageing temperatures between $130^\circ C$ and $200^\circ C$ and at higher ageing temperatures:



Calorimetric measurements [109] indicate that G.P. zones may form at low ageing temperatures. Henes and Gerold [107,108] studied both systems with X-ray techniques and found that regions of short range order existed in both alloys and in the Mg-Pb alloy these can grow to G.P. zones having diameters of approximately 10.0 nm. These zones have an $Mg_3Cd DO_{19}$ structure and a composition Mg_3Pb . Work by Van der Planken [110,111] has also confirmed the presence of short range order.

In these alloy systems rapid quenching from the melt can greatly extend the range of solid solubility. Abe, Ito and Suzuki [112,113] showed that when the metal had been splat cooled a metastable phase with the $\text{Cu}_3\text{Au} - \text{I}$ superlattice formed which, on prolonged ageing, transformed to Mg_2Pb and Mg .

Summary

Age hardening behaviour in magnesium alloys is caused by the formation of transition phases, in a manner analagous to those observed in the classical Al-Cu system. G.P. zones can with confidence be said to be present in Mg-Ag and Mg-Nd alloys, although this does not necessarily preclude their presence in various other systems where less direct methods have indicated some form of low temperature reaction. The formation of transition precipitates is well documented and in several systems useful strength increments are obtained by ageing alloys to contain transition precipitates.

CHAPTER 3

EXPERIMENTAL DETAILS

3.1 Preparation of Alloys

All alloys used in the investigation were prepared using high purity materials. Induction melting of the alloys was carried out under an atmosphere of argon, at slightly less than atmospheric pressure to help degas the melt. All alloys were heated to a temperature of approximately 800°C and immediately cast into a metal mould. The rapid chilling and turbulent conditions during melting helped to minimise the segregation of solute. In the cast billet the head of the ingot was removed for chemical analysis and the remainder of the ingot homogenised for several days near the solidus temperature. This temperature was determined by the "quench and microexamination" method where specimens of the alloy are quenched from various temperatures and examined for areas of grain boundary liquation. After homogenisation, the ingots were scalped and extruded into either strip or bar. A further homogenisation process was followed by hot rolling the strip to the desired thickness.

3.2 Solution Treatment Procedures

Solution treatment, whether for resistivity measurements or electron microscope observations, was carried out for a period of one hour, after which the specimens were rapidly quenched into water at 20°C. Ageing was commenced as soon as possible after the quench.

The solution treatment was carried out in either a salt bath of dichromate salts or in an air-circulation furnace. Specimens solution treated in the air-circulation furnace were first sealed in pyrex ampules containing pure, dry argon. Quenching conditions were arranged so that the tube broke and therefore the quenching rate was comparable with that achieved by quenching directly from the salt bath.

The effectiveness of the solution treatment procedure was checked by measuring the resistivity of a sample of Mg 3.0% Th at 250°C until precipitation was complete and then re-solution treating and ageing. The fact that the curves were identical showed that no loss of thorium was occurring and that precipitates readily redissolve during heat treatment.

3.3 Ageing Environments

High temperature ageing ($> 350^{\circ}\text{C}$) was carried out in a salt bath, which had a composition similar to that used for solution treatment. Ageing temperatures of $250^{\circ}\text{C} - 350^{\circ}\text{C}$ were achieved by air-circulation furnaces with eurotherm type controllers arranged to give a control $\pm 1^{\circ}\text{C}$. Low temperature ageing ($< 250^{\circ}\text{C}$) was carried out in silicone oil baths, again arranged to give a temperature control of $\pm 1^{\circ}\text{C}$.

3.4 Resistivity Measurements

The specimens used for resistivity work were machined from 1 mm thick strip, the cross-sectional area and gauge length being 4 mm^2 and 180 mm respectively. The specimen forms a four terminal resistor with potential connections of the same material.

The kinetics of the precipitation processes were followed by means of resistivity measurements taken whilst the specimens were ageing in an air-circulation furnace. Two different techniques were used and these will be described briefly.

(i) Continuous heating curve

A specimen was continuously heated at a constant rate of $1^{\circ}\text{C}/\text{mm}$. The potential developed by the passage

of a stable current of 1 A was continuously recorded on a millivolt recorder. Simultaneous measurement of the temperature of the specimen was also made. The results were plotted as absolute resistivity against temperature.

(ii) Isothermal transformation curves

The precipitation process in this case was followed by comparing the resistivity of the specimen to that of a standard, while both were contained in the ageing environment. Both specimen and standard were firmly held in a jig in which the current leads were made by screwing the specimen to silver bars. Potential connections were made by welding magnesium wire to the potential arms of the specimen. To prevent error due to thermal electro-motive forces, the current through the specimen was reversed and the mean of the two readings taken. Potential measurements were made using a Kelvin double bridge or a Vernier potentiometer.

Kelvin double bridge circuit

The double bridge circuit is shown in Figure 3.1 and the star connected equivalent in Figure 3.2. The star connected circuit is equivalent to a wheatstone bridge circuit whose balance condition is

$$\frac{R_3}{S + \frac{R_1 \alpha}{R_1 + R_4 + \alpha}} = \frac{R_3}{X + \frac{R_4 \alpha}{R_1 + R_4 + \alpha}} \quad (3.1)$$

where α is the resistance of the bar connecting specimen and standard $R_1 = R_2 = 100 \Omega$ and $R_3 = R_4$ but are both variable.

Therefore

$$X = \frac{R_3}{R_2} S + \frac{\alpha R_3 \left[\frac{R_1}{R_2} - \frac{R_4}{R_3} \right]}{R_1 + R_4 + \alpha}. \quad (3.2)$$

The leads were all of heavy gauge copper wire and were of equal resistance so that lead resistance need not be taken into account. Also, contacts between the specimens were of silver and therefore of extremely low resistance. The term α in equation (3.2) is correspondingly small, making the second term in the equation negligible.

Thus

$$\frac{X}{S} \approx \frac{R_3}{R_2}. \quad (3.3)$$

Since the changes in ratio and not absolute values are being considered, any error introduced by use of equation (3.3) will not affect the results. This equation has been used throughout the present work.

Potentiometric circuit

The potentiometric circuit employed a Vernier potentiometer and automatic current controllers which provided stable currents in both the potentiometer and the external circuit shown in Figure 3.3. It is advantageous to be able to use this method at the higher ageing temperature to give more accurate results in the early stages of ageing where precipitation is extremely rapid.

At the balance condition no current flows in the measuring circuit, so connecting wires were made of fine gauge copper wire rather than the heavy low resistance leads used in the Kelvin bridge circuit.

At the balance condition

$$\frac{V_X}{X} = \frac{V_S}{S}$$

or

$$\frac{X}{S} = \frac{V_X}{V_S} \quad (3.4)$$

where X and S are the values of the resistances of the unknown and standard respectively and V_X and V_S are the potentials developed across them.

In both the Kelvin double bridge and potentiometer techniques the parameter

$$\frac{R_t - R_o}{R_o} = \frac{\Delta R}{R_o}$$

was plotted against the logarithm of ageing time where R_t is the ratio of resistances of standard and specimen at time t , and R_o is the ratio at the commencement of ageing.

The use of this parameter, of course, requires a knowledge of R_o . In some cases a long incubation period preceded the subsequent fall in resistance due to precipitation and graphical extrapolation to obtain R_o was possible. In other cases, however, this was found not to be possible and a computer program was developed to obtain the optimum value of R_o from the ratios measured. The program is based on analysis of the transformation curves according to the Avrami or Johnston-Mehl equation, in which the fraction transformed, Y , after time t , is given by

$$Y = \frac{R_o - R_t}{R_o - R_F} = 1 - \exp\left(-\left(\frac{t}{\tau}\right)^m\right) \quad (4.5)$$

where m and τ are the equation constants and R_F is the ratio of resistances of standard and specimen at the completion of precipitation.

3.5 Electron Microscopy

Transmission electron microscopy has been used to study the distribution and morphology of the precipitates. An A.E.I. EM6 G. microscope operated at 100 K.V. and fitted with high-tilt goniometer, decontaminator and dark-field equipment was the instrument employed. The quantitative nature of certain aspects of the work made it necessary to calibrate the microscope for magnification, image rotation and effective camera length.

Preparation of thin foils

Specimens for transmission microscopy were generally prepared from 0.5 mm thick rolled strip but this was found to suffer from pronounced $\{0001\}$, $[2\bar{1}\bar{1}0]$ preferred orientation, which severely limited the number of zone axes available. To make available a wider range of orientations, specimens were also cut from extruded rod at 0 and 30° to the face to give $\{2\bar{1}\bar{1}0\}$ and $\{10\bar{1}0\}$ orientations respectively.

Specimens were prepared for microscopy by cleaning on emery paper and electrothinning by the window technique at 0°C in a solution containing 30% nitric acid in ethanol. A stainless steel cathode and applied potential of 10 volts were found to give the required polishing

conditions for the majority of the alloys studied.

After perforation specimens were quickly removed from the solution, washed in ethanol and dried between filter papers. To remove the film of oxide formed during polishing the specimen was cut and cleaned in orthophosphoric acid at 10°C for thirty seconds, and finally washed in ethanol and dried.

Calibration of the electron microscope

The microscope had previously been calibrated for true magnification using the standard technique involving a replica of a diffraction grating [114]. This calibration curve is shown in Figure 3.4. The effect of image-selected area diffraction pattern rotation had also been calibrated using a series of diffraction patterns and bright field images taken at different intermediate lens currents of a crystal of Mo O₃, which form with long straight edges parallel to the [100] (ref. [114]). This calibration is shown in Figure 3.5.

The camera constant (λL) was determined by obtaining several diffraction patterns from an evaporated polycrystalline film of aluminium. The camera constant was then found by the relationship

$$r_{hkl}^* \cdot d_{hkl} = \lambda L$$

where r_{hkl}^* is the reciprocal lattice distance measured from the diffraction pattern and d_{hkl} is the spacing of the $\{hkl\}$ plane in the direct lattice.

3.6 Creep Testing

Creep testing was carried out in a Mand creep machine. The machine was of the lever loading type with the specimen at one end of the lever arm and a constant load at the other. Facility was provided, by means of an adjustable counterbalance, to compensate for the weight of the levers and weight pan. The mechanical advantage of the system was determined by insertion of a proving ring in the position normally occupied by the creep specimens and the deflection for various loads was noted.

The extension was measured by a dial gauge type extensometer attached to the specimen by knife edges, enabling the extension to be measured on a 5 cm gauge length with an accuracy of 1 part in 10^4 .

Temperature measurement was achieved by attaching a chromel/alumel thermocouple to the specimen gauge length. All specimens were allowed a period of one hour in which to attain the furnace temperature before the tests were commenced.

Figure 3.1 Kelvin Double Bridge Circuit

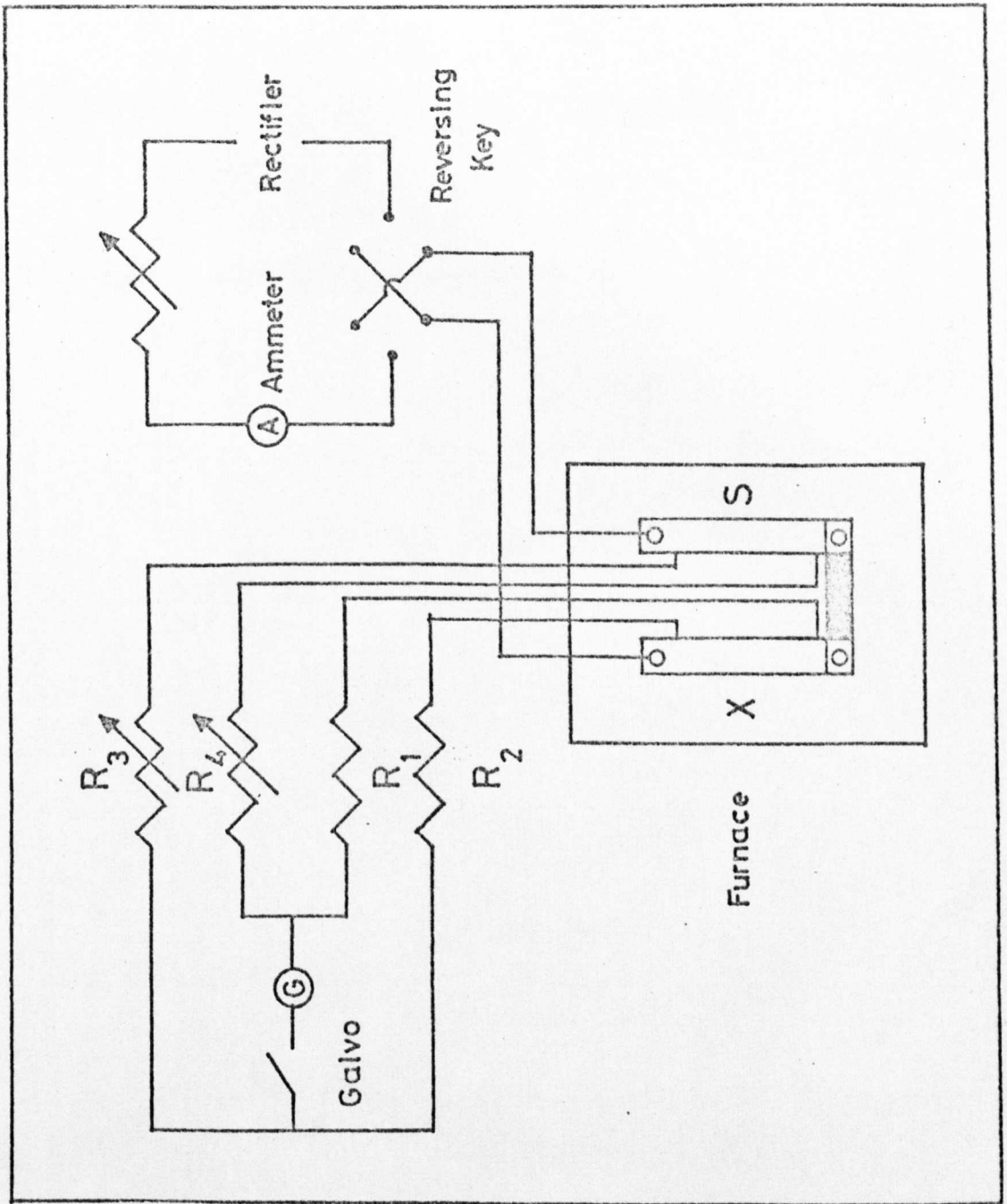


Figure 3.2 Kelvin Double Bridge Circuit

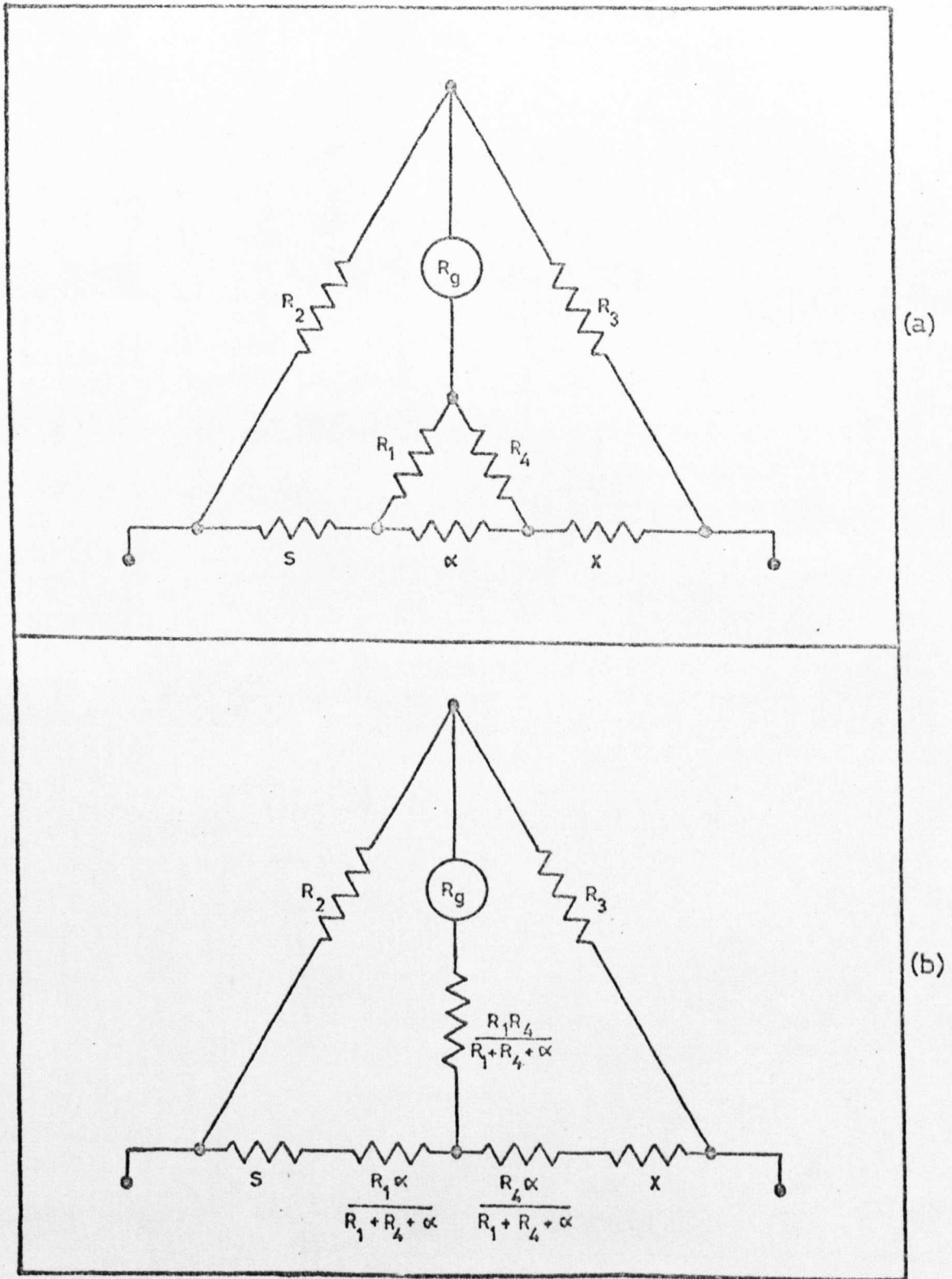


Figure 3.3: Potentiometer Circuit

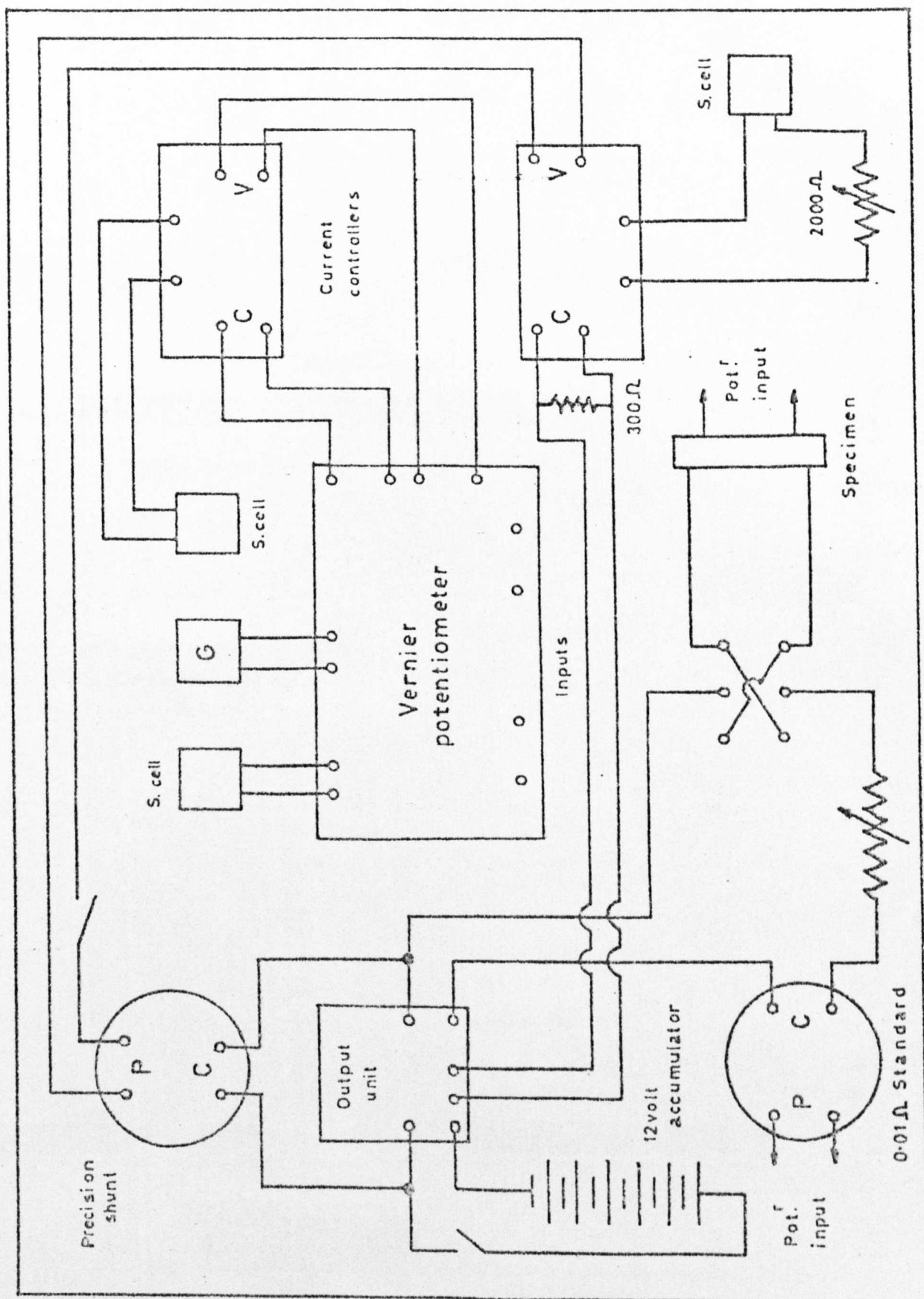


Figure 3.4: Magnification calibration curve for electron microscope
Accelerating potential 100 kV objective current 145 mA

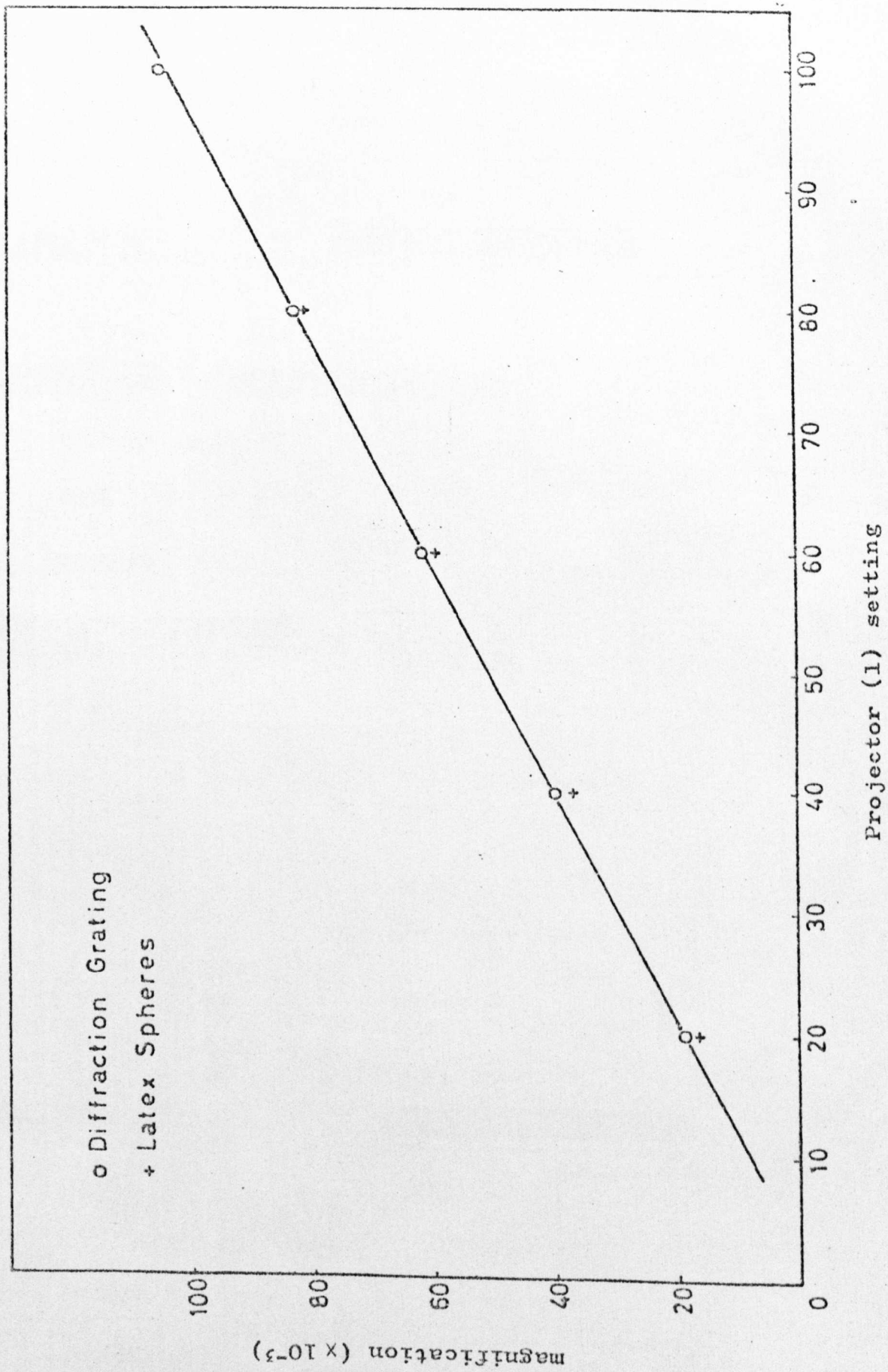
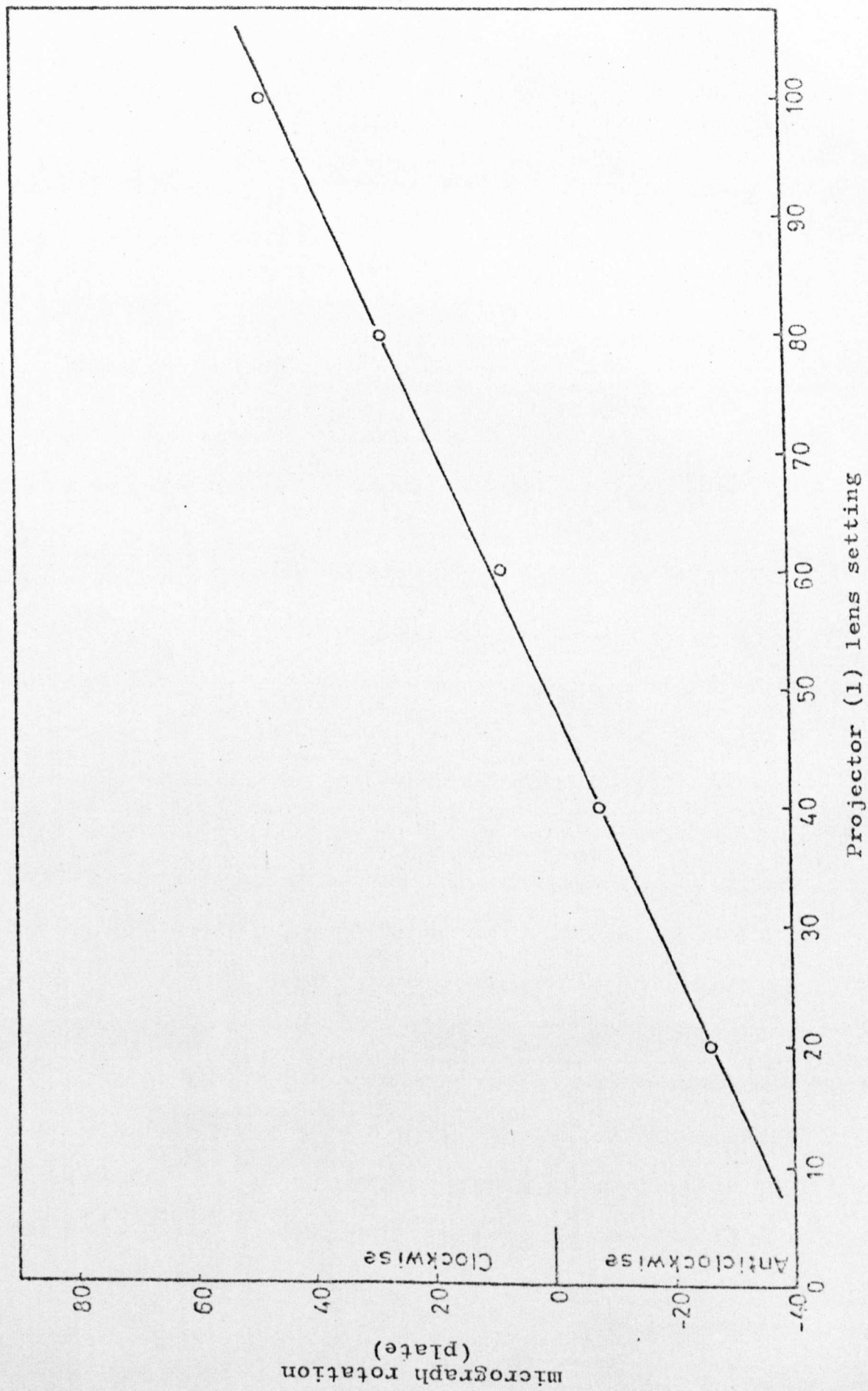


Figure 3.5: Rotation of Electron Microscope image relative to diffraction pattern
Accelerating potential 100 kV



CHAPTER 4THE Mg-Th SYSTEM: EFFECT OF ZIRCONIUM ADDITIONS

Mg-Th alloys are extensively used in creep resistant applications, generally with an addition of approximately 0.7% Zr, which is added as a grain refiner. Until recently, it had been assumed that the binary Mg-Th alloys and the ternary alloy containing zirconium were structurally equivalent since no Th-Zr, Mg-Zr or Mg-Th-Zr compounds are known to exist. Recent work, however, has shown that the two systems are not equivalent and by comparing the results of Noble and Crook [61] on a binary alloy with those of Stratford on the ternary, it has been deduced [63] that an additional phase is present in the ternary alloy. This phase, Mg_2Th , has been previously shown to exist in two polymorphic forms [64]. It has a C 15 structure (f.c.c. $a_0 = 0.857$ nm) at temperatures of 800°C and above, and a C 36 type (hexagonal $c = 1.964$ nm $a = 0.6086$ nm) at temperatures below 700°C. For the purposes of this thesis these polymorphs have been designated β' cubic and β' hex.

The object of this chapter is to re-examine both binary and ternary alloys in the light of recent results and to arrive at a coherent view of precipitation in both systems. It was then hoped to deduce the rôle of

zirconium in the precipitation process in the ternary alloy.

The investigation has used alloys of nominal composition 3.0% Th, 3.0% Th 0.4% Zr and 3.0% Th 0.7% Zr.

4.1 The β' hex Phase

In specimens quenched and aged at temperatures in the range 325 - 425°C the β' hex polymorph was found to be present in the ternary alloy. For foils in or near basal orientation this β' hex was found to precipitate in two entirely different forms:

- (i) as isolated particles rather similar in appearance to β particles (Fig. 4.1a);
- (ii) as rings of precipitate around large irregular shaped particles (Fig 4.1b).

Attempts to identify the particles at the centre of the rings of precipitates by selected area diffraction were unsuccessful as in all cases the particles were too thick to transmit electrons.

Diffraction patterns taken from areas containing these β' hex precipitates were obtained and trace analysis showed that the majority of these rings lay in the basal plane of the magnesium matrix. For this situation the orientation relationship proved to be

$$(0001) \text{ Mg } \parallel (0001) \beta' \text{ hex}$$

$$(11\bar{2}0) \text{ Mg } \parallel (10\bar{1}0) \beta' \text{ hex.}$$

The full stereographic relationship is shown plotted in Figure 4.2. A small amount of precipitation of β' hex was also noted on prism planes, an example of this is shown in Figure 4.3. Diffraction patterns taken from the precipitate showed a completely different orientation relationship

$$(0001) \text{ Mg } \parallel (\bar{2}110) \beta' \text{ hex}$$

$$(\bar{2}110) \text{ Mg } \parallel (0001) \beta' \text{ hex.}$$

Examination of thin foils in several orientations showed the β' hex to have the shape of an oblate spheroid with the major axes parallel to (0001) and (10 $\bar{1}$ 0) for precipitation on basal and prism planes respectively. For β' hex in the form of basal rings, streaks were observed in electron diffraction patterns. Examples of these streaks are shown in Figure 4.4. The streaks can be interpreted as $\langle 10\bar{1}0 \rangle^{*\dagger}$ relrods, the fact that they are present in the $[10\bar{1}1]$ zone axis β' hex pattern (Fig. 4.4b) in the $\langle 10\bar{1}1 \rangle^*$ direction being due to the finite thickness of the Ewald sphere intersecting these $\langle 10\bar{1}0 \rangle^*$ relrods causing discontinuous streaks. Since the precipitate has

\dagger Denotes vectors in reciprocal space

been shown not to be thin in the $[10\bar{1}0]$ directions, it is assumed that the streaks arise from faulting of the $\{10\bar{1}0\}$ planes of the β' hex precipitate.

In an attempt to study the kinetics of β' hex formation, electrical resistivity isotherms were plotted at 325°C and 350°C , these being the optimum temperatures for β' hex formation. The results are shown in Figure 4.5 compared with work by Crook [115] who undertook similar measurements on a binary Mg-Th alloy. The curves are shown to be identical, showing no inflections due to β' hex formation. However, it is possible that the β' hex is forming competitively with the β with similar kinetics since the resistivity technique measures only the rate of removal of solute atoms from solid solution, or, alternatively, that the β' hex is only a small volume fraction of the total precipitate.

Since it appeared that the greater part of the β' hex precipitate was forming on dislocations, it was felt relevant to investigate the effect of deliberately deforming the specimen between solution treatment and ageing. A deformation of 10% was applied to both the binary and ternary alloys. The electron microstructures of the two alloys were seen to be identical (Fig. 4.7). The introduction of a high density of dislocations resulted in a large volume fraction of β' hex nucleating on these dislocations. It appears that the β' hex nucleates

at several points on each individual dislocation line and the small particles grow together giving the impression of intertwined "ribbons" of precipitate. This precipitate proved to have an extremely high resistance to coarsening and all attempts to coarsen the precipitate resulted in transformation to $\beta \text{ Mg}_2\text{Th}_6$. Diffraction patterns taken from the binary and ternary alloys containing the β' hex ribbon precipitate showed that the precipitate has an identical structure and orientation relationship with the matrix to the β' hex previously found in the undeformed alloy. The particles in the deformed alloy, however, were very much smaller (~ 50 nm) than those found in the undeformed alloy (~ 500 nm) in specimens given identical treatments of 24 hours at 350°C .

To compare the precipitation behaviour of deformed and undeformed material the resistivity of two specimens of the ternary alloy, one deformed at 10% and the other undeformed, was monitored while the specimens were heated from room temperature to 580°C at a constant rate of $1^\circ\text{C}/\text{minute}$. The results are shown in Figure 4.6. In the undeformed material it can be seen that two deviations from the interpolated solid solution line occurs. These are due to precipitation of the β'' and β phases respectively. There is no deviation which can be attributed to either β' hex or β' cubic formation, showing that these phases are either absent or else their volume fraction is so small

as to not affect the resistivity behaviour of the undeformed alloy. However, after 10% deformation both binary and ternary alloys show an additional inflection at $\sim 300^{\circ}\text{C}$, which persists until β precipitation becomes dominant at temperatures in excess of 400°C . These results are consistent with a large volume fraction of a third phase, β' hex, precipitating in this temperature range.

4.2 The β and β' cubic Phases

In many of the specimens examined containing β' hex, particles of the equilibrium phase $\beta \text{ Mg}_{23}\text{Th}_6$ were also detected both at grain boundaries and within the grains. The β was found to occur in two forms, small, irregular shaped particles and rod shaped particles. The former particles were unambiguously identified as the β phase (Fig. 4.8) by selected area diffraction. Large numbers of the rod shaped particles were examined by electron diffraction and, although the majority could be indexed as β , a small number were indexed as β' hex and an even smaller number as the other polymorph of Mg_2Th β' cubic $a_0 = 0.857 \text{ nm}$. To give some idea of the distribution of the different phases in the alloy it was estimated that in one grain, out of a total of over 100 particles examined, $\sim 66\%$ were of the β' hex phase, one particle was

identified as β' cubic and the remainder were β . In total 4 β' cubic zone axes patterns were obtained and these are shown in Figure 4.9. They are the $[110]$, $[111]$, $[411]$ and $[332]$ zones. The following common directions were found in diffraction patterns containing β' cubic

$$\begin{aligned} [\bar{1}10] \beta' \text{ cubic} & \parallel [10\bar{1}0] \text{ Mg} \\ [\bar{1}13] \beta' \text{ cubic} & \parallel [2\bar{1}\bar{1}0] \text{ Mg} \\ [\bar{1}11] \beta' \text{ cubic} & \parallel [10\bar{1}1] \text{ Mg}. \end{aligned}$$

On subjecting this information to stereographic analysis, however, it was found that no unique orientation relationship between β' cubic and the magnesium matrix exists.

4.3 Discussion

It has been found in the present investigation that the β' hex phase forms as a transition precipitate during the ageing of Mg-Th-Zr alloys. This phase has been found to precipitate within the grains and also in a "ribbon-like" fashion on dislocations lying in the basal planes of magnesium matrix with an orientation relationship

$$\begin{aligned} (0001) \text{ Mg} & \parallel (0001) \beta' \text{ hex} \\ (10\bar{1}0) \text{ Mg} & \parallel (2\bar{1}\bar{1}0) \beta' \text{ hex}. \end{aligned}$$

The rings of β' hex around irregular shaped particles were particularly interesting. By examining foils in the solution treated condition it was deduced that these particles were left undissolved after the solution treatment operation, as in all magnesium alloys containing zirconium, insoluble zirconium particles are found throughout the matrix, in the form of both stringers and small discrete particles. It is therefore likely that these particles throw out dislocation loops as a result of the different thermal contraction coefficients of matrix and particle and that nucleation of β' hex then takes place on these dislocations. Harris and Partridge [104], in a study of ZrH_2 formation in a binary Mg-Zr alloy, found that in homogenised and hydrided sheet a similar situation caused precipitation of ϵ ZrH_2 on dislocations around insoluble particles. They also were unsuccessful in identifying the insoluble particles, but assumed them to be small particles of undissolved zirconium.

If this is, in fact, the operative mechanism, it is to be expected that β' hex would be more prevalent in the high zirconium alloy H K 31 A studied by Sturkey, due to the high proportion of undissolved zirconium present. The fact that the β' hex phase has been detected in the deformed binary Mg-Th alloy shows that it is a true binary compound and not, as suggested [116], a ternary compound

of the type $Mg_2(Th\ Zr)$.

β' 'cubic has also been shown to be present but it does not form a large volume fraction of the total precipitate present at any time. This latter result is in contrast to previous work by Sturkey [55], Mushovic and Stoloff [59,60], and Stratford [63].

Sturkey used X-ray and reflection electron diffraction techniques to study precipitation in a ternary Mg-Th-Zr alloy aged in the temperature range 335 - 370°C. In alloys aged at 370°C he detected diffractometer peaks representing d spacings of 0.49 - 0.50 nm and 0.30 - 0.31 nm, the intensity of which increased on prolonged ageing and eventually disappeared, indicating the presence of a transition precipitate. These peaks were interpreted as arising from the 111 and 200 reflections of β' 'cubic. However, the values quoted by Sturkey represent uncertainties of ~ 2% - 3% in the position of the peaks; within these uncertainty limits it is equally possible to interpret these peaks as arising from the β' 'hex $10\bar{1}1$ and $11\bar{2}0$ peaks respectively. Additional evidence presented by Sturkey consists of a reflection electron diffraction pattern indexed by Sturkey as $\langle 211 \rangle$ zone axis from β' 'cubic. This pattern is also ambiguous since it can equally well be indexed as arising from $\langle 10\bar{1}2 \rangle$ β' 'hex with very small errors as indicated in Table 4.1.

Table 4.1

Interplanar spacings in β' hex and β' cubic

Reflection	d fcc nm	Reflection	d hex nm
111	0.494	01 $\bar{1}$ 1	0.509
131	0.259	20 $\bar{2}$ 1	0.262
022	0.303	2 $\bar{1}$ $\bar{1}$ 0	0.305

Sturkey noted in his investigation that the formation of the transition precipitate was enhanced by the application of 30% deformation in the interval between quenching and ageing. This has been found to be the case in the present study with β' hex, also no nucleation of β' cubic has been found on dislocations. In view of these observations, together with the ambiguity of previously published evidence, it is strongly felt that the precipitate detected by Sturkey was the hexagonal, not the cubic, polymorph of β' Mg₃Th.

Mushovic and Stoloff [59,60], in their study of the ternary alloy, claim that the β'' Mg₃Th structure transforms to β' cubic on prolonged ageing. The β' cubic remains as plates on the {10 $\bar{1}$ 0} planes of magnesium. The evidence presented for the existence of the β' cubic phase consists of one diffraction pattern purporting to

show an orientation relationship

$$(111) \text{ ppt} \parallel (0001) \text{ Mg}$$

$$[220] \text{ ppt} \parallel [11\bar{2}0] \text{ Mg}$$

between matrix and precipitate. However, the reflections claimed to be due to the Mg_2Th β' cubic phase can be indexed as arising from MgO , which forms as an epitaxial film on magnesium on prolonged exposure to the electron beam. The structure of MgO is f.c.c. with $a = 0.421$ nm, i.e. approximately half that of β' cubic 0.857 , which explains the apparent confusion. The pattern published by Mushovic and Stoloff indexes as a $[0001]$ Mg zone axis and a $[111]$ zone axis of MgO . This is the orientation relationship found by Hales, Dobson and Smallman $[117]$ for an epitaxial film of MgO on magnesium. In the light of this evidence it can be seen that the micrographs published by Mushovic and Stoloff showing precipitates on $\{10\bar{1}0\}$ planes, are of the β'' phase.

Stratford $[63]$ found evidence of both β' hex and β' cubic in a ternary Mg-Th-Zr alloy aged at 330°C . However, in contrast to several other workers, he found no evidence of intergranular β precipitation, even after periods of up to 96 hours at 330°C . The electron diffraction pattern shown for β' cubic had a $\langle 310 \rangle$ zone axis and indicated an orientation relationship of

$$[310] \parallel [0001].$$

The present investigation has found orientation relationships

$$[\bar{1}10] \parallel [1010] \text{ Mg}$$

$$[\bar{1}13] \parallel [2\bar{1}\bar{1}0] \text{ Mg}$$

$$[\bar{1}11] \parallel [10\bar{1}1] \text{ Mg}$$

but it has been found that no unique relationship exists.

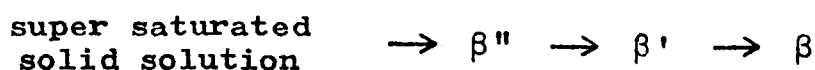
In a later communication [116], it was shown that the $[310]$ zone axis β' cubic pattern originated from a particle similar in form to those observed in the present investigation, i.e. a pointed, rod-shaped particle. Stratford, however, appears from this evidence to have assumed that all particles similar in appearance to this rod-shaped particle are in fact β' cubic. This has been shown in the present work not to be so. The large majority of rod-shaped particles identified conclusively by electron diffraction proved to be $\beta \text{ Mg}_{23} \text{ Th}_8$. Many of these β particles were shown to have their long axes parallel to $[2\bar{1}\bar{1}0]$ and to be identical in appearance to the particles Stratford refers to as β' cubic particles in an $[0001]$ foil aged for one hour at 425°C . It should be noted that difficulty is often obtained in identifying conclusively particles in this condition as they are often too thick to transmit electrons. However, it is

strongly felt, in view of the results of this and other investigations where β has been found, in a variety of orientations and morphologies, under conditions similar to those used by Stratford, that the majority of the rod-shaped particles are β , not β' cubic.

Summary

The results of the present investigation, together with the results of several recent papers on precipitation in Mg-Th-Zr and Mg-Th alloys, can be summarised as follows.

- (i) The precipitation sequence in Mg-Th-Zr alloys is

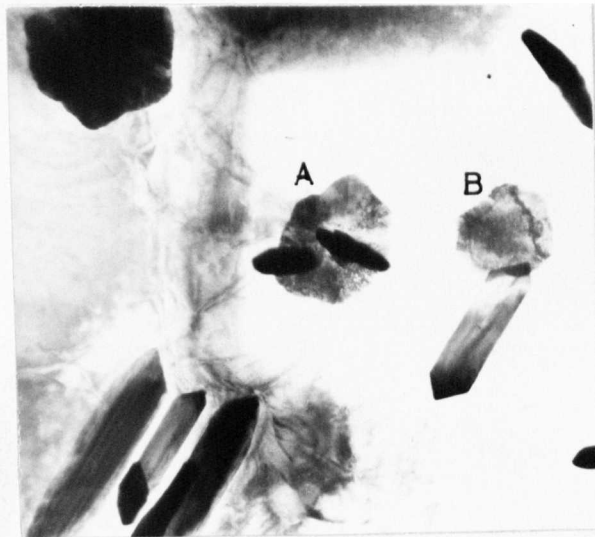


where the symbol β' is taken to include both polymorphs β' hex and β' cubic but strongly weighted in favour of the β' hex polymorph.

- (ii) The β' hex phase has been shown to nucleate extensively on dislocations and does not occur in the super-pure Mg-Th alloy unless deformation is applied before ageing due to the lack of suitable nucleation sites. It has been shown to precipitate with the orientation relationship

$$\begin{aligned}(0001) \text{ Mg} & \parallel (0001) \beta' \text{ hex} \\ (2\bar{1}\bar{1}0) \text{ Mg} & \parallel (10\bar{1}0) \beta' \text{ hex}.\end{aligned}$$

- (iii) β' cubic has been shown to occur in a ternary alloy in extremely small proportions. It has been shown not to have a unique orientation relationship.
- (iv) The $\beta \text{ Mg}_{23} \text{ Th}_8$ phase precipitates both within the grains and at grain boundaries. In the former case it can assume a variety of orientations and morphologies.



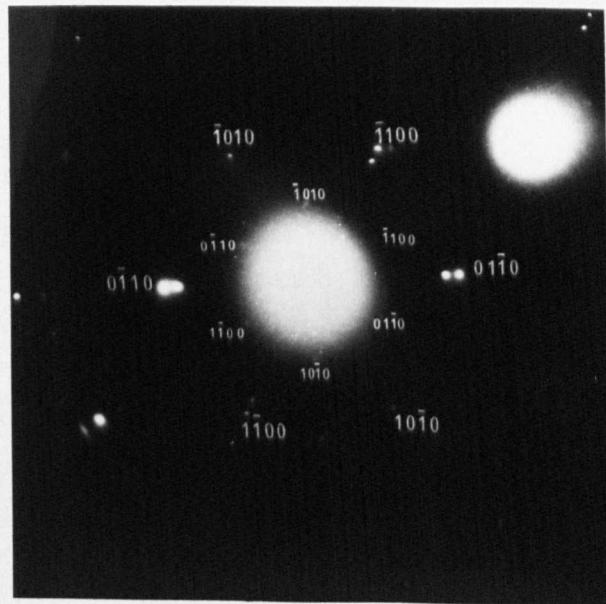
(a)

Figure 4.1(a) Mg-Th-Zr alloy aged for one day at 350°C. Particles A and B were identified by electron diffraction as β' hexagonal. Other particles were identified as β $Mg_{23}Th_6$.

Mag 16,000 x



(b)



(c)

Figure 4.1(b) Mg-Th-Zr alloy aged 16 hrs at 350°C showing β' hex precipitation on dislocation around insoluble particles. Mag 10,000 x

(c) Diffraction pattern showing
 $[0001] \text{Mg} \parallel [0001] \beta' \text{hex}$
 $[2\bar{1}\bar{1}0] \text{Mg} \parallel [10\bar{1}0] \beta' \text{hex}$

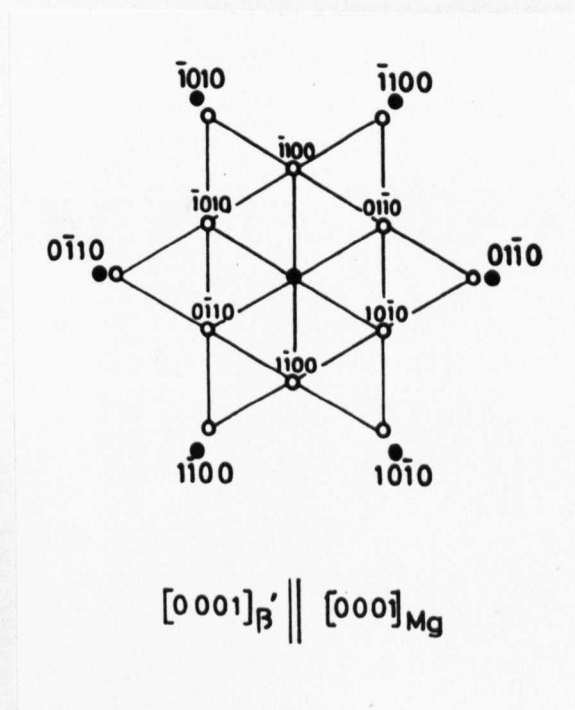
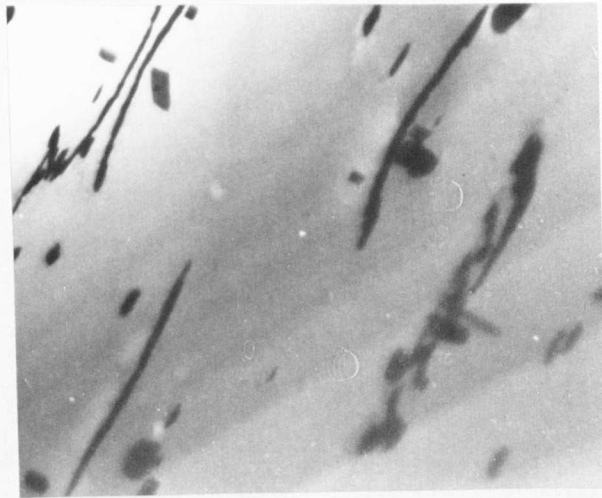
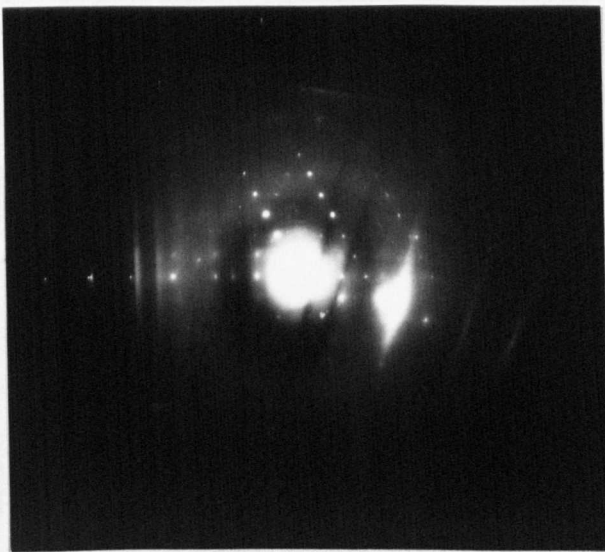


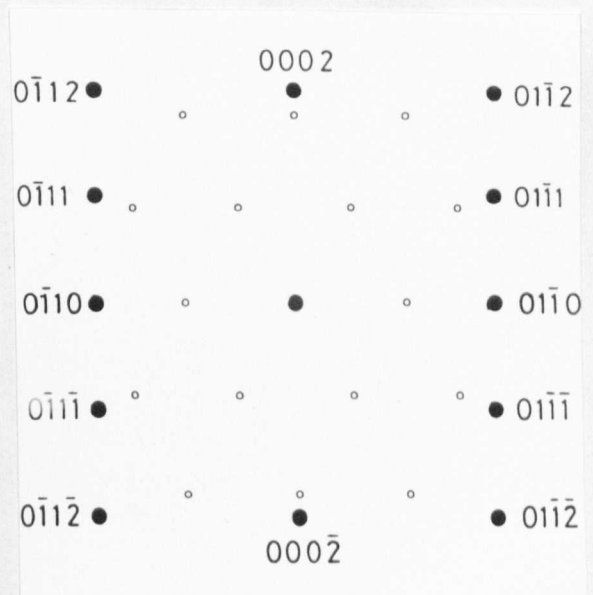
Figure 4.2 Schematic illustration of
 $[0001]_{Mg} \parallel [0001]_{\beta'hex}$
 pattern showing orientation relationship
 $[10\bar{1}0]_{Mg} \parallel [2\bar{1}\bar{1}0]_{\beta'hex}$
 $[2\bar{1}\bar{1}0]_{Mg} \parallel [10\bar{1}0]_{\beta'hex}$



(a)



(b)

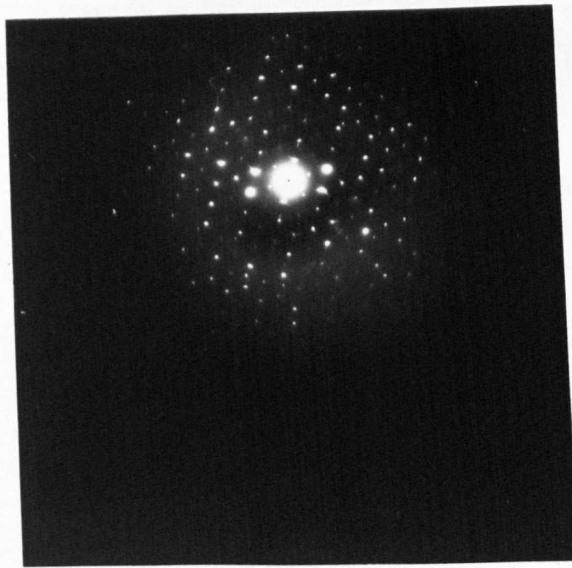


(c)

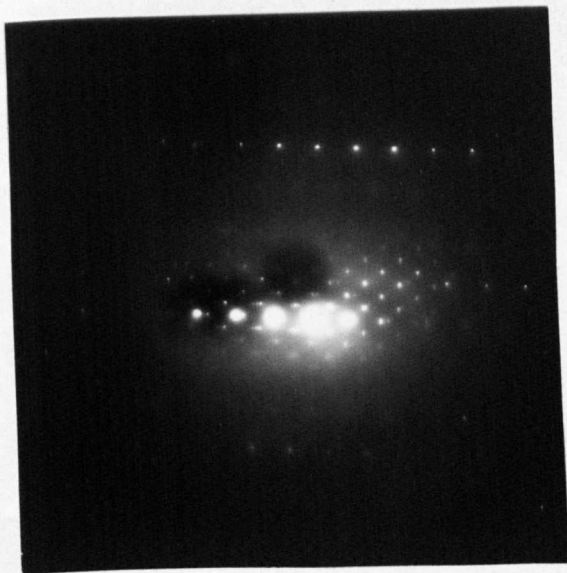
Figure 4.3 Mg-Th-Zr alloy aged 30 hrs at 330°C

- (a) β' hex precipitating on dislocations Mag 10,000 x
- (b) Diffraction of above showing $[2\bar{1}\bar{1}0]\text{Mg} \parallel [0001]\beta'$ hex
- (c) Schematic of above

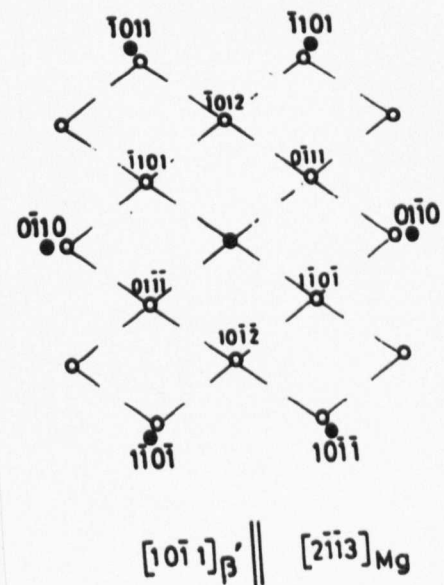
Text cut off in original



(a)



(b)

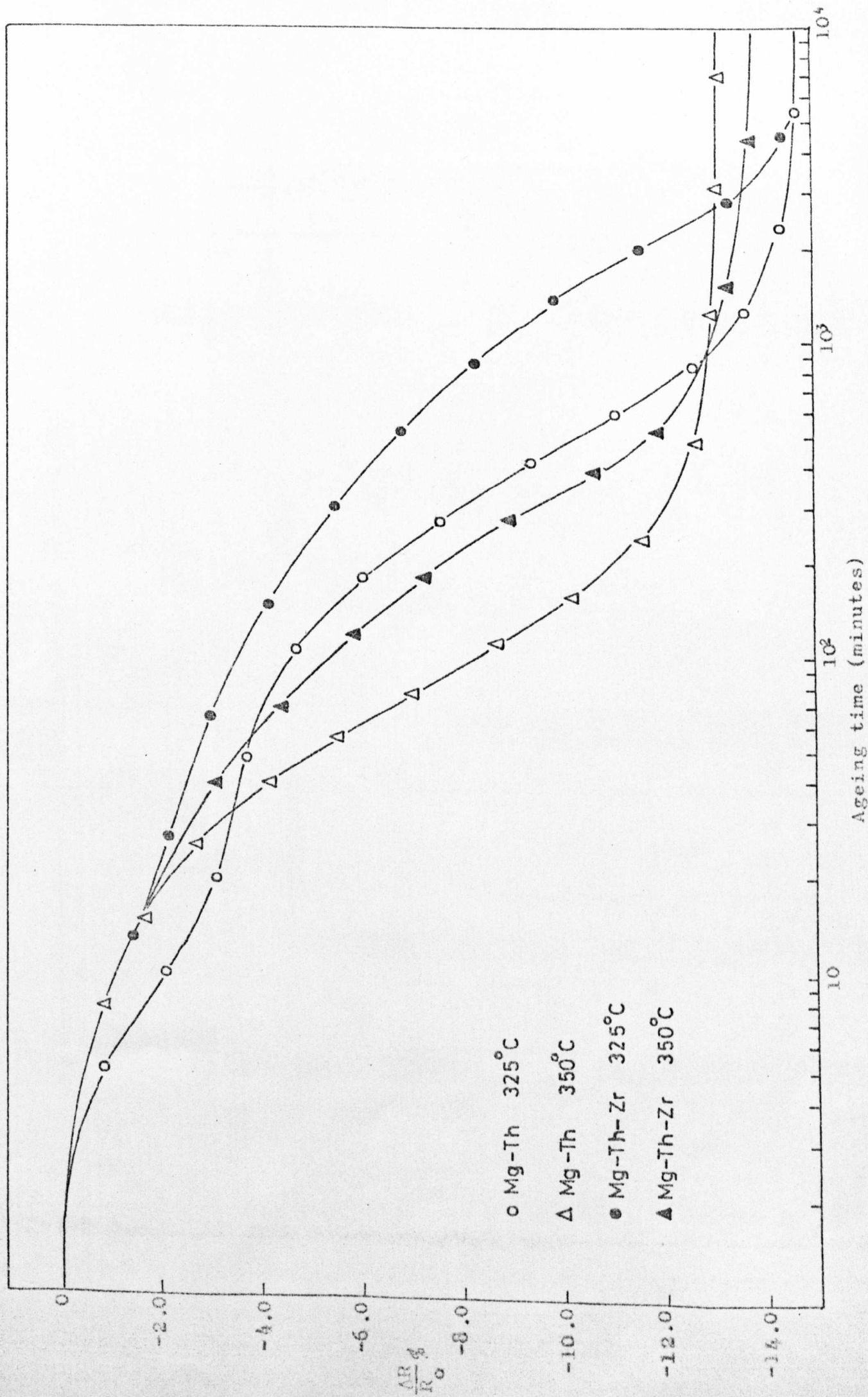


(c)

Figure 4.4 Mg-Th-Zr aged 24 hrs at 350°C

- (a) Electron diffraction pattern $[0001]$ zone axis β' hex showing continuous streaks in all $[10\bar{1}0]^*$ directions
- (b) Electron diffraction pattern showing $[2\bar{1}13]_{Mg} \parallel [10\bar{1}1]_{\beta'}$ hex discontinuous streaks in $[10\bar{1}1]^*$ directions
- (c) Schematic of (b)

Figure 4.5: Mg-Th and Mg-Th-Zr alloys: resistivity isotherms at 325 and 350°C



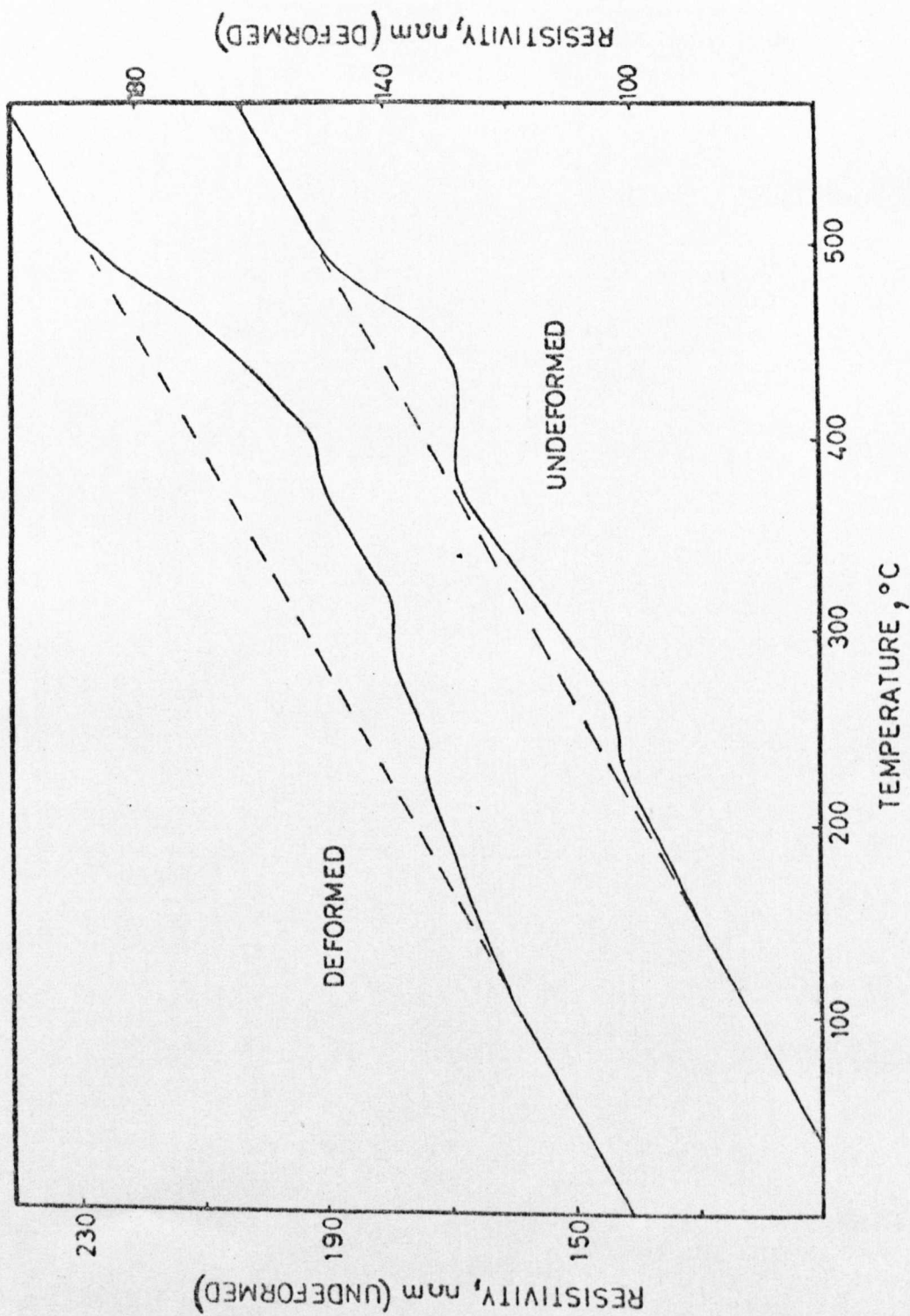
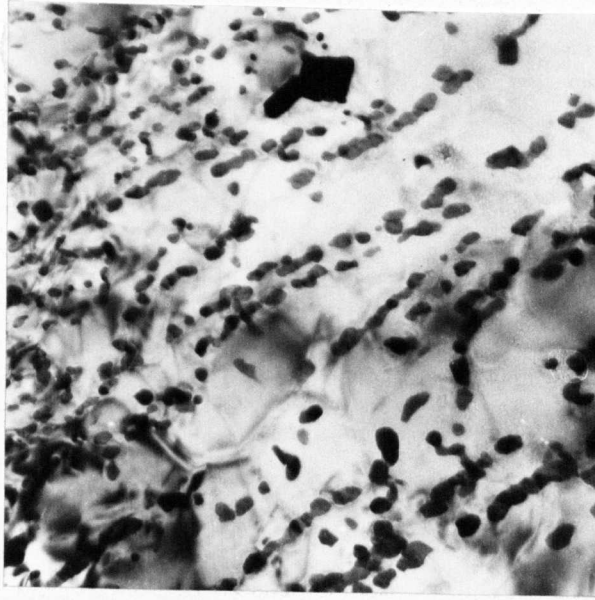
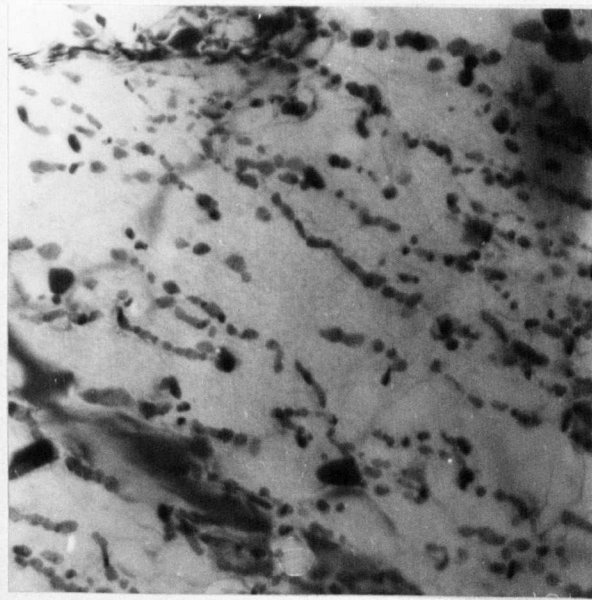


Fig.4.6 Continuous-heating electrical-resistivity curves for Mg-3wt.-% Th-0.7 wt.-% Zr alloy, showing effect of prior deformation (10%).



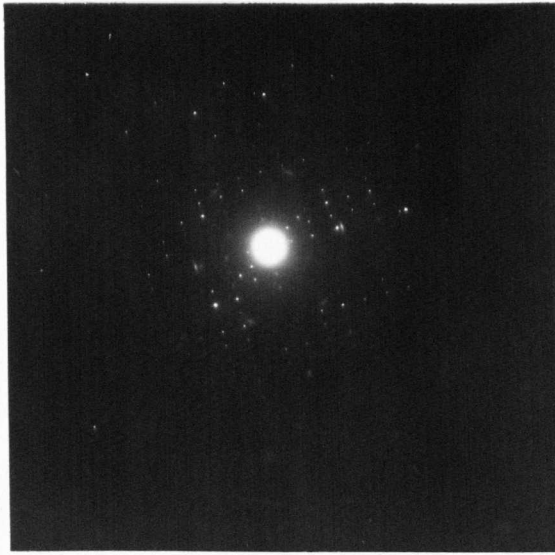
(a)



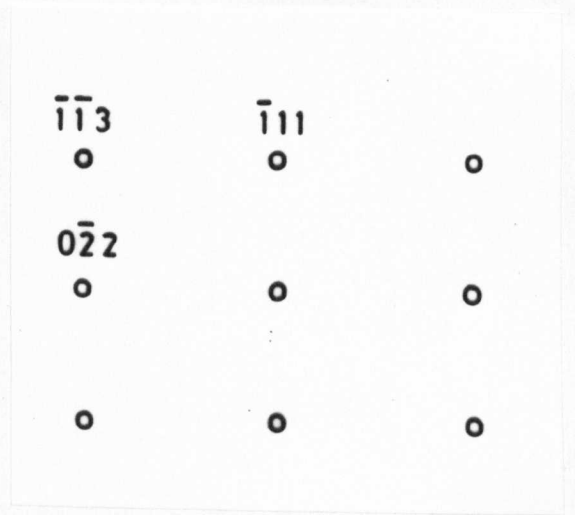
(b)

Figure 4.7

- (a) Mg-Th alloy deformed 10% before ageing 1 hr at 275°C
 β' hex precipitate on dislocations Mag 50,000 x
- (b) Mg-Th-Zr alloy deformed 10% before ageing 1 hr at 275°C
 β' hex precipitate on dislocations Mag 50,000 x



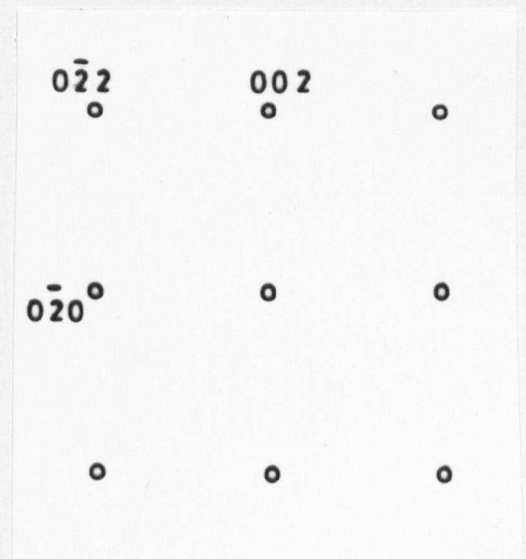
(a)



(b)



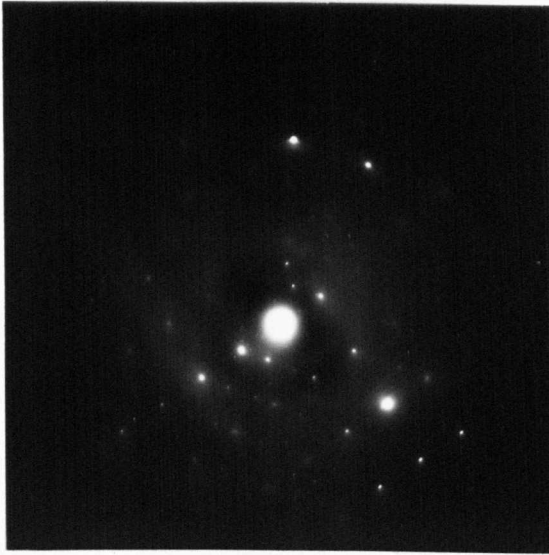
(c)



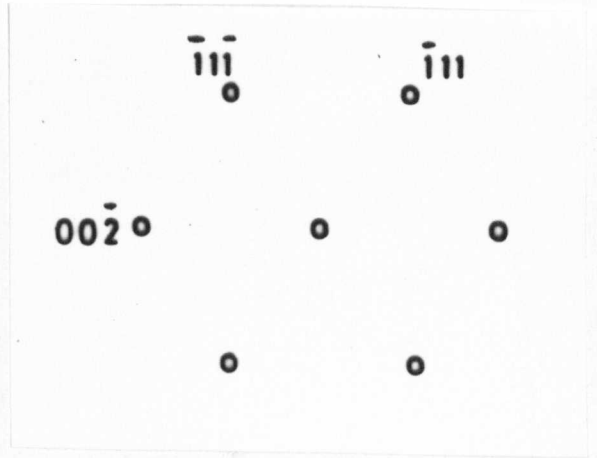
(d)

Figure 4.8 Mg-Th-Zr aged one day at 350°C

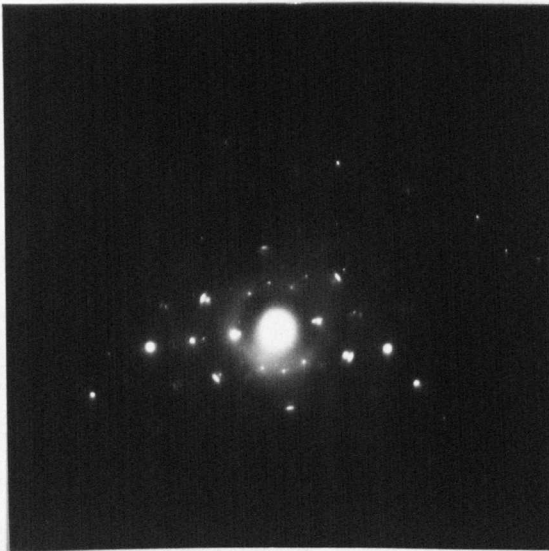
- (a) S.A.D. showing $[211]$ β zone axis
- (b) Schematic (a)
- (c) S.A.D. showing $[001]$ β zone axis
- (d) Schematic (c)



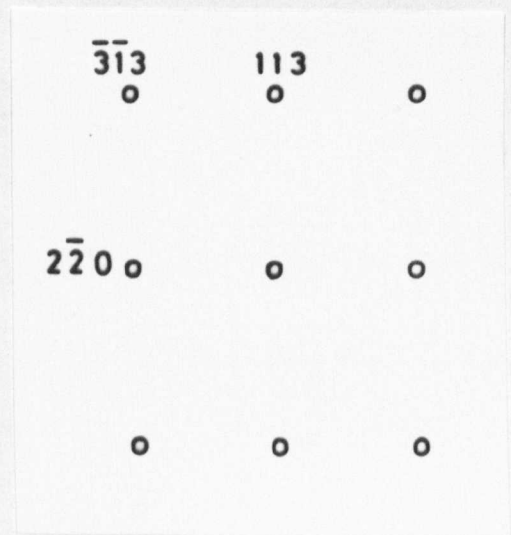
(a)



(b)



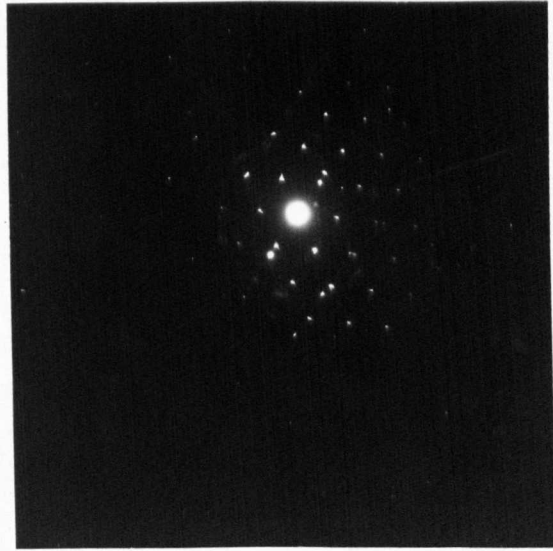
(c)



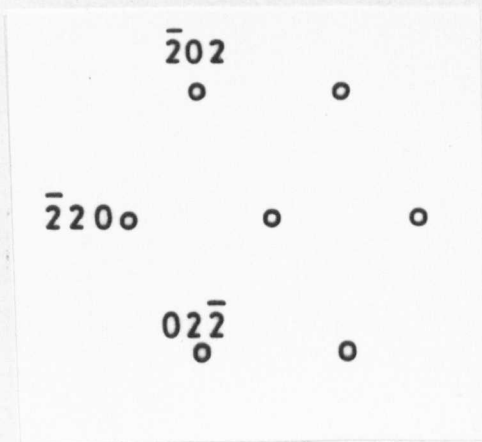
(d)

Figure 4.9 Mg-Th-Zr alloy aged 16 hrs at 330°C

- (a) Diffraction from rod-shaped particle $[110] \beta'$ cubic
- (b) Schematic (a)
- (c) Diffraction from rod-shaped particle $[3\bar{3}\bar{2}] \beta'$ cubic
- (d) Schematic (c).



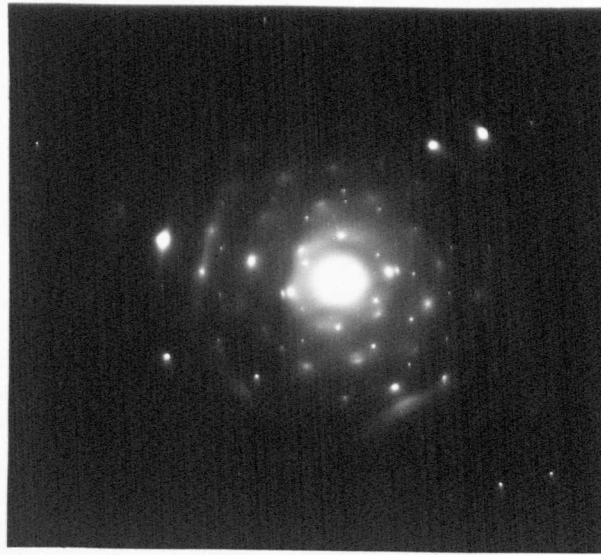
(e)



(f)

Figure 4.9 Mg-Th-Zr alloy aged 16 hrs at 330°C

- (e) Diffraction from rod-shaped particle $[111]$ β' cubic
- (f) Schematic (e)



(g)



(h)

Figure 4.9 Mg-Th-Zr alloy aged 16 hrs at 330°C.

(g) Diffraction from rod shaped particle $[114] \beta'$ cubic

(h) Schematic (g)

CHAPTER 5

THE Mg-Th SYSTEM: EFFECT OF Mn, Zn AND Ag ADDITIONS

The elevated temperature properties of Mg-Th alloys have been ^{referred to} in earlier chapters. These properties are enhanced by additions of other elements. In some cases the additions are small and their influence on mechanical properties may be due to a change in the size and distribution of the strengthening Mg-Th precipitates. Manganese and zinc, however, are frequently added in quantities that amount to several per cent and in this case the improvement in properties could reasonably be expected to be due to the precipitation of phases other than those present in the binary Mg-Th system. In the present investigation alloys containing both trace additions (0.1 at %) and larger ternary additions (~ 0.5 at %) of the elements zinc and manganese have been studied. Trace additions of silver have also been investigated.

5.1 Trace Additions of Zn, Ag and Mn

Electrical resistivity experiments carried out on a Mg-Th alloy containing 0.1 at % additions of Zn, Mn or Ag showed that the kinetics of precipitation were only markedly altered by the presence of zinc (Figures 5.1, 5.2 and 5.3).

All the curves were analysed according to the Johnson-Mehl equation in which fraction transformed, y , after time t is given by

$$y = \frac{R_o - R_t}{R_o - R_F} = 1 - \exp\left[\left(-\frac{t}{\tau}\right)^m\right]. \quad (5.1)$$

Rearrangement leads to:

$$\log_{10} \log_{10} \frac{(R_o - R_t)}{(R_t - R_F)} = m \log_{10} t - \log_{10} \tau - \log_{10} 2.305 \quad (5.2)$$

where m and τ are the equation constants. The resulting time exponents m were determined from plots of

$$\log_{10} \log_{10} \frac{R_o - R_t}{R_t - R_F} \text{ vs. } \log t \text{ and found to lie in the range}$$

0.3 - 0.5 for alloys aged at 150°C and, excluding the zinc containing alloy, for alloys aged at 250°C and 350°C time exponents were 1.5 ± 0.1 and 1.0 ± 0.1 respectively.

These values correspond well with the values found by Noble and Crook [61] in their study of the binary alloy. The value of $m = 1.5$ can be associated with diffusion controlled growth and the value $m = 1.0$ can be associated with dislocation nucleation.

The alloy containing zinc, however, when aged at 250°C was seen to be completely different to the other alloys. Analysis according to equation(5.1) gave a linear log log y vs. $\log t$ from which a time exponent of

0.4 was calculated, similar to that obtained for all alloys at 150°C. The 350°C isotherm for the alloy containing zinc shows a time exponent of 0.8. However, ageing at this temperature produces extended dislocations in addition to the β Mg₂Th₆ precipitate and it is to be expected that this dissociation process would make a significant contribution to the resistivity of the alloy and so affect the kinetic analysis of the alloy.

Electron microscope observations showed the precipitation behaviour in the silver and manganese bearing alloy to be identical to that of the binary alloy. In all alloys including the binary alloy aged at temperatures < 150°C no structural changes could be detected in spite of the substantial resistivity decrease that occurs at this ageing temperature. The resistivity decrease is too large to be explained in terms of vacancy annealing but can be explained by assuming some type of atomic rearrangement is taking place, possibly short range order, which would lead to a resistivity drop, but would give little or no diffraction evidence.

At higher ageing temperatures the β'' (DO₁₉) phase was found in all alloys except the zinc bearing system; the number densities ($\sim 10^{22}/\text{m}^3$) of the β'' were similar to the binary alloy. In the zinc containing alloy, in spite of long ageing treatments at 250°C and 275°C, no evidence of the β'' phase could be found. The only precipitate found

in this latter alloy was β , $Mg_{23}Th_6$ which formed at temperatures of $300^{\circ}C$ and above. The β formation in the Mg-Th-Zn alloy was accompanied by stacking fault type defects (Figure 5.3a) These have been extensively studied [66] and shown to be extended dislocations bounded by $\frac{1}{3} \langle 10\bar{1}0 \rangle$ partial dislocations.

5.2 Precipitation in the Mg-Th-Mn System

Magnesium-thorium alloys with manganese additions are used commercially, a typical composition being Mg 2.0% Th 1.0% Mn (HM 21). At the start of this investigation very little work had been reported in the literature on the precipitation behaviour of this alloy. However, during the course of the present study a paper by Stratford and Beckley [62] was published on the structural characteristics of the HM 21 alloy. The present work merely confirms their findings and therefore a brief study of the structural and ageing characteristics will be presented here.

Ageing at $350^{\circ}C$ produces a phase which is not present in the precipitation sequence of the binary alloy (Figure 5.4). Trace analysis showed the precipitate to be of the form of discs on (0001) Mg. Diffraction patterns taken from areas containing this precipitate showed it to be a highly ordered hexagonal structure with

lattice parameters $c = 3.12$ nm, $a = 0.556$ nm. The orientation relationship from the pattern in Figure 5.5(a) is seen to be

$$\begin{aligned} (0001) \text{ ppt} & \parallel (0001) \text{ Mg} \\ (11\bar{2}0) \text{ ppt} & \parallel (10\bar{1}0) \text{ Mg}. \end{aligned}$$

This structure proved to be extremely stable, being present in foils aged 48 hours at 400°C . Continued ageing at this and higher temperatures produced a microstructure as seen in Figure 5.6. Some of the particles were identified as $\beta \text{ Mg}_{23}\text{Th}_8$ and others were assumed to be $\text{Mn}_{23}\text{Th}_8$. Positive confirmation of the latter was not possible as the thickness of most of the particles made it impossible to achieve good diffraction conditions.

5.3 Precipitation in the Mg-Th-Zn System

Additions of up to 2% Zn improve the creep properties of Mg-Th alloys [118]. This improvement is dependent on the Th/Zn ratio and is thought to be due to a grain boundary precipitate which is present in the cast alloys [119]. Yamamoto, Klimek and Rostoker [120] in a detailed study of the Mg-Th-Zn system, detected a phase not present in either the systems Mg-Th or Mg-Zn, which they designated θ . This phase was found in alloys containing large amounts of thorium and zinc and the structure was

determined as hexagonal with lattice parameters $c = 0.702$ nm, $a = 0.436$ nm, $c/a = 1.61$. Crook, in a later study [115], did not detect the θ precipitate, but found evidence of another phase, designated γ'' , in a 3.0% Th 2.0% Zn alloy. This precipitate was found to have the unusual habit plane $\{20\bar{2}5\}$; the structure of the precipitate was not determined. In view of the mechanical property enhancement produced by zinc additions to Mg-Th alloys, it was felt worthwhile to examine the alloy to determine the cause of the improvement and, if possible, to develop the optimum ageing conditions for peak properties.

Alloys were prepared with Zn/Th (weight) ratios between 0.67 and 2.67. Electron microscopy did not reveal the θ or the γ'' phases in any of the alloys; the only precipitate identified by electron diffraction was β , $Mg_{23}Th_6$. Solution treatment of these alloys had been carried out by immersing the specimen in a mixture of dichromate salts. Since commercial practice often uses an SO_2 protective atmosphere for heat treatment, and since it was known also that Crook [115] had used this type of atmosphere for the heat treatment of some of his alloys, it was decided to repeat the electron microscopy of the alloys using this type of protective atmosphere. Again, no θ phase was detected but the γ'' was found in these samples (Figure 5.7). Due to the very fine nature

of the precipitate, no diffraction evidence was obtained from the precipitate, but presumably it forms by diffusion of sulphur into the alloy, which reacts with the zinc to produce the finely dispersed phase.

Solution treatment of the alloy in dichromate salts produced a material completely free of second phase except after high temperature ageing when the β phase was precipitated. The action of zinc in improving the creep properties of the Mg-Th system appears therefore to be one of keeping the thorium in solid solution.

5.4 Discussion

The trace element additions to the system Mg-Th appear to have little or no effect on the precipitation sequence with the exception of zinc. An addition of 0.1 at % Zn ~ 0.25 at % completely suppressed the β reaction and extended the "low temperature reaction" up to 250°C. In Mg-Th it has been suggested that the resistivity drop on low temperature ageing is due to short-range ordering taking place. This phenomenon has been noted in Mg-Pb alloys where it also precedes the formation of a highly ordered, DO_{19} precipitate. The fact that the rate of the low temperature reaction, as measured by the resistivity technique, is unaffected by the addition of zinc appears to show that the zinc atoms

are not associating with quenched-in vacancies. It is possible that the ordering reaction involves zinc atoms and that a relatively stable short range ordered structure is formed containing both thorium and zinc atoms. The relative sizes of the atoms involved appear to favour this as the zinc atom is $\sim 12\%$ smaller than magnesium and the thorium atom is $\sim 13\%$ larger.

The phase formed initially in the Mg-Th alloy containing large additions of manganese is quite different from those formed in the binary Mg-Th systems. The highly ordered structure precipitates as discs on the Mg (0001) with $c = 3.16$ nm and $a = 0.556$ nm $c/a = 5.68$. The c parameter is $6 \times c_{\text{Mg}}$ and the a parameter $\sqrt{3} \times a_{\text{Mg}}$. The structure and orientation relationship confirm that reported by Stratford and Beckley [62] in a study of the HM 21 alloy. They considered that the phase forms by the introduction of manganese atoms into the $\text{Mg}_3\text{Th DO}_{19}$ structure with ordering to produce the large c spacing. The composition of the compound would then be $\text{Mg}_3(\text{ThMn})$. The precipitate has remarkable temperature stability; the phase was still found in samples aged 48 hours at 400°C . The stability of this phase undoubtedly contributes to the good high temperature strength of this alloy.

In the system Mg-Th-Zn the effect of zinc appears to be to keep the thorium in solid solution and the

improvement in creep properties could possibly be due to a solid solution strengthening effect. However, the alloys studied in the present investigation have been worked and homogenised, unlike the commercial alloy, which is generally used in the cast state. In this condition a grain boundary precipitate is formed [118] which has not been found in the present study and is possibly the θ phase detected by Yamamoto et al. [120]. Further work is necessary on both the microscopy of the cast alloy and the creep properties of both homogenised and cast alloys before the true effect of zinc can be determined.

Figure 5.1: Mg-Th ternary alloys
resistivity isotherms 150°C

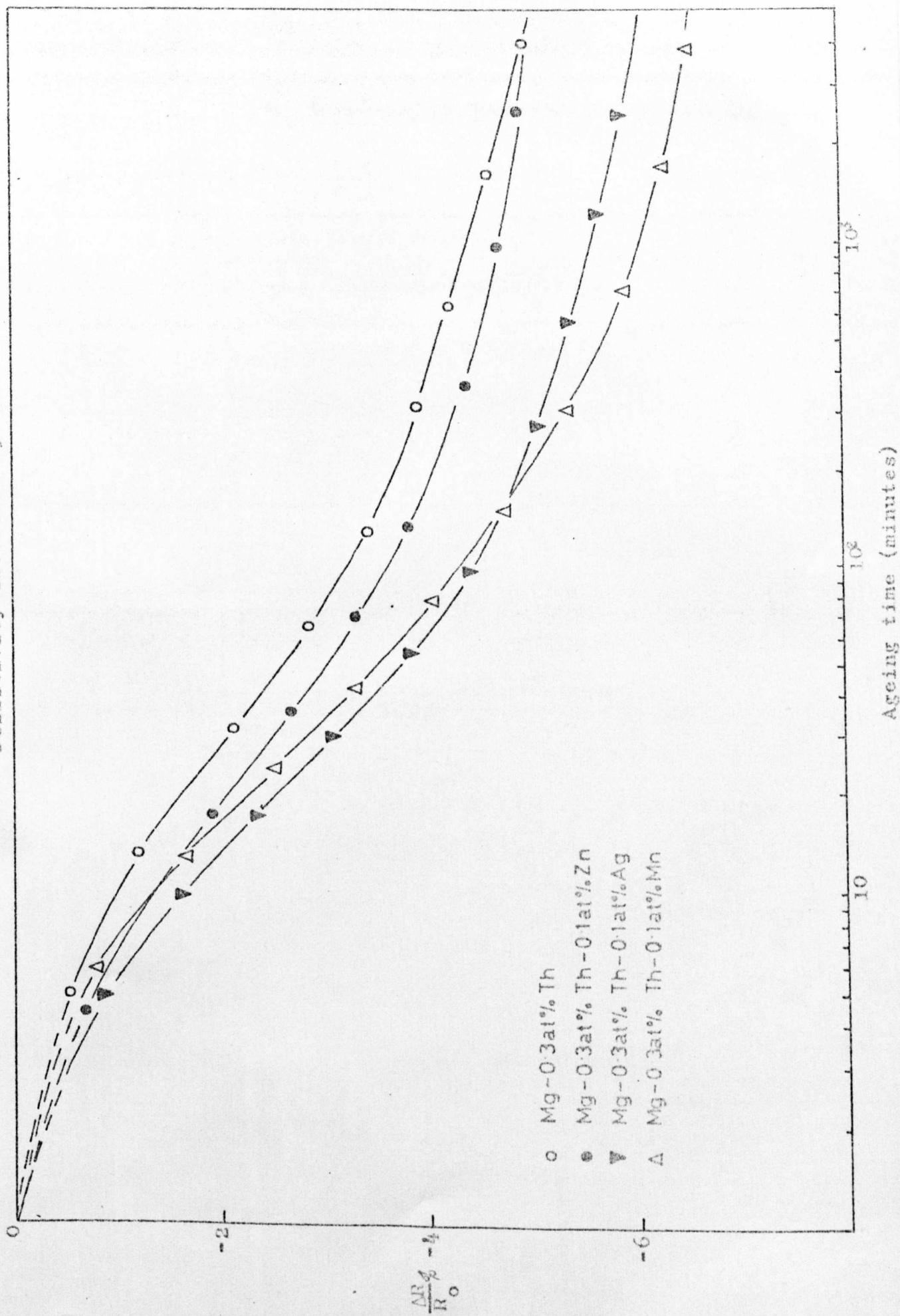


Figure 5.2: Mg-Th ternary alloys resistivity isotherms 250°C

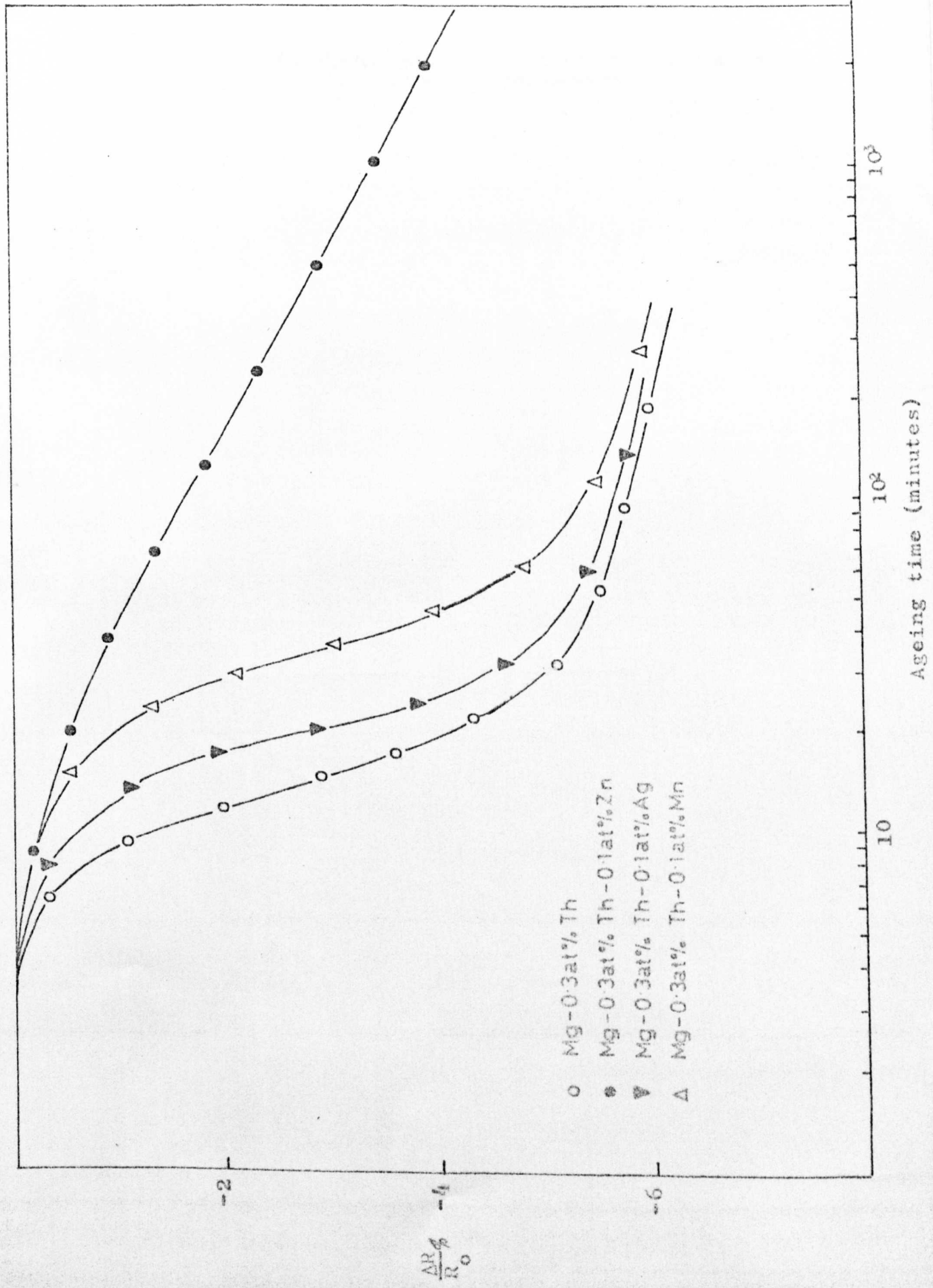
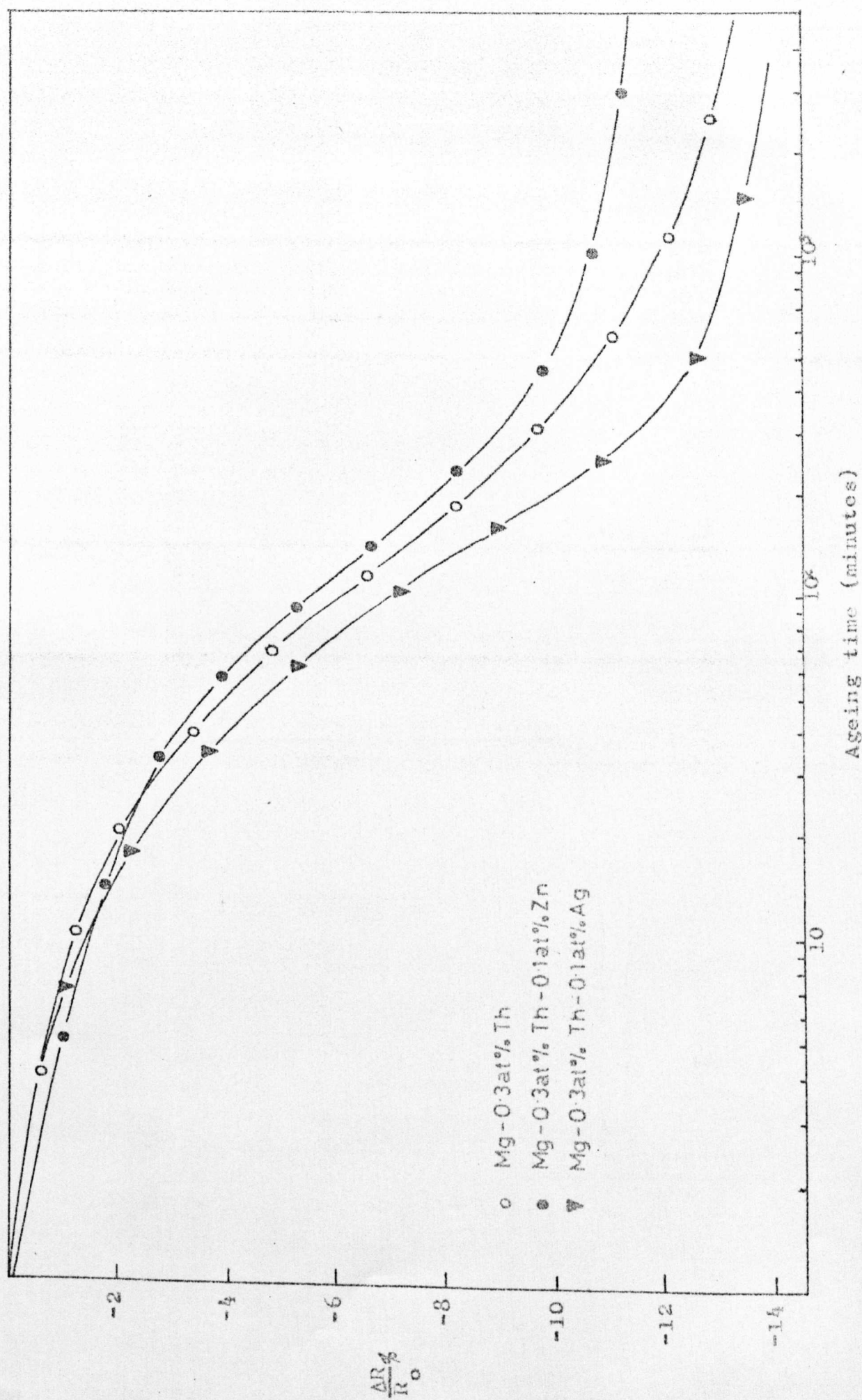
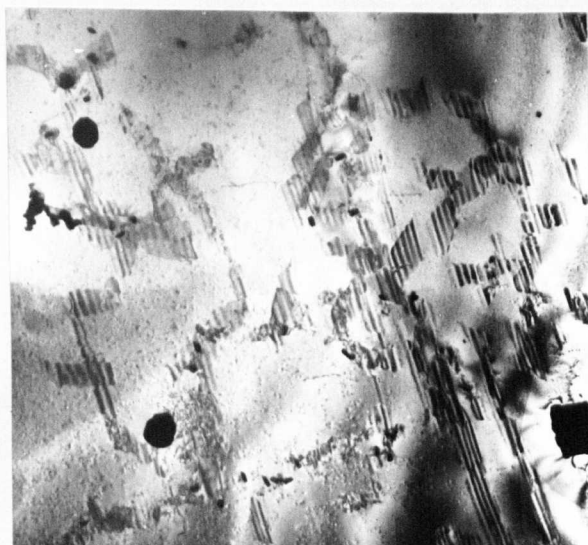


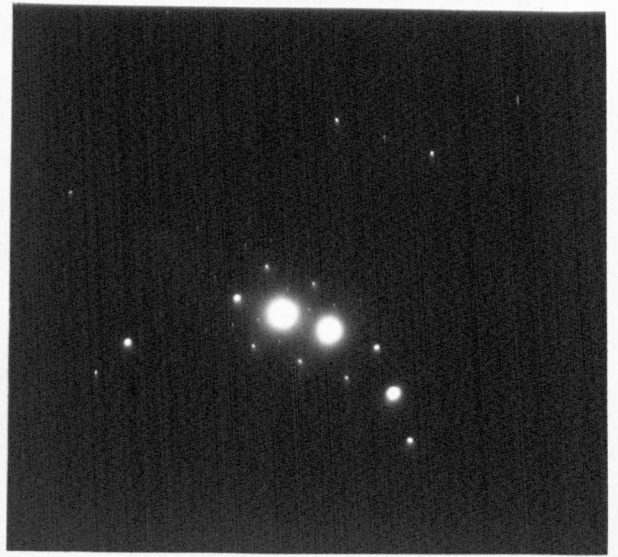
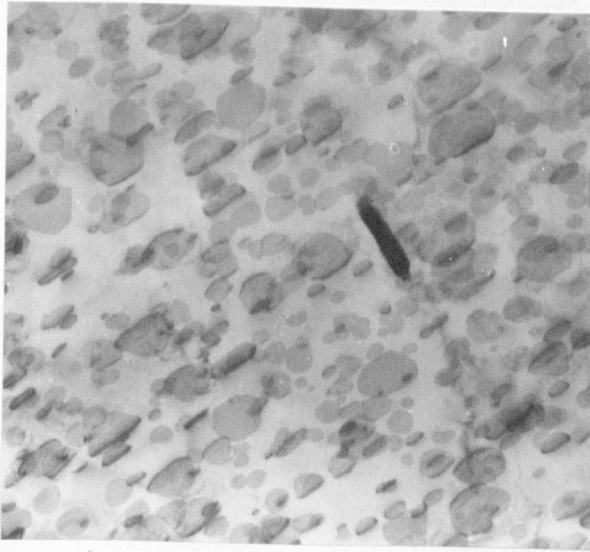
Figure 5.3: Mg-Th ternary alloys
resistivity isotherms 350°C





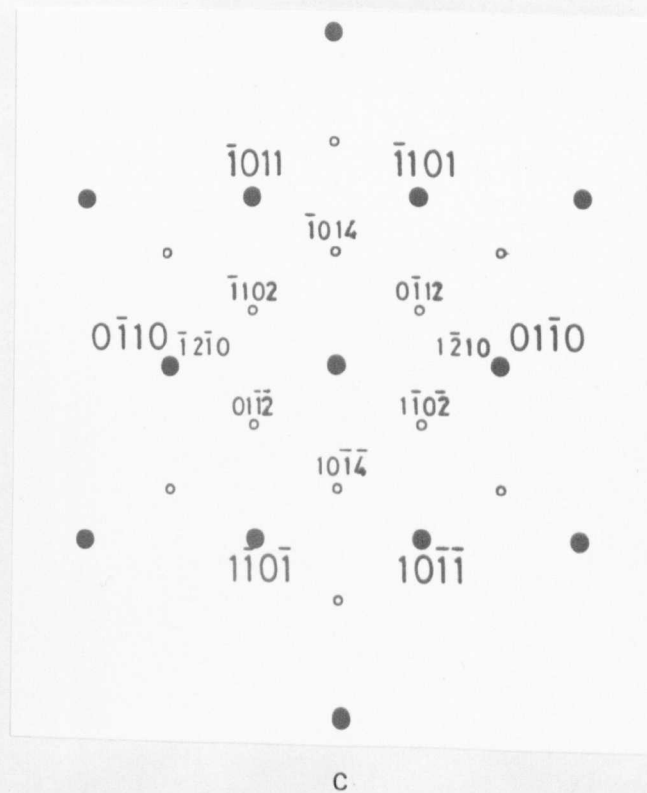
Mg-Th-Zn

Figure 5.3(a) Mg 3.0% Th 0.25% Zn aged 3 hrs at 350°C
showing stacking faults Mag 40,000 x



(a)

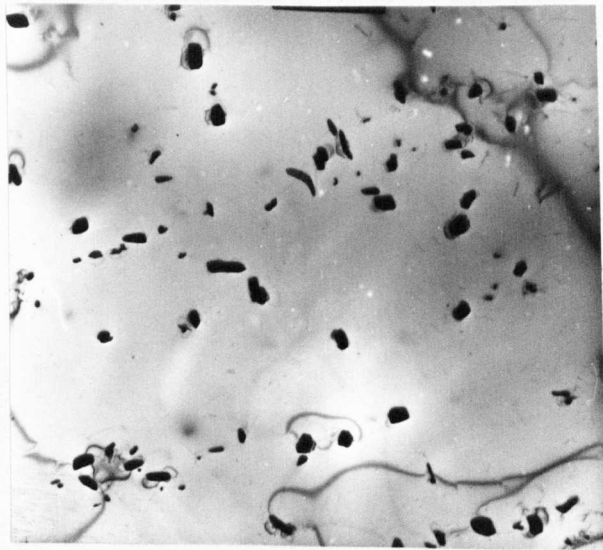
(b)



Mg-Th-Mn

Figure 5.4 Mg 3.0% Th 2.0% Mn

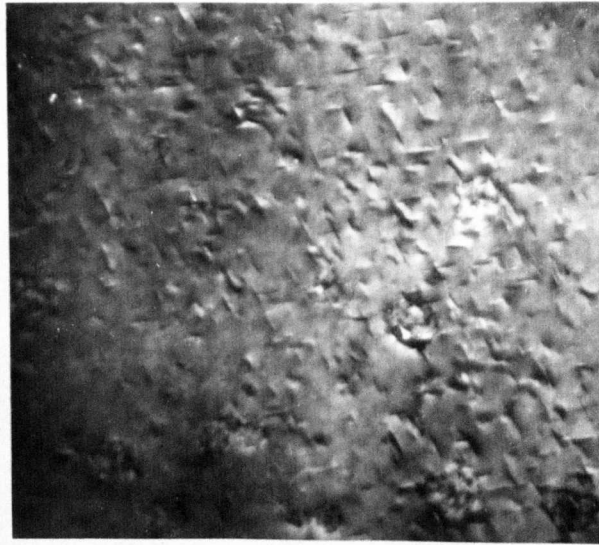
- (a) Aged 100 hrs at 350°C Mag 20,000 X
- (b) Diffraction above $[2\bar{1}\bar{1}3]$ Mg \parallel $[20\bar{2}1]$ ppt
- (c) Schematic (b)



Mg-Th-Mn

Figure 5.6 Aged 48 hrs at 450°C

Mag 10,000 x



Mg-Th-Zn

Figure 5.7 Mg 3.0% Th 2.0% Zn
Heat treated in SO₂ and aged 24 hrs at 350°C
Mag 40,000 x

CHAPTER 6

THE Mg-Nd SYSTEM:

EFFECT OF ZINC ADDITIONS ON MICROSTRUCTURE

The addition of zinc to magnesium-neodymium alloys has been claimed [121] to have a beneficial effect on the creep properties. However, little systematic work has been done on the creep properties of this alloy system and no work has been published on the reasons for the improvement of the creep properties. In this and the following chapters Mg-Nd-Zn alloys of various concentrations have been studied and the creep properties correlated with the microstructure of the alloys.

6.1 Preliminary Investigations

A Mg 2.8% Nd 1.35% Zn alloy was chosen for the initial investigation. This alloy contains equiatomic proportions of zinc and neodymium and is near to the composition of the commercial alloy.

A general survey of the precipitation behaviour of the alloy was determined by heating a solution-treated specimen at a rate of 1°C/min and continuously measuring the changes in resistivity. The resulting curve of resistivity vs temperature is shown in Figure 6.1.

Deviations from the interpolated solid solution line occur in the range $80^{\circ}\text{C} - 480^{\circ}\text{C}$. It is convenient to divide the deviation into three separate regions

- (i) low temperature processes (up to 200°C)
- (ii) medium temperature processes ($200^{\circ}\text{C} - 250^{\circ}\text{C}$)
- (iii) high temperature processes ($250^{\circ}\text{C} - 480^{\circ}\text{C}$).

It should be noted that the temperature ranges indicated above for the three precipitation ranges are expected to exceed the corresponding limits found during isothermal experiments since non-equilibrium conditions existing during continuous heating should cause a hysteresis effect. However, the continuous heating curve does provide information on which to base isothermal experiments; these will now be described.

6.2 Low Temperature Processes

Resistivity isotherms at temperatures between 50°C and 150°C are shown in Figure 6.2. The curves approximate to the typical sigmoidal reaction curves but show no distinct induction periods, in fact the 125°C and 150°C isotherms indicate a substantial amount of the transformation is over by the time measurements could be taken, i.e. approximately 4 to 5 minutes from the commencement of ageing. However, the remaining isotherms

were sufficiently complete to be analysed in terms of equation 5.1. Linear plots resulted from the data obtained and these are shown in Figure 6.3. The time exponent in all cases is 0.5 ± 0.05 . To examine the nature of the reaction foils were aged at 100°C for 24 hours, this being the time required for completion of the reaction as indicated by the kinetic curve, and examined in the electron microscope. No evidence of any precipitation reaction was found either by direct observation or by electron diffraction. Representative electron diffraction patterns are shown in Figure 6.4.

The fact that a substantial resistivity drop ($\sim 4\%$) was observed, however, indicates that some form of atomic re-arrangement is taking place. Resistivity changes of comparable magnitude have been detected during the low temperature ageing of other magnesium based alloy systems and have been attributed to the formation of regions of short range order [61].

6.3 Medium Temperature Processes

The resistivity isotherms for ageing temperatures 200°C , 225°C and 250°C are shown in Figure 6.5. At all three temperatures the curves can be seen to be the sum of at least two precipitation reactions. The 200°C curve is the sum of three reactions, a part of the initial drop

being due to the low temperature mechanism previously discussed. In this section, however, only the first reaction is considered.

This reaction gave a drop of approximately 12% and the kinetics of the reaction became appreciably faster with the increase in ageing temperature, until at 250°C the reaction was complete after approximately 30 minutes. For the analysis according to equation 5.1 only the first part of the curve was used, the second transformation being dealt with in the following section. The data fitted this equation well and time exponents of 1.5 ± 0.1 were determined for all three curves. The analysis of the three curves is shown in Figure 6.6.

Specimens were prepared for microscopy after ageing for a time that corresponded to completion of the reaction. The resulting structure after 35 minutes at 300°C is shown in Figure 6.7. The accompanying diffraction pattern shows that the precipitate is highly coherent with the matrix. It proved very easy to obtain diffraction patterns from the precipitate and examples of patterns are shown in Figures 6.8 and 6.9 with schematic diagrams. Trace analysis showed that the morphology of the precipitate, which has been designated γ'' , was that of discs on $\{0001\}$ Mg. The precipitate proved to be very thin in the $[0001]$ direction and this gave rise to relrods in the $[0001]^*$ direction in diffraction patterns with $[10\bar{1}0]$ and $[2\bar{1}\bar{1}0]$

zone axes. These $[0001]^*$ relrods passed through all magnesium relpoints and through positions one-third of the distance between spots in $[1\bar{2}10]^*$. By ageing at 325°C for one hour the precipitate was able to be coarsened sufficiently to give rise to diffractions, which appear as maxima in the streaks (Figure 6.8 b). From this data the structure of the precipitate was determined to be hexagonal $c = 1.56 \text{ nm}$, $a = 0.55 \text{ nm}$, $c/a = 2.81 \text{ nm}$. Diffraction patterns from $[30\bar{3}2]$, $[5\bar{1}\bar{4}3]$ and $[10\bar{1}2]$ magnesium zone axes, however, contain non-matrix reflections which cannot be explained in terms of the structure proposed. The reflections, however, can be explained in terms of relrod intersections with the Ewald sphere. Figure 6.10 shows a portion of the reciprocal lattice of magnesium together with the $[0001]^*$ relrods from the γ'' structure. The section shown represents the $[30\bar{3}2]$ zone axis and for the sake of clarity the relrods have been terminated in the diffraction plane. The finite thickness of the Ewald sphere in the diffraction plane leads to the intersection of the relrods and the diffraction plane leaving short streaks on the diffraction pattern elongated in the $[\bar{1}013]^*$ direction. The pattern from $[30\bar{3}2]$, together with the schematic illustration, is shown in Figure 6.11. The patterns from $[10\bar{1}2]$ and $[5\bar{1}\bar{4}3]$ can be explained in a similar manner. Of course the relrods give streaks on

patterns from all zone axes except $[0001]$ Mg, where the intersection is at 90° . However, this does not lead to an uncertainty in determining the structure since true precipitate spots have been observed in prism orientation and this, together with the basal pattern, allows a unique solution to the structure.

The orientation relationship of the precipitate with the matrix is

$$\begin{aligned} [0001] \text{ Mg} & \parallel [0001] \gamma'' \\ [\bar{1}0\bar{1}0] \text{ Mg} & \parallel [2\bar{1}\bar{1}0] \gamma''. \end{aligned}$$

This relationship is demonstrated in Figure 6.7(c). All the patterns proved to be consistent with this orientation relationship and a stereogram showing common magnesium/precipitate zone axes is shown in Figure 6.13.

6.4 High Temperature Processes

The high temperature precipitating phase has been found to form at temperatures above 200°C and has been designated γ .

The two stage isotherms for the formation of γ from γ'' have been shown in the previous section (Figure 6.5) and the curves for ageing temperatures of $275^\circ\text{C} - 350^\circ\text{C}$ are shown in Figure 6.14. These curves again show the typical characteristics of nucleation and growth reaction

and the analysis of the curves is shown in Figure 6.15. The values of the time exponent n decreased from 1.4 to 1.0 at ageing temperatures in the range $250^{\circ}\text{C} - 350^{\circ}\text{C}$.

Electron microscopy revealed the structure shown in Figure 6.16 after ageing for 3 hours at 325°C , i.e. ageing conditions for the completion of the γ reaction. The grain shown is in $[0001]$ orientation and the γ phase is seen to have six traces, 60° apart in all $\langle 10\bar{1}0 \rangle$ and $\langle 2\bar{1}\bar{1}0 \rangle$ directions. Further microscopy and trace analysis showed the γ phase to have a morphology of rods lying on the basal plane with the long directions in $\langle 10\bar{1}0 \rangle$ and $\langle 2\bar{1}\bar{1}0 \rangle$ directions.

Diffraction patterns taken in various orientations were solved in terms of a f.c.c. structure with $a_0 = 0.72 \text{ nm}$. The orientation relationship was determined as

$$\begin{aligned} [0001] \text{ Mg} & \parallel [220] \gamma \\ [2\bar{1}\bar{1}0] \text{ Mg} & \parallel [111] \gamma \\ [10\bar{1}0] \text{ Mg} & \parallel [211] \gamma. \end{aligned}$$

Diffraction patterns, together with schematic illustrations, are shown in Figure 6.18. From the schematics of the $[10\bar{1}0]$ and $[2\bar{1}\bar{1}0]$ patterns the reason for the development of two growth directions can be seen. The diffraction patterns show that $5d(11\bar{2}0)\text{Mg} = 2d(111)\gamma$ and $d(10\bar{1}0)\text{Mg} \simeq d(112)\gamma$. The good matching between these planes enables the precipitate to grow with the minimum

of strain energy.

The lattice parameter for the γ phase was calculated from several precipitate cross grating patterns which were not closely related to that of the matrix, e.g. the [001] zone axis pattern shown in Figure 6.18(a). From this parameter the misfits for the two situations $(111) \gamma \parallel (11\bar{2}0) \text{Mg}$ and $(112) \gamma \parallel (10\bar{1}0) \text{Mg}$ were calculated. The misfits proved to be 3.5% and 5.9% respectively but the diffraction evidence outlined earlier indicates that in the former case, at least, this misfit is accommodated by elastic strains.

Precipitation of the γ phase was seen to occur on dislocations at all temperatures above 250°C. Nucleation of precipitates on dislocations takes place due to the relief of strain energy by the interaction of strain fields of precipitate and dislocation. This can only occur if the Burgers vector \underline{b} is not normal to the misfit vector \underline{R} of the precipitate, i.e. $\underline{b} \cdot \underline{R} \neq 0$. The misfit vector may be defined as the direction in which the matrix planes close to the precipitate suffer the greatest elastic displacements. This occurs for plate precipitates such that \underline{R} is perpendicular to the plane of the plate and for rod shaped precipitates such that \underline{R} cannot be uniquely defined but occurs in all directions in a plane perpendicular to the axis of the rod.

In magnesium the commonest stable dislocations are

the $\frac{1}{3}\langle 11\bar{2}0 \rangle$ type, whose slip plane is (0001); all six habits of the γ phase occur such that the axes of their rods lie in the basal plane. The $\underline{b} \cdot \underline{R} \neq 0$ condition for any particular Burgers vector (e.g. $\frac{1}{3}[11\bar{2}0]$) is fulfilled by only five out of the possible six habits of the γ precipitate, since for the remaining one (the rod whose long axis is $[11\bar{2}0]$) \underline{R} is always normal to \underline{b} . Thus up to five habits of γ could be expected to occur on any one dislocation; all observations of precipitation of γ on dislocations were in accordance with this observation. The situation is analagous to that in Al-Cu [1], where θ' nucleates on two of a possible three habits on any $\frac{a}{2}\langle 110 \rangle$ type dislocation.

6.5 Discussion

The resistivity results presented in the earlier sections may be analysed to yield the reaction activation energies. The temperature dependence of the reaction kinetics usually obeys an equation of the Arrhenius type:

$$K' = A \exp - \left(\frac{Q}{kT} \right) \quad (6.1)$$

where K' is the rate constant, kT is the thermal energy, A is a frequency factor and Q is the empirical activation energy. Provided the rate constant K' is the only

temperature dependent term in the empirical rate equation representing the reaction, k' is proportional to ty^{-1} , [122], where ty is the time required for a fixed amount of transformation X .

Therefore:

$$ty \propto A^{-1} \exp\left(\frac{Q}{kT}\right)$$

or

$$\log_{10} ty = \text{constant} - \log_{10} A + \frac{Q}{2.303kT} \quad (5.2)$$

and a linear relationship should exist between $\log_{10} ty$ and T^{-1} , the gradient of which should be $\frac{Q}{2.303k}$.

Figure 6.19 shows that such a relationship does exist for the kinetic curves presented in the previous sections. The curves have been plotted on the basis of ty being equal to the time to 50% transformation ($t_{0.5}$). Uncertainty does exist, however, in assigning $t_{0.5}$ values to many of those curves which have a very short incubation period. In these cases a considerable part of the reaction may be over before readings can be taken. These curves have been extrapolated back to zero time assuming a total resistance change equal to that shown by transformation curves for the same phase, but at lower temperatures where a longer incubation time exists, so that none of the reaction is missed.

Uncertainty also exists in the kinetic analysis of

those curves that show two distinct reactions. Here the time for 50% transformation is taken from the first curve in the normal way and the second is extrapolated back to a "false zero" on the resistance scale. The $t_{0.5}$ value is then taken as the 50% transformation from the false zero reading to the completion of the reaction. To illustrate this technique the 225°C isotherm (Figure 6.5) shows two distinct resistance drops. The first part of the curve, giving a drop of approximately 12%, is caused by precipitation of the γ'' phase. This reaction gives a value for $t_{0.5}$ of 100 minutes. The second reaction due to the γ phase causes a further drop of 6%, giving a $t_{0.5}$ value of 2,000 minutes.

In this way the results reported can be interpreted, as shown in Figure 6.19, where part of three curves representing the low temperature reaction, the γ'' reaction and the γ reaction are shown. The lower temperature portions of each curve are linear and from the gradients the following activation energies were obtained.

	KJ/mol	eV/atom
Low temperature reaction	82	0.85
γ''	147	1.53
γ	132	1.37

The values for the γ'' and γ phases are similar to the value quoted in the literature for the self diffusion of

magnesium; 134 KJ/mol (1.39 eV/atom). This indicates that the precipitation reactions for these two phases are rate-controlled by solute atoms diffusing to the growing nuclei. The low temperature reaction, however, is governed by a much smaller activation energy and it seems likely that this can be associated with the value of 48 KJ/mol (0.5 eV/atom) [123] for vacancy migration in magnesium. The rather high value for the activation energy may be explained assuming a binding energy of approximately 0.3 eV/atom between a neodymium atom and a vacancy. This is similar to the typical solute-vacancy binding energies found in aluminium alloys.

The analysis of the resistivity data yields values for n , the time exponent, of 0.5, 1.5 and 1.4/1.0 for the low temperature reaction, γ'' and γ phases respectively.

The value of 0.5 is similar to the value obtained for G.P. zone formation in Al-Cu [124] and binary Mg-Nd [65] alloys and is assumed to relate to some vacancy assisted atomic rearrangement process. The value of $\frac{3}{2}$ for the γ'' reaction is typical of a reaction involving diffusion controlled growth of a fixed number of particles [125], i.e. zero nucleation rate. It appears that this should be the case with the γ'' phase because, due to the coherent nature of the phase, no nucleation difficulty seems to exist. After the initial part of the reaction

very little nucleation should be taking place.

The values of n for the γ reaction are approximately 1.4 at 250°C, where the γ is forming from γ'' , to the value of 1.0 at 325°C and 350°C. This latter figure is in agreement with the value associated with the diffusion controlled growth of cylinders or rods [125].

The low temperature reaction is similar to that observed in other magnesium alloys, e.g. Mg-Th [61] and Mg-Mn [105], where solute clustering has been deduced from resistivity measurements and other methods but no diffraction evidence for G.P. zones has been found. It would appear that the zinc addition to the Mg-Nd system is completely suppressing the G.P. zone reaction found in the binary alloy and in its place some atomic rearrangement process is preceding the formation of the ordered hexagonal (γ'') phase.

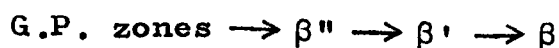
The γ'' phase shows a strong coherence with the matrix. The lattice parameters of this phase are related to those of the matrix by the relationships

$$a\gamma'' = \sqrt{3}a \text{ Mg} \text{ and } c\gamma'' = 3c \text{ Mg.}$$

The precipitate appears to be a true ternary phase as no phases with the above lattice parameters are formed in the systems Mg-Nd [65], Mg-Zn [89] or Nd-Zn [126]. The γ'' phase, however, does bear a resemblance to a phase recently observed in a Mg-Th-Mn alloy [62]. This phase

has an identical morphology and orientation relationship. The lattice parameters are also similar, they are quoted as being $a = \sqrt{3}a_{\text{Mg}}$, $c = 6.c_{\text{Mg}}$, it can be seen that the a parameters in the systems Mg-Nd-Zn and Mg-Th-Mn are identical but the c parameter of the manganese bearing alloy is twice that of the alloy in the present investigation. The binary Mg-Nd and Mg-Th systems show a preference for ordering in the early stages of precipitation, both forming structures of the DO_{19} type $a = 2.a_{\text{Mg}}$, $c = c_{\text{Mg}}$ with probable composition Mg_3Th and Mg_3Nd . Both Nd and Th have atomic sizes greater than that of magnesium and the introduction of a small third atom, zinc or manganese, presumably alters the stacking sequence and leads to the promotion of the ordered ternary compounds. The different c parameters of the ternary phases in the two alloys presumably result from different matching in the c direction due to the different sizes of the atoms concerned.

The equilibrium, γ phase is also not found in the systems Mg-Nd, Mg-Zn or Nd-Zn and therefore must be a true ternary phase. This means that the effect of an addition of 1.3% Zn to a binary Mg 2.8% Nd alloy is to completely suppress the binary precipitation sequence which has been shown to be [65]



and to replace it with a pseudo-binary system involving two ternary Mg-Nd-Zn phases previously unreported

low temperature reaction $\rightarrow \gamma'' \rightarrow \gamma$.
(possibly involving S.R.O.)

Text cut off in original

Figure 6.1 Continuous heating curve for Mg 2.8% Nd 1.3% Zn

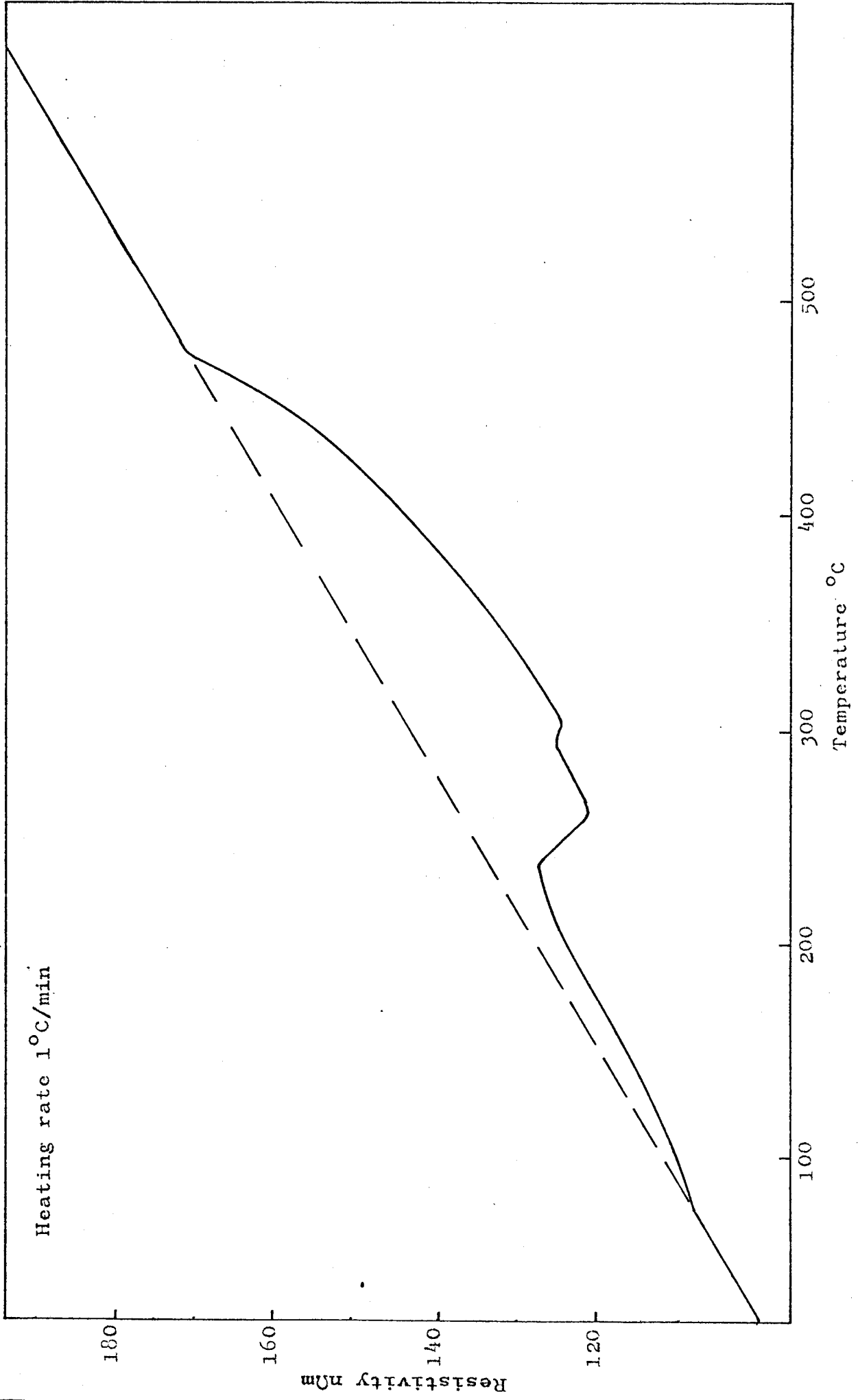


Figure 6.2 Mg 2.8% Nd 1.3% Zn

Low temperature resistivity isotherms

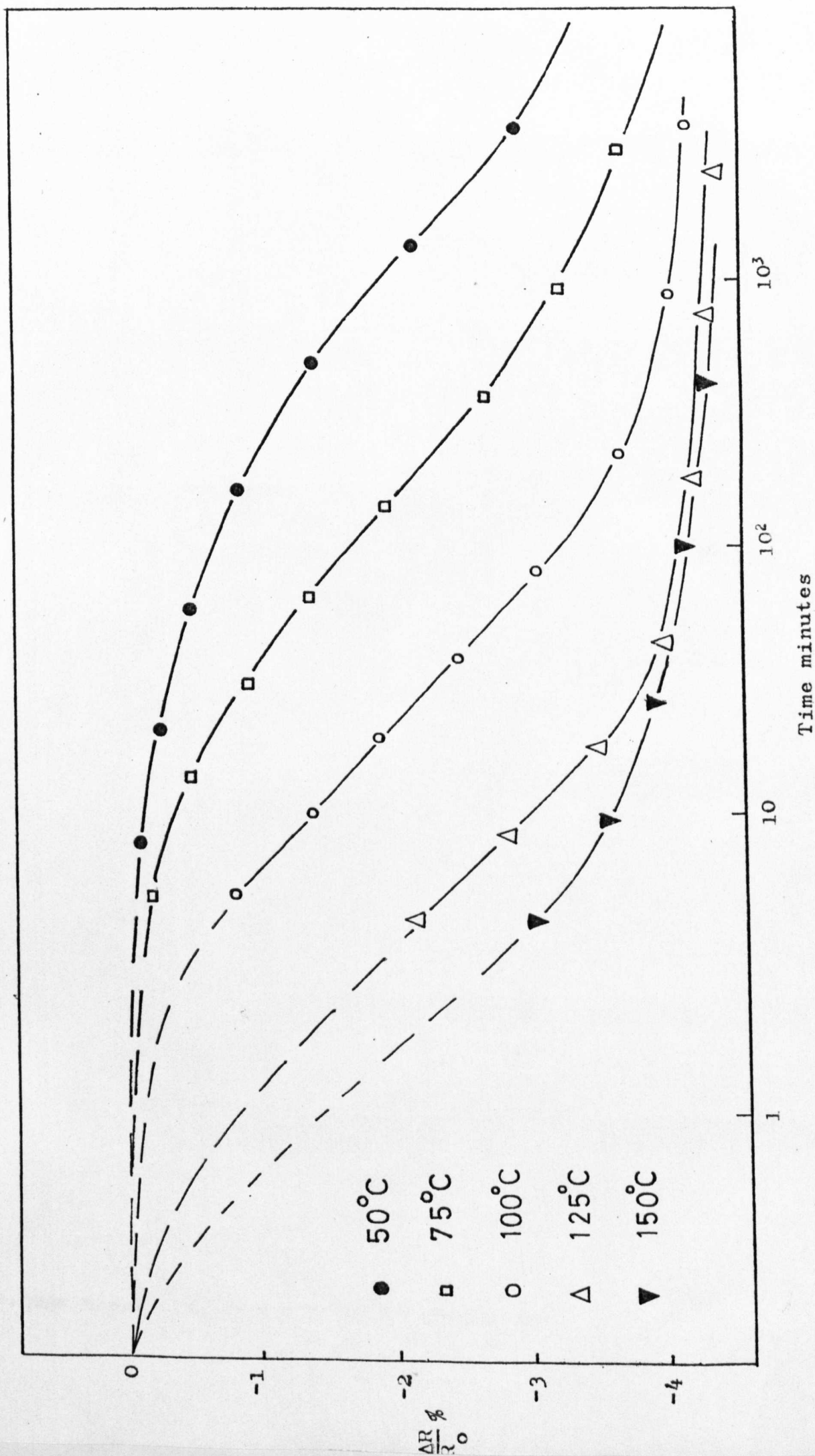
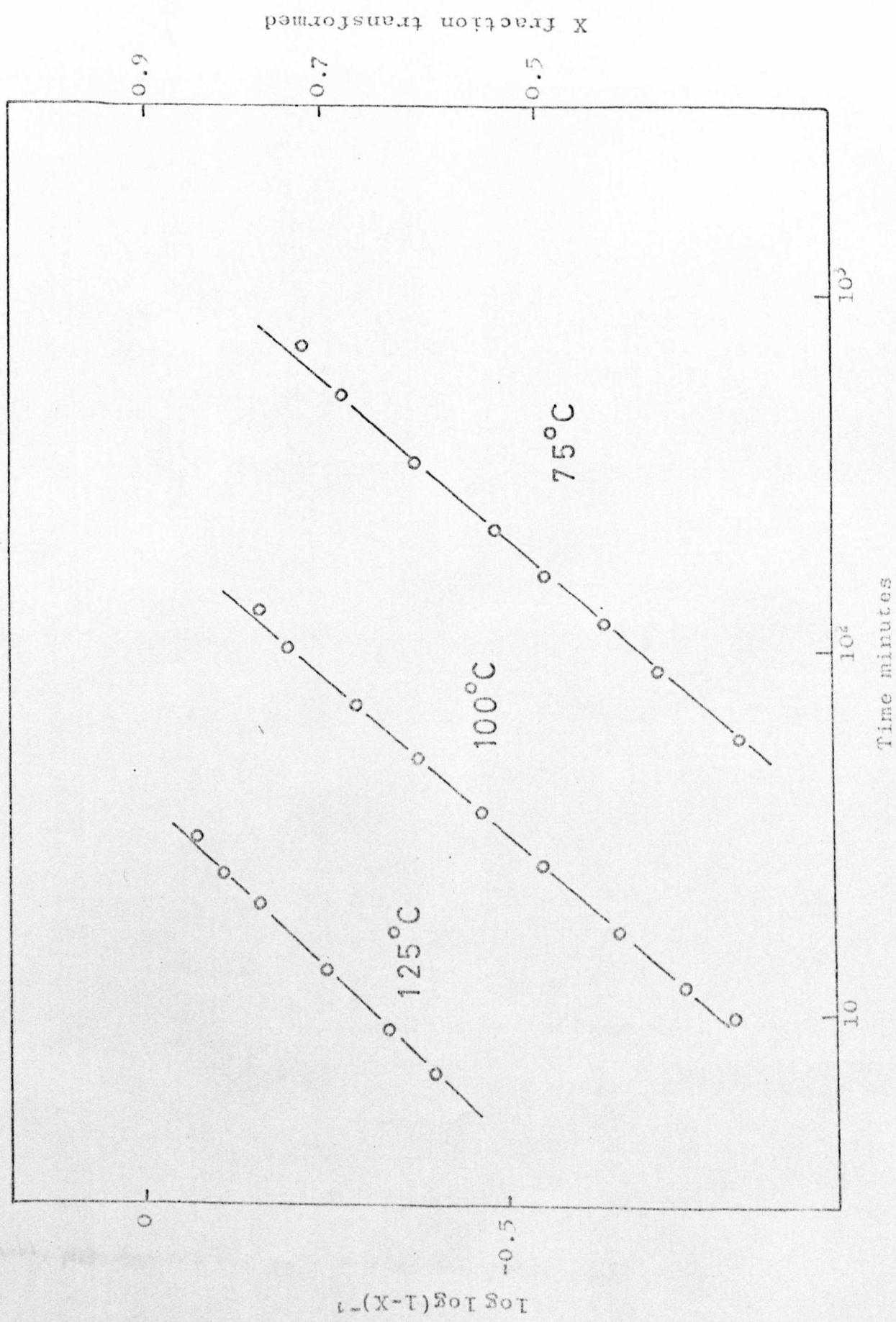


Figure 6.3 Avrami analysis of low temperature isotherms

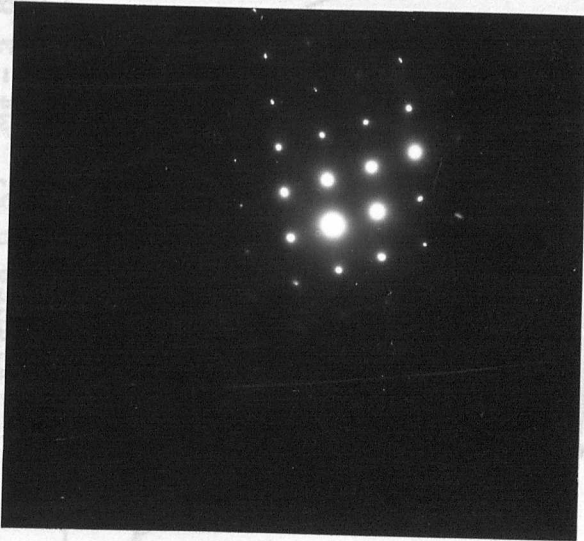




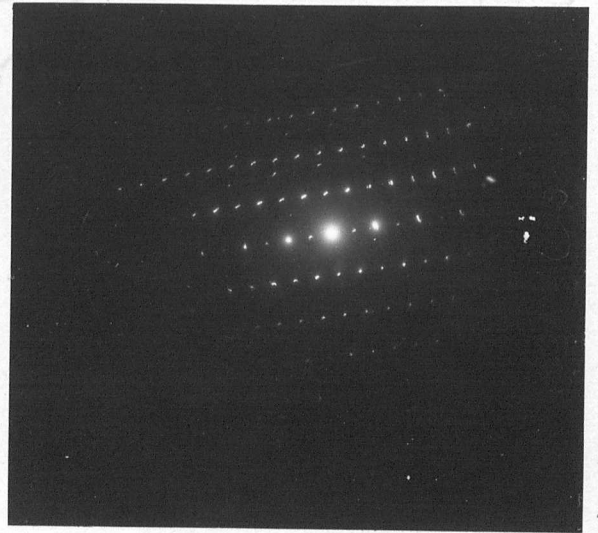
(a)



(b)



(c)



(d)

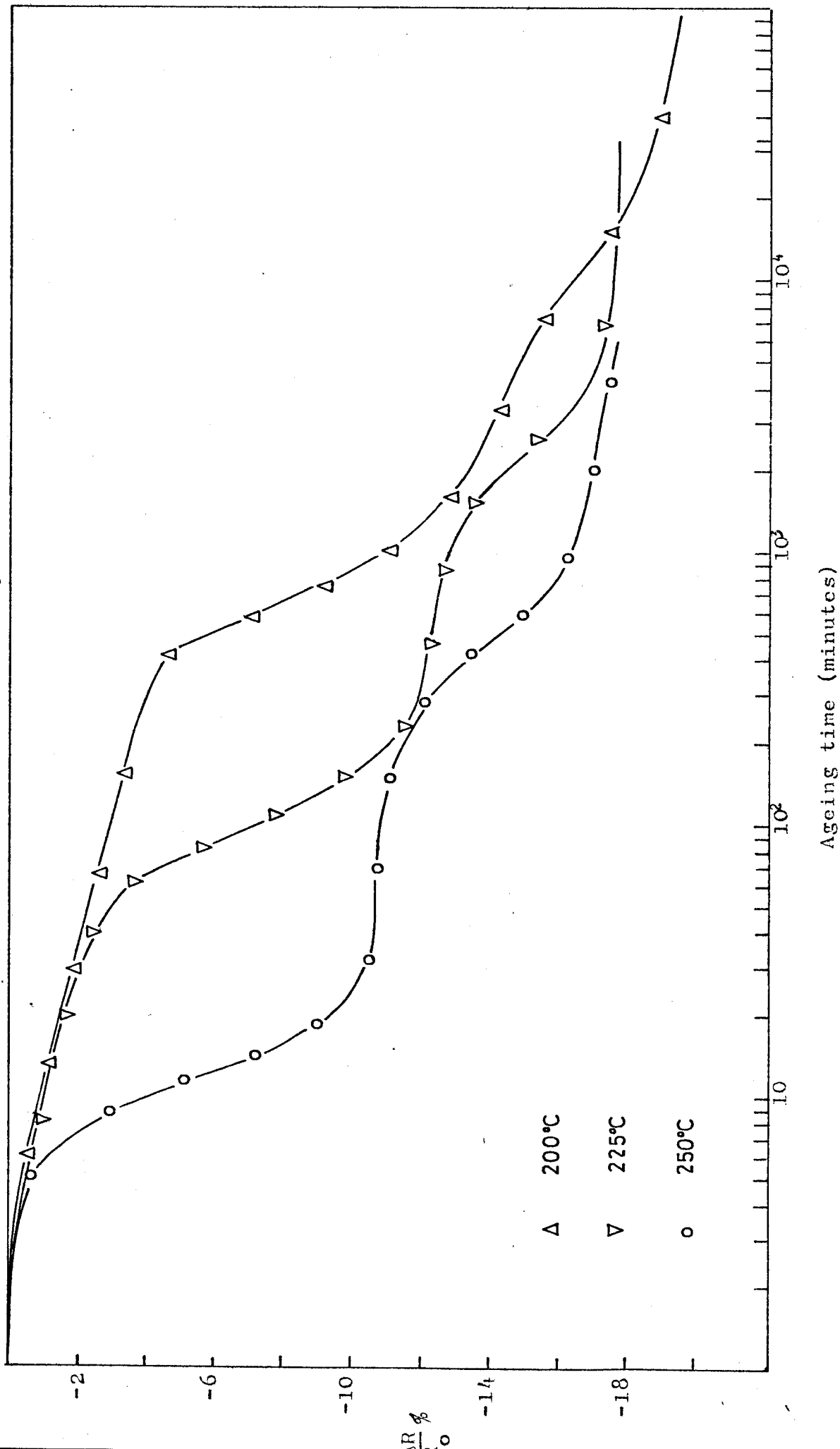
Figure 6.4 Mg-Nd-Zn

Aged 24 hrs at 100°C

Representative selected area diffraction patterns

- (a) $[0001]$ zone axis
- (b) $[2\bar{1}\bar{1}3]$ zone axis
- (c) $[10\bar{1}1]$ zone axis
- (d) $[2\bar{1}\bar{1}0]$ zone axis

Figure 6.5: Mg - 2.8%Nd - 1.3%Zn
Medium temperature resistivity isotherms



Text cut off in original

Figure 6.5: Mg - 2.8%Nd - 1.3%Zn
Medium temperature resistivity isotherms

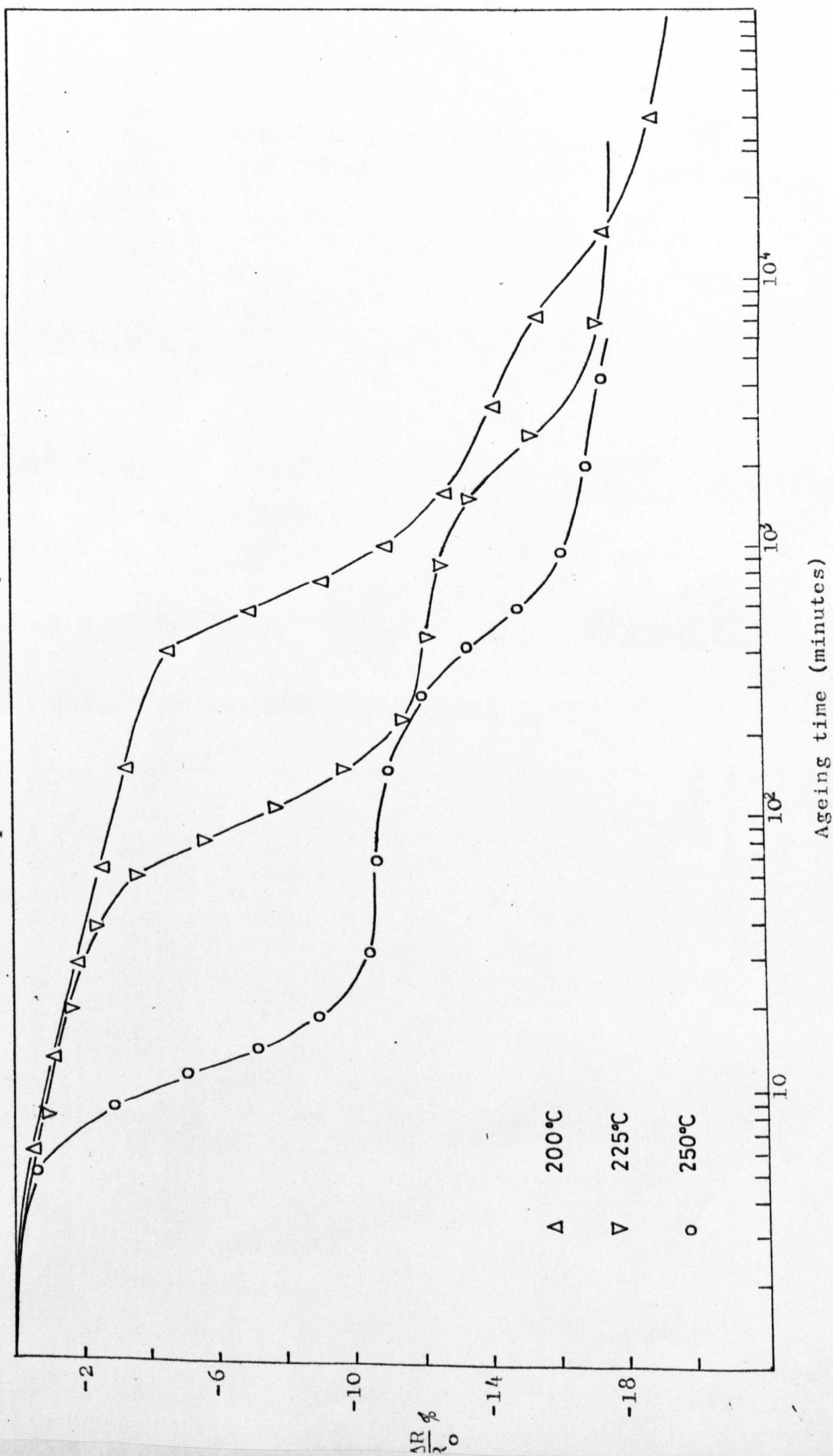
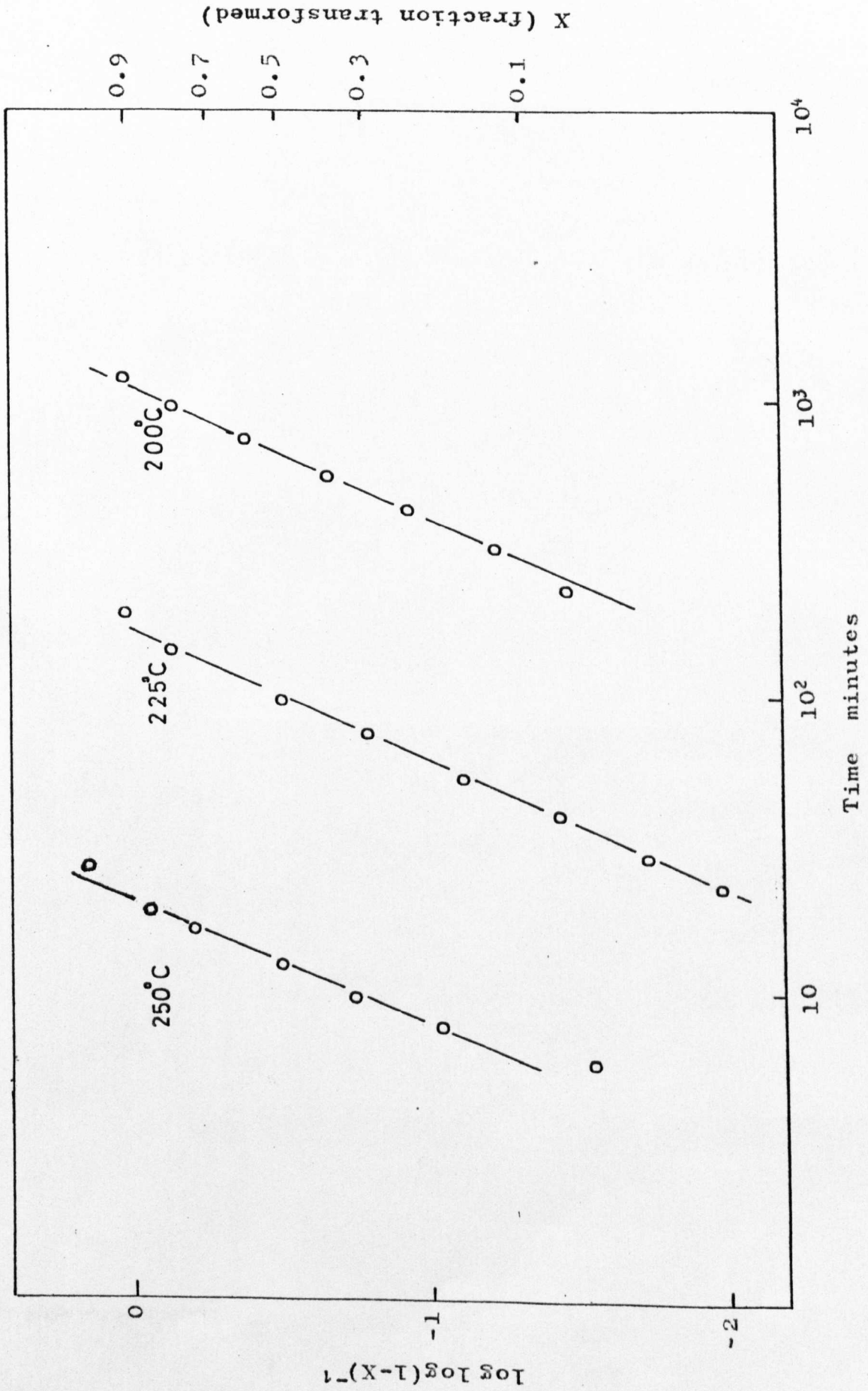
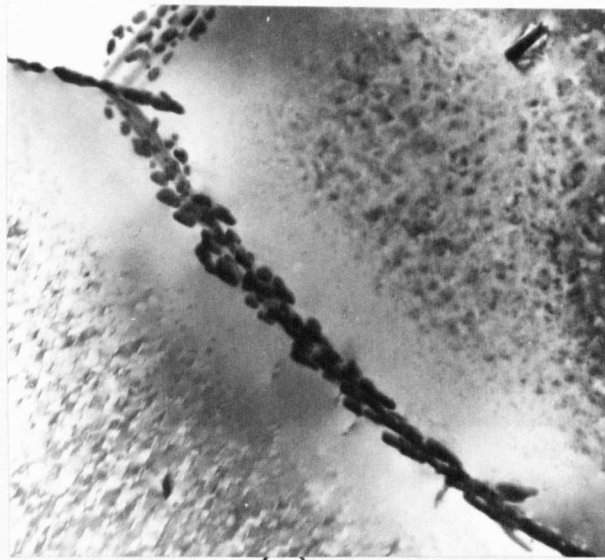


Figure 6.6 Avrami analysis of γ'' isotherms





(a)



(b)

Figure 6.7 Mg-Nd-Zn

- (a) Aged 35 minutes at 300°C. Pronounced precipitate free zone. Mag. 40,000 x
- (b) Aged 1 hour at 300°C. γ with background γ'' . Mag. 10,000 x

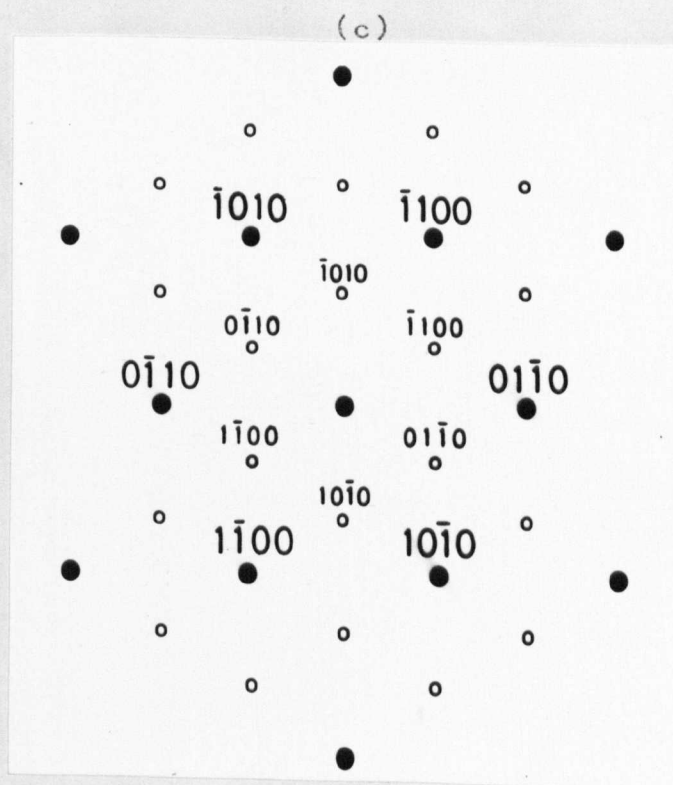
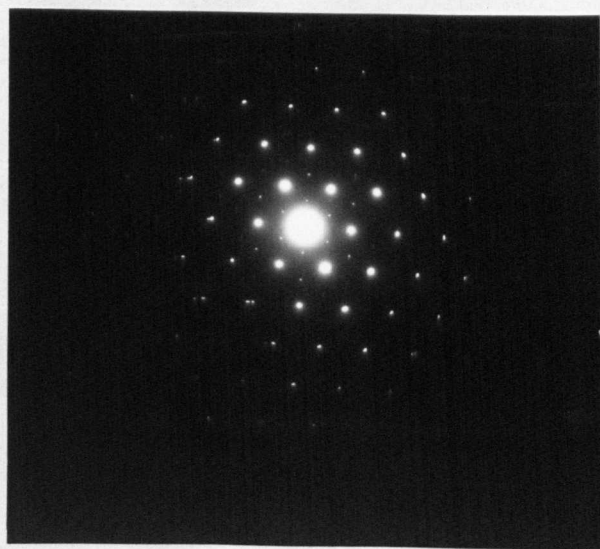
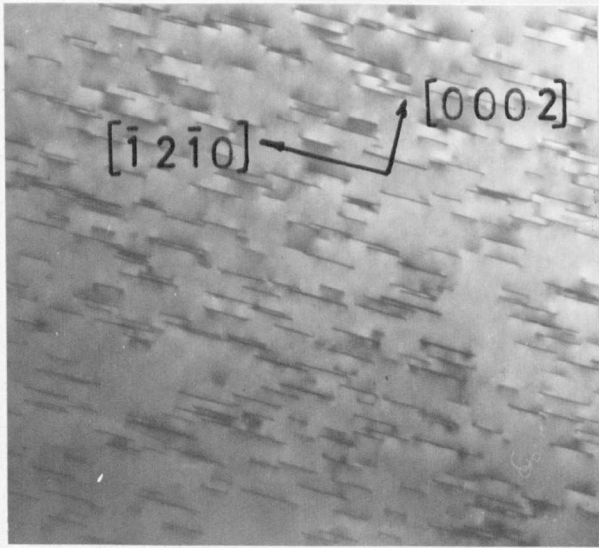


Figure 6.7 Mg-Nd-Zn

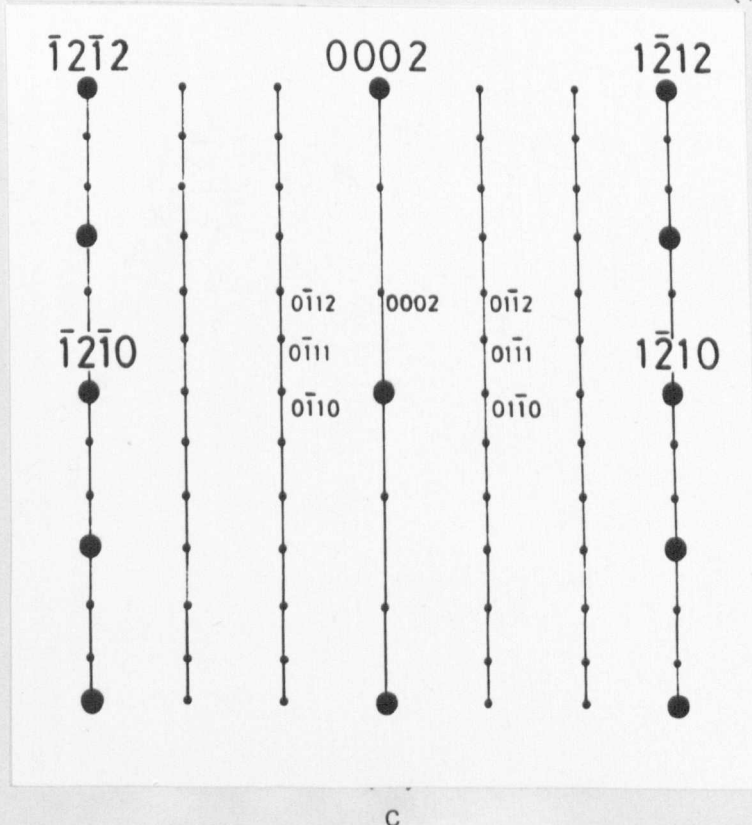
(c) Diffraction pattern showing
 $[0001]_{\text{Mg}} \parallel [0001]_{\gamma''}$
 $[10\bar{1}0]_{\text{Mg}} \parallel [2\bar{1}\bar{1}0]_{\gamma''}$

(d) Schematic (c)



(a)

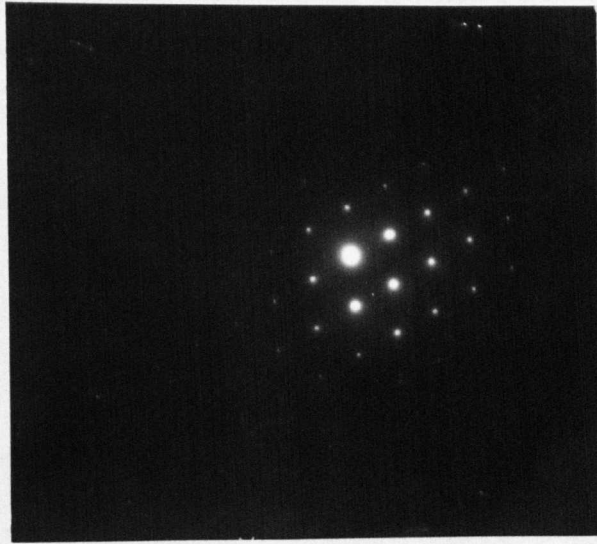
(b)



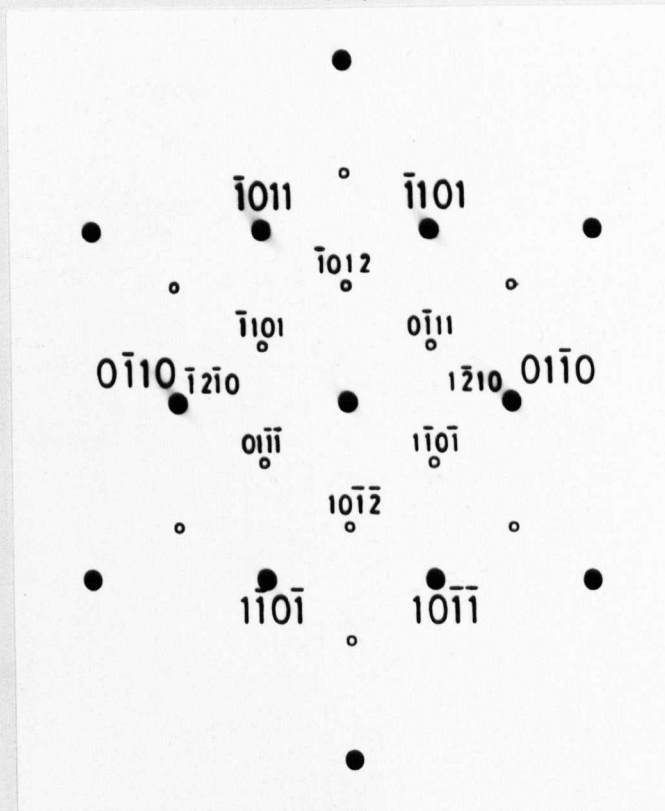
c

Figure 6.8 Mg-Nd-Zn

- (a) Aged 1 hr at 325°C coarse γ'' $[10\bar{1}0]$ zone axis
 (b) Diffraction above showing maxima in streaks
 $[10\bar{1}0]_{\text{Mg}} \parallel [2\bar{1}\bar{1}0]_{\gamma''}$
 (c) Schematic (b)



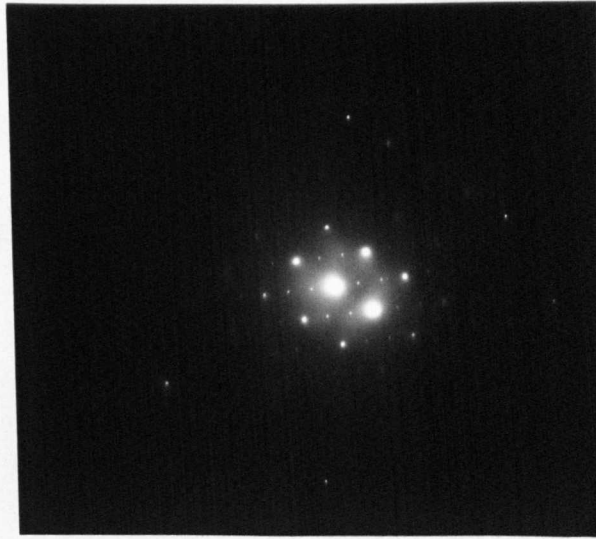
(a)



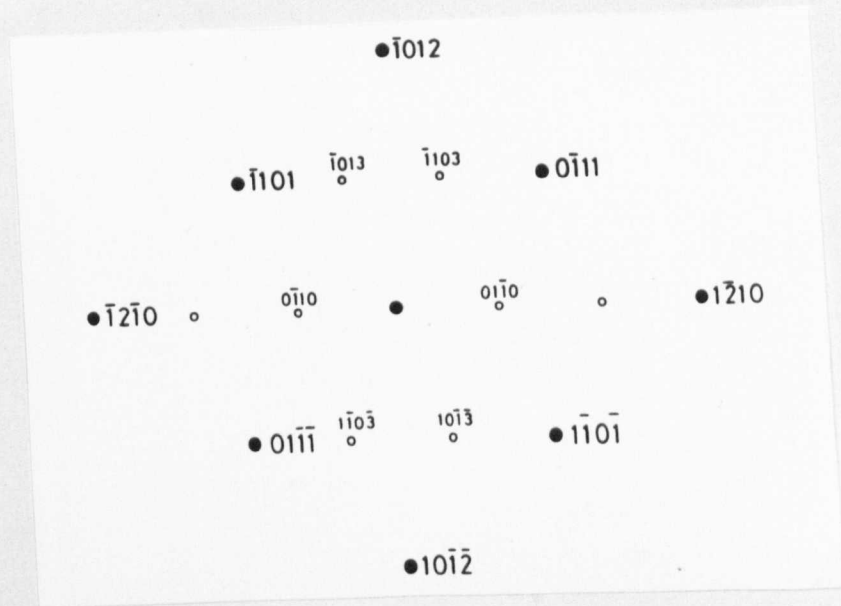
b

Figure 6.9 Mg-Nd-Zn
Aged 8 hrs at 240°C

- (a) Selected area diffraction pattern showing
 $[2\bar{1}\bar{1}3]_{\text{Mg}} \parallel [10\bar{1}1]_{\gamma''}$
- (b) Schematic (a)



(c)

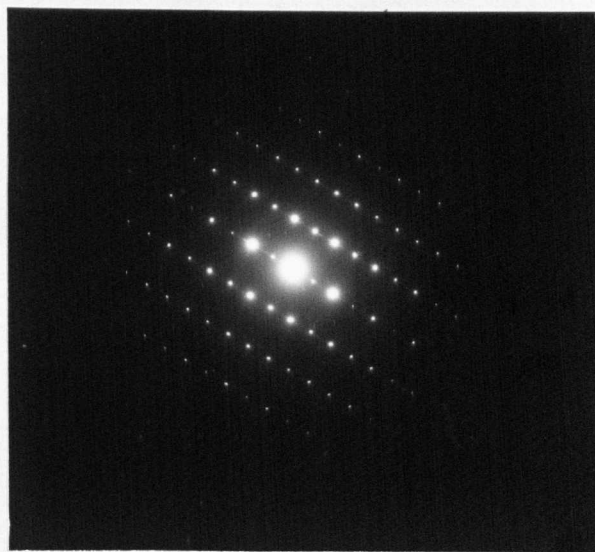


(d)

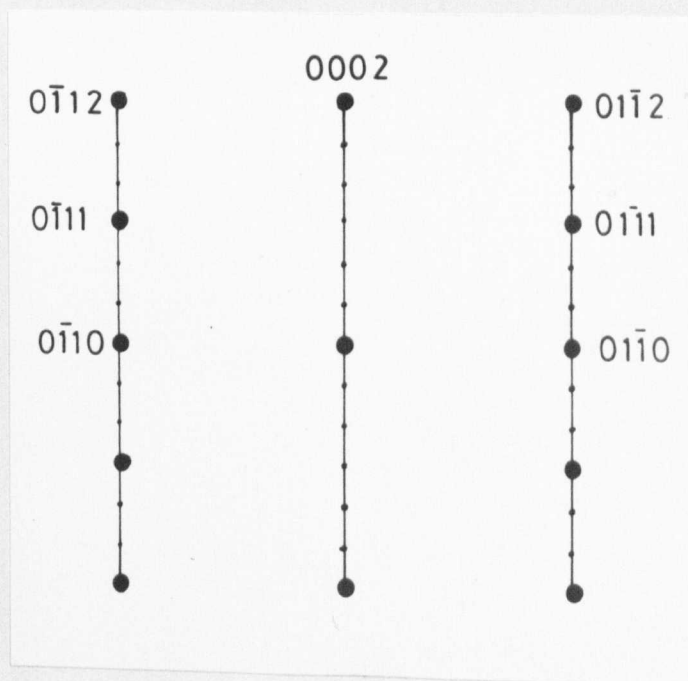
Figure 6.9 (cont.) Mg-Nd-Zn

(c) Selected area diffraction pattern showing
 $[10\bar{1}1]_{\text{Mg}} \parallel [2\bar{1}\bar{1}1]_{\gamma''}$

(d) Schematic (c)



(e)



(f)

Figure 6.9 (cont.) Mg-Nd-Zn

- (e) Selected area diffraction showing $[2\bar{1}\bar{1}0]_{\text{Mg}}$ with streaks and maxima from $[10\bar{1}0]_{\gamma''}$ pattern
- (f) Schematic (e)

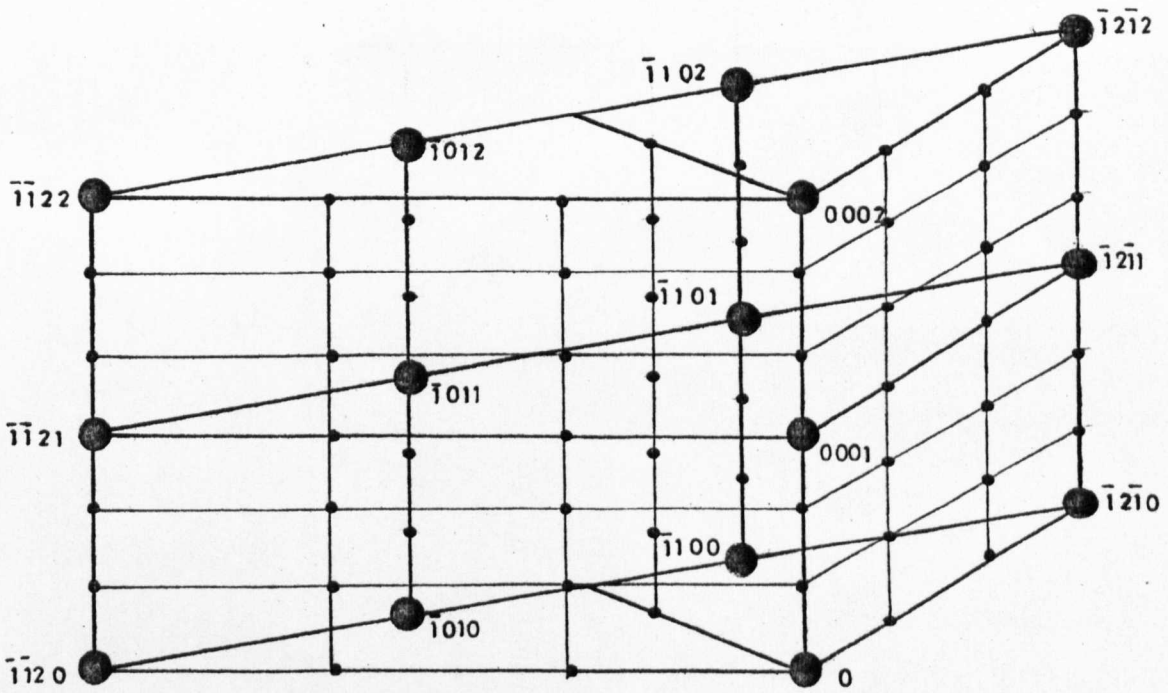
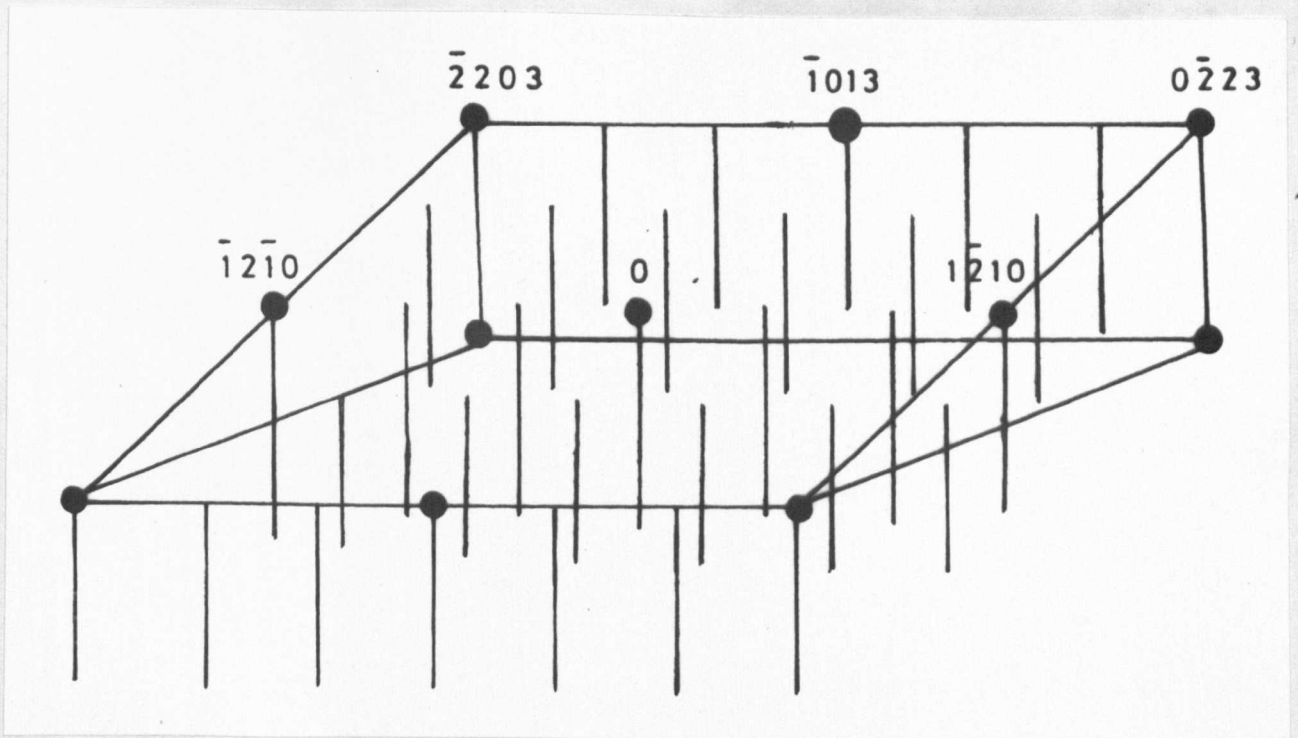


Figure 6.10

Section of the reciprocal lattices
of magnesium and γ'' superimposed

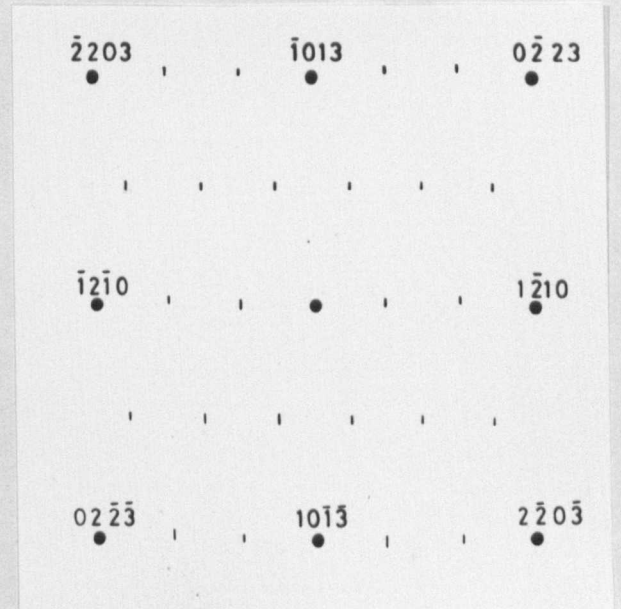
Large circles denote magnesium relpoints
and small circles denote γ'' relpoints



(a)



(b)



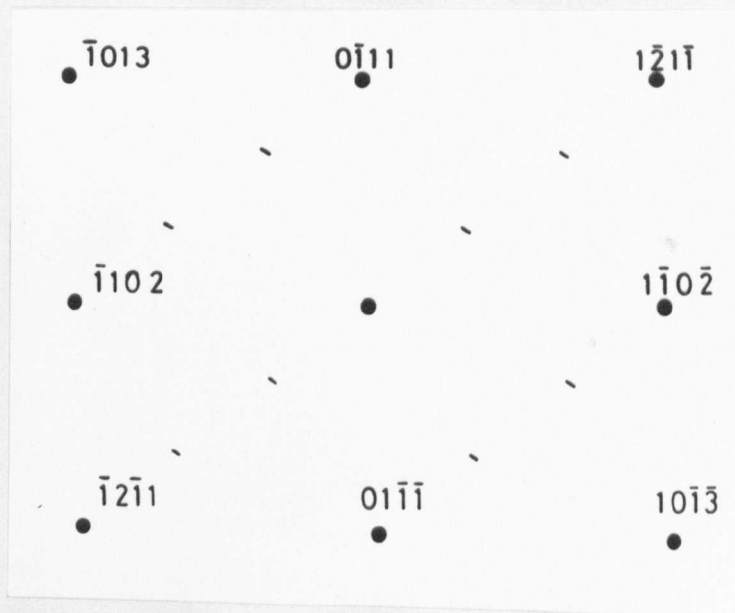
(c)

Figure 6.11 Mg-Nd-Zn

- (a) Schematic representation of $[30\bar{3}2]$ section of magnesium reciprocal lattice with $[0001]$ rellods from γ'' structure superimposed
- (b) Selected area diffraction pattern $[30\bar{3}2]$ zone axis
- (c) Schematic (b) showing streak intersections



(a)



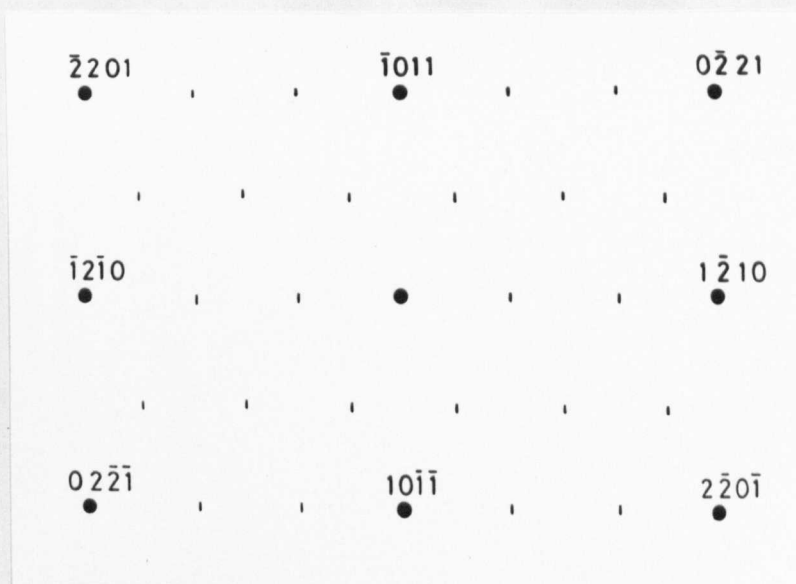
(b)

Figure 6.12 Mg-Nd-Zn
Aged 8 hrs at 250°C

- (a) Selected area diffraction pattern showing $[5\bar{1}\bar{4}3]$ Mg zone axis with streak intersections from γ'' phase
- (b) Schematic (a)



(c)



(d)

Figure 6.12 (cont.) Mg-Nd-Zn

- (c) Selected area diffraction pattern showing $[10\bar{1}2]$ Mg zone axis with streak intersections due to γ'' phase
- (d) Schematic (c)

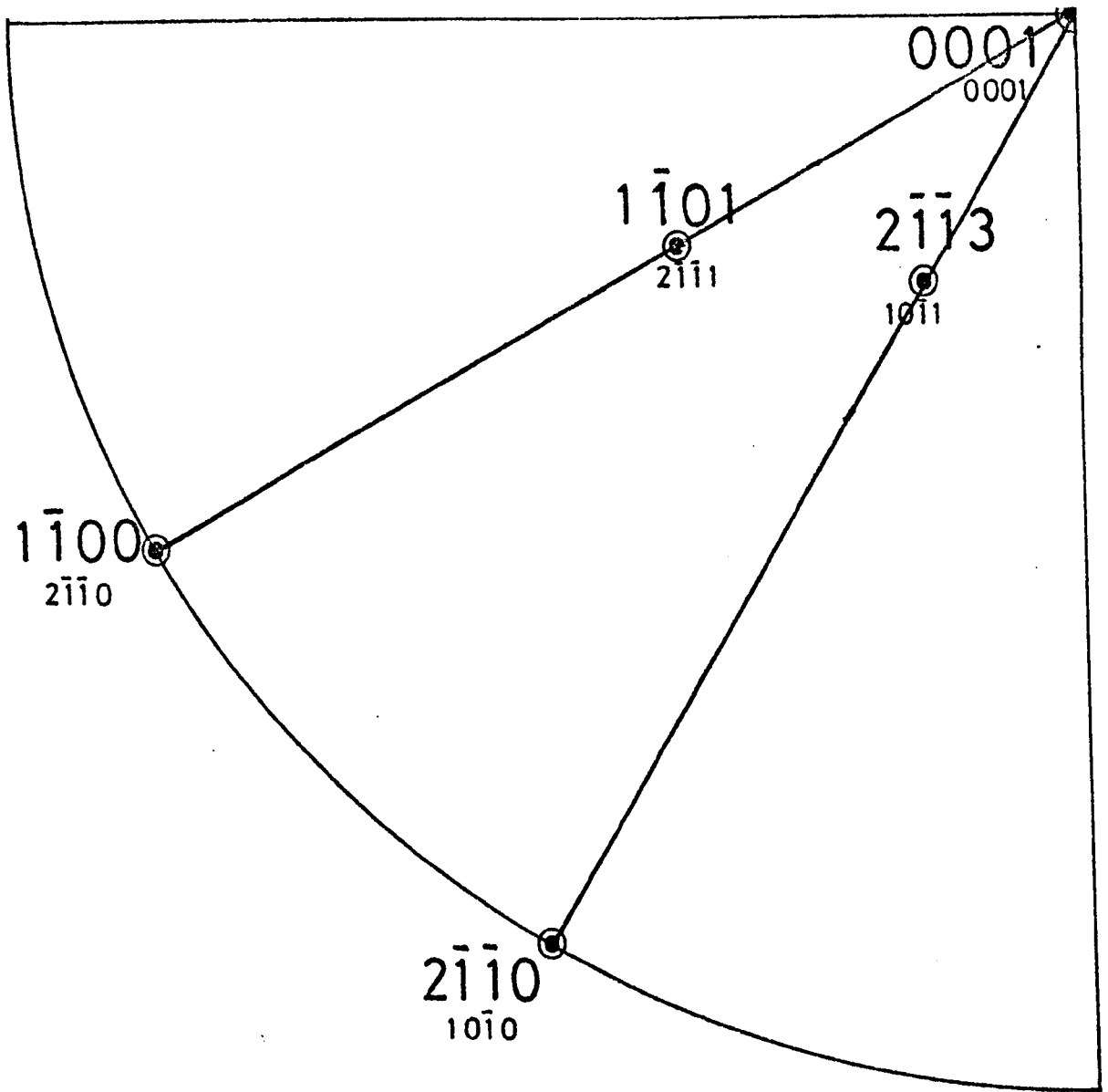


Figure 6.13 Stereogram showing common zone axes patterns from γ'' structure and magnesium matrix.

[Magnesium zone axes in large print]

Figure 6.14 Mg 2.8% Nd 1.3% Zn
High temperature resistivity isotherms

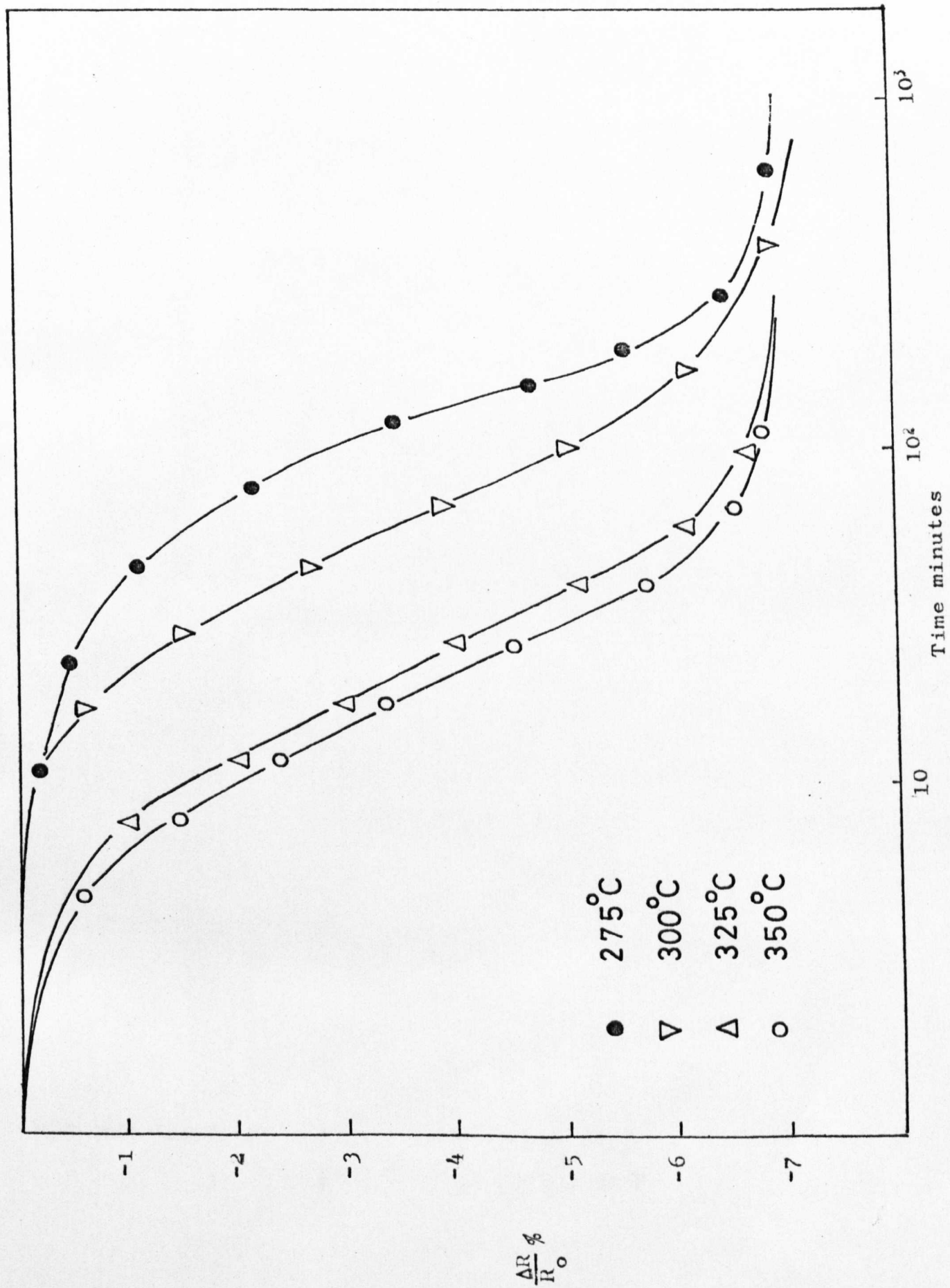
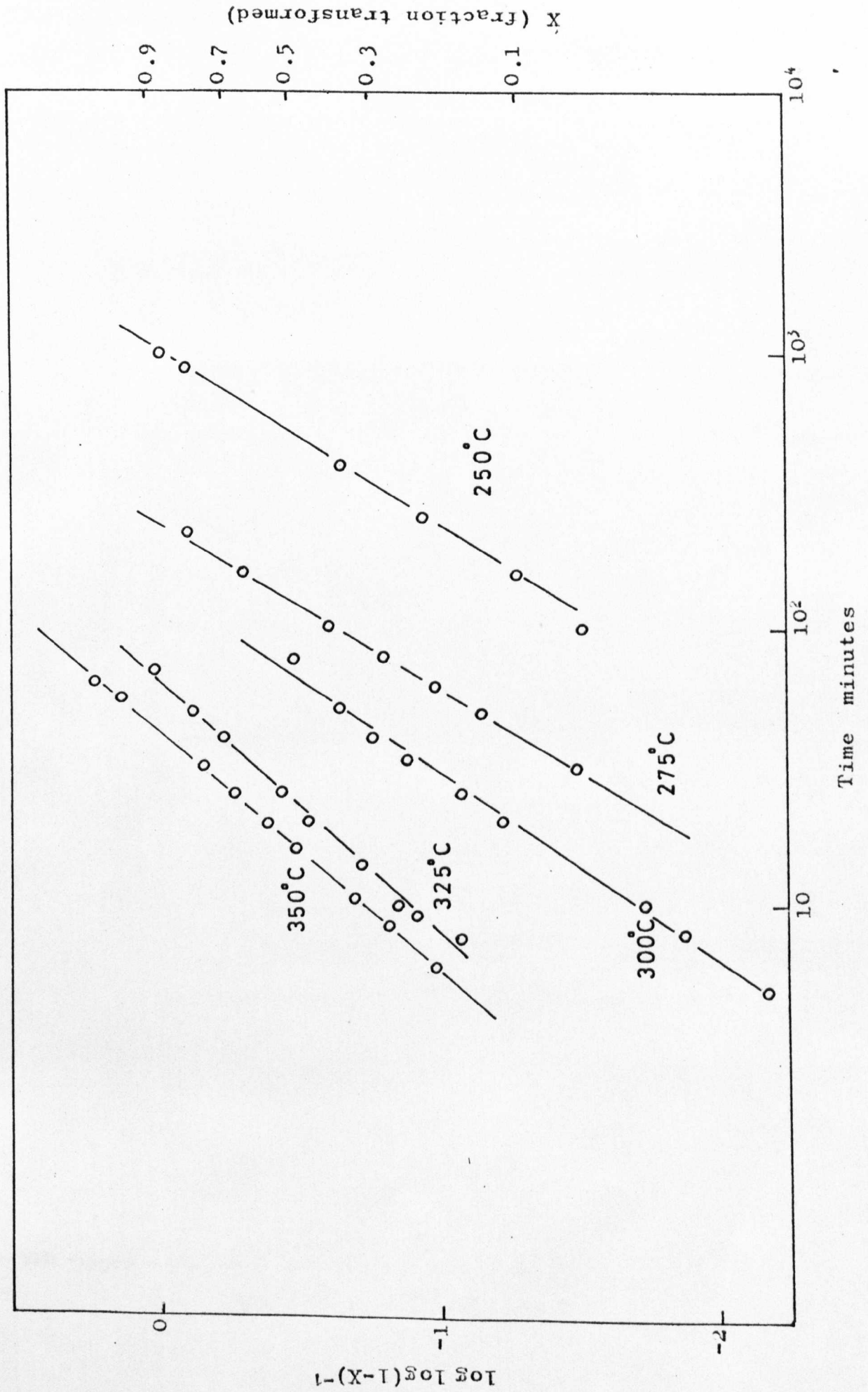


Figure 6.15 Avrami analysis of γ isotherms





Mg-Nd-Zn

3hrs at 325°C

Figure 6.16 Aged

Orientation [0001] Mag 11,000 x

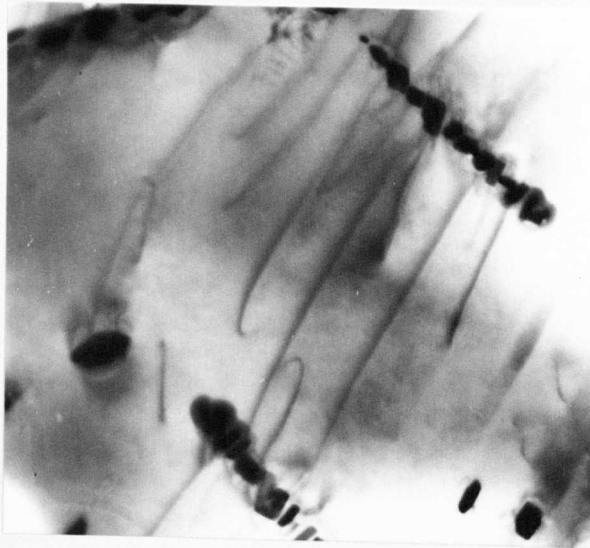
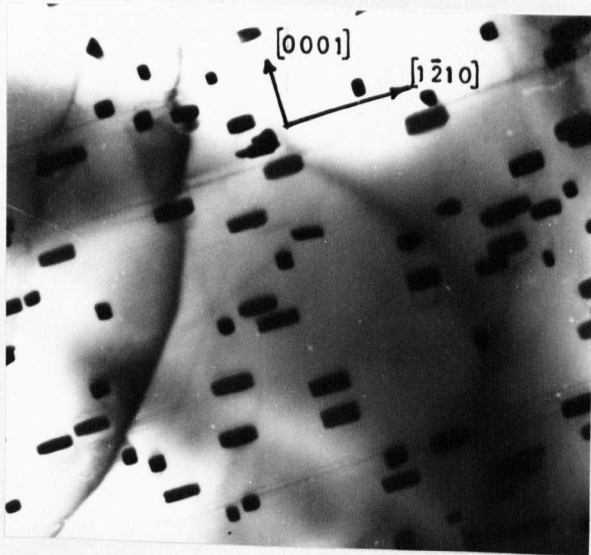
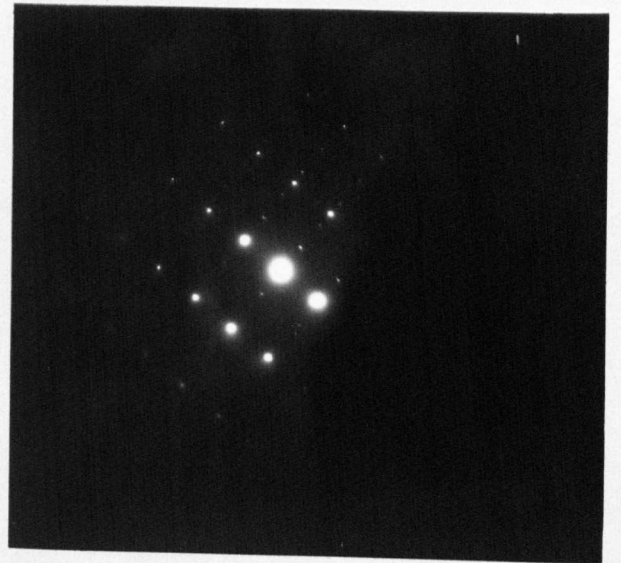


Figure 6.16(b) Mg-Nd-Zn

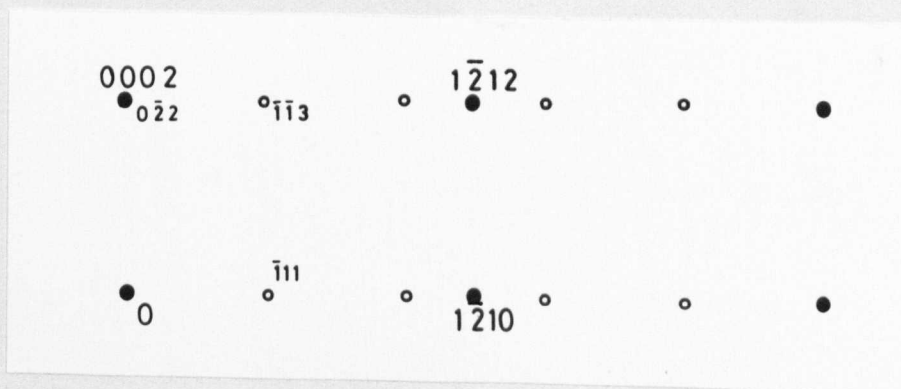
Aged 1 hour at 325°C
γ precipitation on dislocations
Mag 40,000 x



(a)



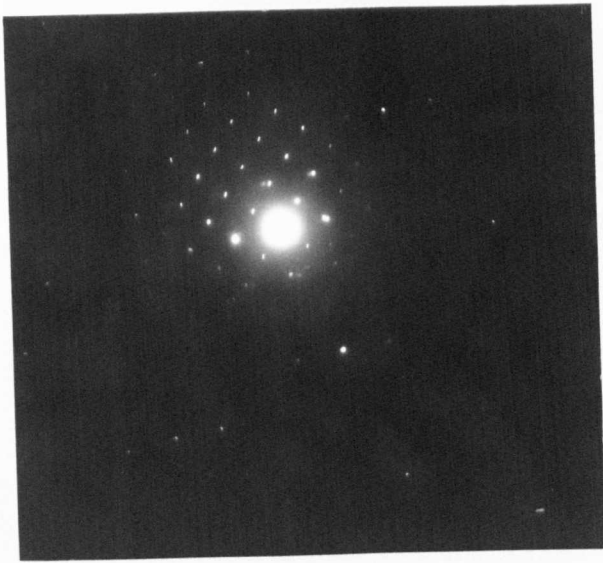
(b)



(c)

Figure 6.17 Mg-Nd-Zn

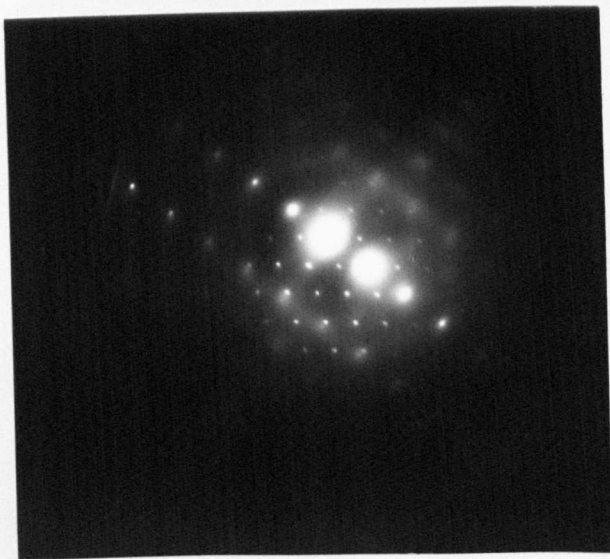
- (a) Aged 10 days at 300°C Mag 16,000 x
- (b) Diffraction above $[10\bar{1}0]_{\text{Mg}} \parallel [211]_{\gamma}$
- (c) Schematic (b)



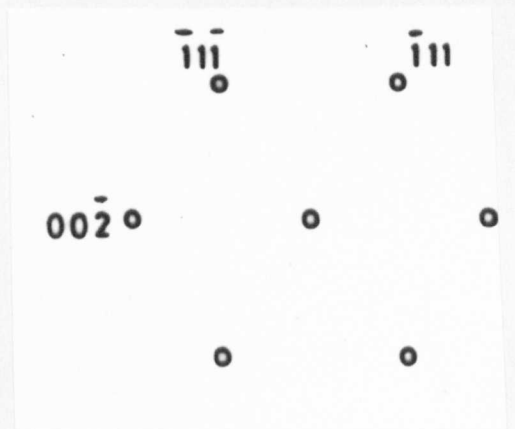
(a)



(b)



(c)



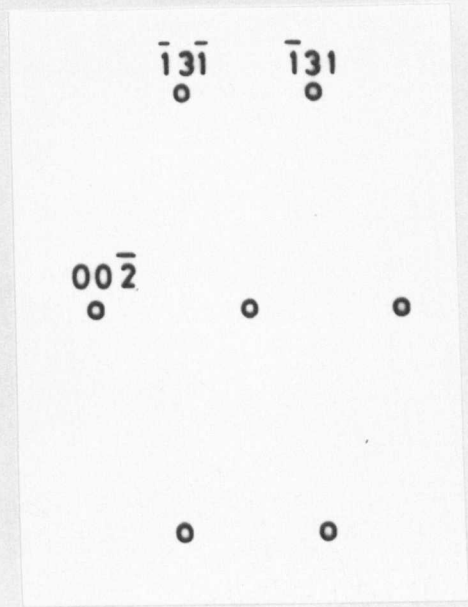
(d)

Figure 6.18 Mg-Nd-Zn
Selected area diffraction patterns from γ phase

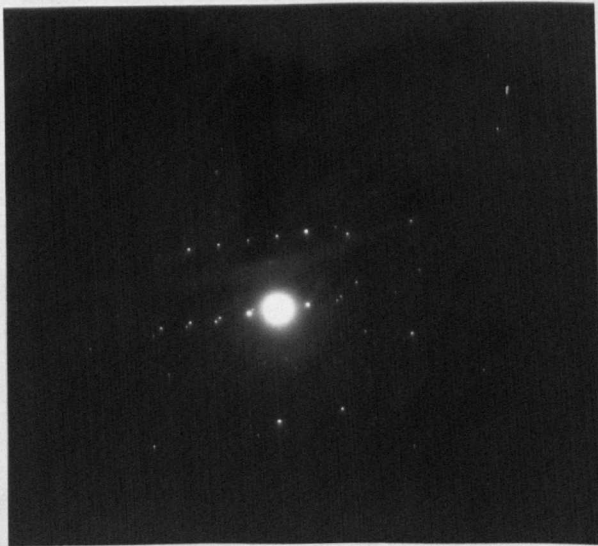
- (a) $[100]\gamma$ zone axis
- (b) Schematic (a)
- (c) $[\bar{1}\bar{1}0]\gamma$ zone axis
- (d) Schematic (b)



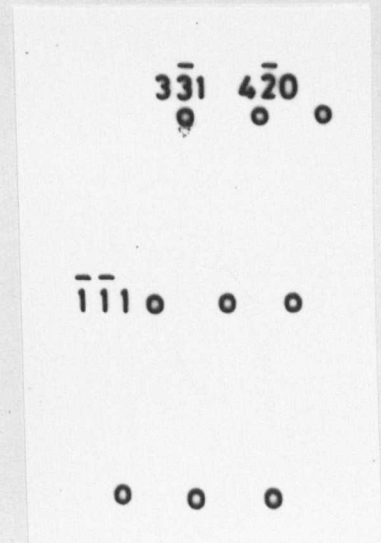
(e)



(f)



(g)



(h)

Figure 6.18 (cont.) Mg-Nd-Zn
Selected area diffraction patterns from γ phase

- (e) $[310]\gamma$ zone axis
- (f) Schematic (e)
- (g) $[123]\gamma$ zone axis
- (h) Schematic (g)

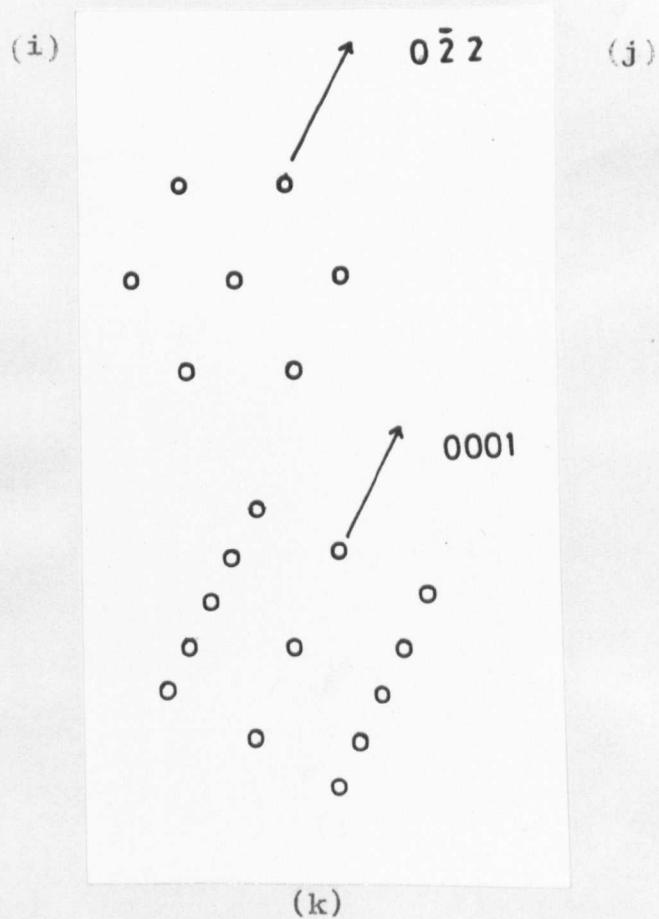
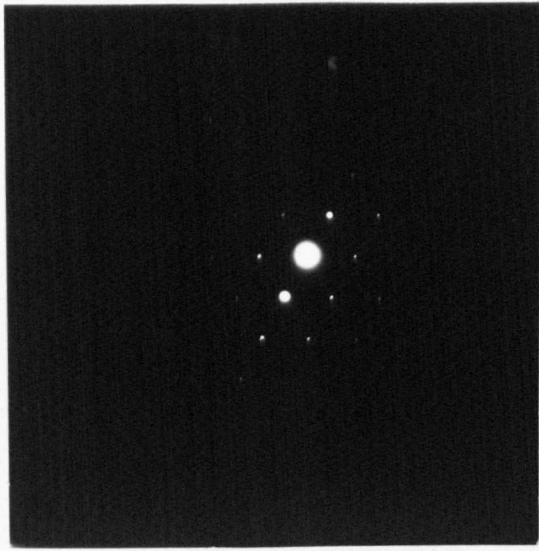
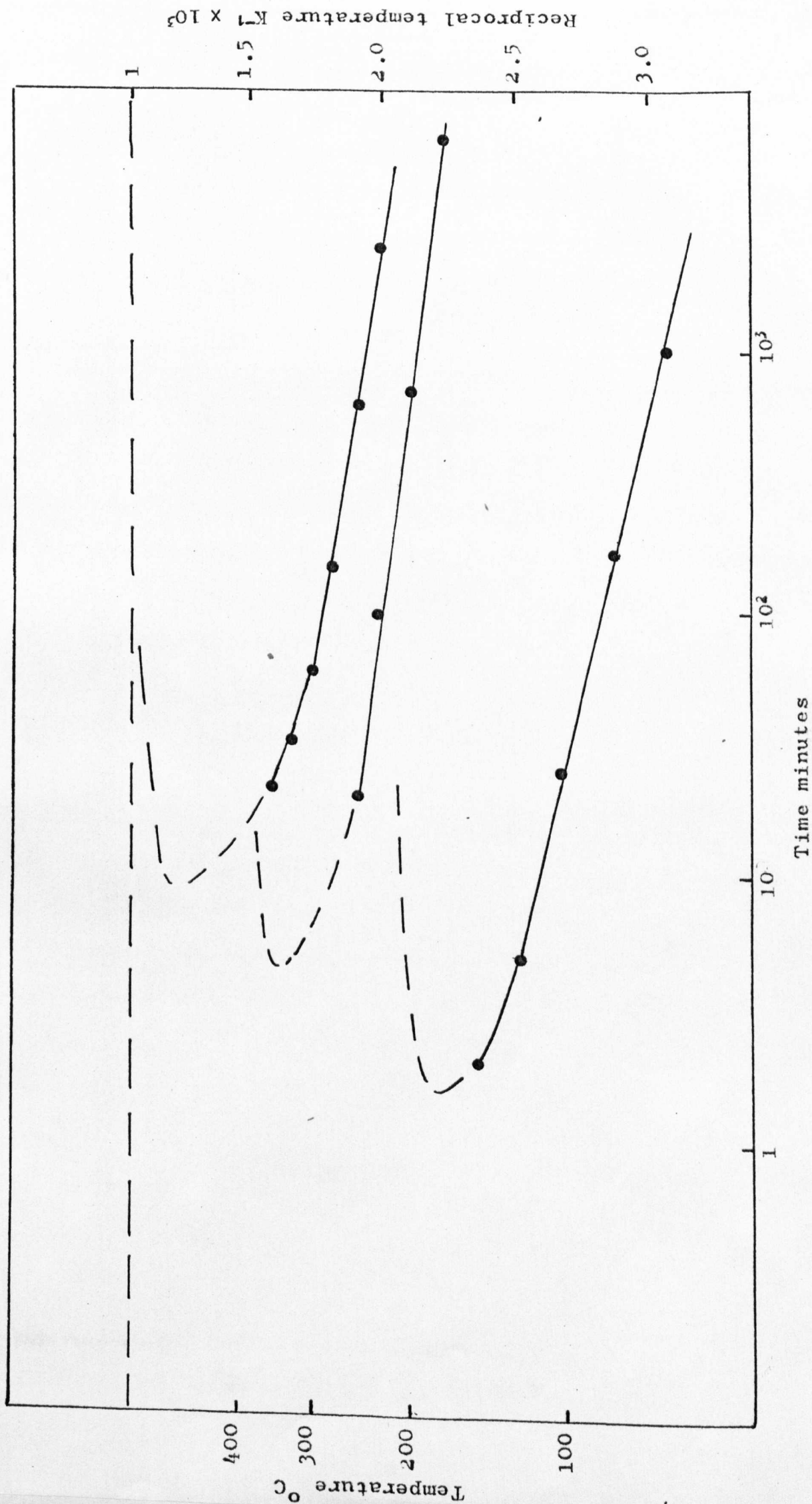


Figure 6.18 Mg-Nd-Zn

- (i) Selected area diffraction of precipitate in $[2\bar{1}\bar{1}0]$ grain
- (j) Matrix above
- (k) Schematic (a) and (b) showing $[2\bar{1}\bar{1}0] \text{ Mg} \parallel [111] \gamma$
 $[0001] \text{ Mg} \parallel [0\bar{2}2] \gamma$

Figure 6.19 Mg-Nd-Zn
C-curves for 50% transformation



CHAPTER 7

THE Mg-Nd SYSTEM:

EFFECT OF ZINC ON MECHANICAL PROPERTIES

To determine the influence of zinc on the mechanical properties of the Mg-Nd system, alloys were prepared with nominal compositions 2.8% Nd, 2.8% Nd 0.3% Zn, 2.8% Nd 0.7% Zn and 2.8% Nd 1.3% Zn. The compositions correspond to additions of zinc of 0.1 atomic %, 0.25 atomic % and 0.5 atomic %. The chemical analyses of these alloys are shown in Appendix II.

7.1 Room Temperature Proof Stress

Proof stress ageing curves were determined for the binary alloy and the alloy containing 1.3% zinc at ageing temperatures of 200°C and 250°C. These temperatures were chosen as the ageing temperatures most likely to give peak properties and also because this is the temperature used in commercial practice [127]. The results are presented in Figure 7.1. It can be seen from this that peak properties are attained after ageing for approximately four days at 200°C.

7.2 Creep Testing

The commercial alloys based on the system magnesium-rare earths are claimed to have good creep properties at temperatures up to 250°C and therefore in the present investigation creep testing has been carried out at 200°C and 250°C on all alloys. In all cases specimens were allowed one hour after insertion into the creep furnace and prior to application of the load, this being sufficient for the specimen to attain the test temperature.

Prior to all testing, all alloys were aged to a standard condition, this being an ageing time to peak proof stress at 200°C.

The parameter chosen for comparison purposes was the steady state creep rate. Due to the limited time available, the tests were of comparatively short duration and it was felt that this parameter provided a better basis for comparison than, for example, the permanent elongation after fifty hours. In the latter measurement a large amount of the elongation would occur during loading and in the first few minutes of the test. Typical creep curves are shown in Figure 7.2, they show the classical two stage reaction of primary and secondary creep; in only one case, the alloy containing 0.3% Zn, was any evidence of tertiary creep found. This alloy, on analysis, proved to be low in neodymium, 2.5%

instead of 2.8% (see Appendix II). In an attempt to rationalise the result for this alloy, binary Mg-Nd alloys of various neodymium contents were aged for four days at 200°C and their room temperature 0.1% proof stresses determined (Figure 7.3). As can be seen from the graph, the proof stress is lowered some 30% by reducing the neodymium content from 2.8% to 2.5%. The alloy containing 0.3% zinc, as will be shown in a later section, contains only binary phases and the creep resistance of the alloy is assumed to arise almost entirely from these phases with only a small contribution, in the form of solid solution strengthening, from the zinc. It has been felt reasonable, therefore, to adjust the results for the alloy with low neodymium concentration by a factor of 0.3.

Also, a short investigation was carried out on the stress dependence of creep in the binary alloy. Specimens of the binary alloy were tested with applied loads of 11.5, 12.0 and 12.5 Kg/mm². The results are presented in Figures 7.5 and 7.6. The stress exponent n in the equation [128]

$$\dot{\epsilon} = K\sigma^n$$

where $\dot{\epsilon}$ is the steady state creep rate, K is a

function of temperature and structure only, and σ is the applied stress, was found to be 23.8. This compares with values of 4.5 [129], 4.0 - 5.5 [130] and 7.5 - 19.0 [131] found by various workers for magnesium; the latter values were associated with non-basal cross-slip of screw dislocations and the slip motion of dislocations in pyramidal slip.

7.3 Microstructure of the Alloys

To determine the effect of the microstructure on the creep properties of magnesium-neodymium alloys, it was necessary to examine all alloys in the conditions they were creep tested. In this way the phases influencing the creep properties can be identified. All alloys were examined in the undeformed state but it was felt that, under creep conditions, precipitation would be expected to be rather more rapid due to pipe diffusion along dislocation lines and increased precipitation on dislocations. The alloys were examined after ageing for

- (a) four days and six days at 200°C and
- (b) four days at 200°C plus a further one hour and two days at 250°C.

These conditions are equivalent to those at the beginning and end of the creep tests at 200°C and 250°C respectively.

Binary Mg 2.8% Nd alloy

The structure, after ageing at 200°C for four days, is shown in Figure 7.7(a). The foil is in [0001] orientation and the precipitate is seen to have three traces 60° apart in all $\langle 10\bar{1}0 \rangle$ directions. Diffraction evidence showed the precipitate to be plates of β' phase [65] with lattice parameters of $a = 0.52$ nm and $c = 1.30$ nm. The β' phase showed little coarsening after a further two days at 200°C. However, on ageing at 250°C, the β' coarsened considerably, until after two days at 250°C the structure was coarse β' together with the equilibrium β ($Mg_{12}Nd$) phase.

Mg 2.8% Nd 0.25% Zn alloy

The microstructure of this alloy was very similar to the binary alloy in all conditions. No evidence of any ternary phase, either by direct observation or by electron diffraction, was found. On further ageing at 250°C, as in the binary alloy, the β' became very coarse and partially transformed to the β phase.

Mg 2.8% Nd 0.7% Zn alloy

The structure, after ageing for four days at 200°C,

is extremely complex. The diffraction pattern in Figure 7.8(b) indicates the structure to consist of binary β'' and β' phases together with the ternary γ'' phase. In this pattern the γ'' reflections can be clearly seen at $\frac{1}{3}\langle 11\bar{2}0 \rangle^*$, and streaks in the $\langle 11\bar{2}0 \rangle^*$ directions and the $\langle 10\bar{1}0 \rangle^*$ directions indicate the presence of the β'' and β' phases respectively. On ageing for six days at 200°C all the β'' had transformed and the structure was a mixture of γ'' and β' . No evidence of any ternary phases were found after ageing at 250°C , the structure being composed of coarse β' and the equilibrium β phase.

Mg 2.8% Nd 1.3% Zn alloy

The precipitation sequence in this alloy has been discussed in the previous chapter; only the ternary phases γ'' and γ are precipitated. In the alloy aged four days at 200°C (Figure 7.9(a)), the microstructure was observed to be very fine γ rods with their long directions in all $\langle 10\bar{1}0 \rangle$ and $\langle 11\bar{2}0 \rangle$ directions. Diffraction evidence (Figure 7.9(b)) shows that fine γ'' is observed in the background. The situation is not significantly altered by ageing for a further two days at 200°C but on ageing at 250°C the γ'' transforms to γ . After four days at 200°C followed by a two day treatment at 250°C no γ'' is present and the structure is coarse γ (Figure 7.9(c)).

7.4 Discussion

The deformation of polycrystalline magnesium at elevated temperatures has been studied by several workers [129-133] and it has been found that non-basal slip occurs. The predominant mode of deformation at room temperature is slip on the (0001) plane in the $\langle 11\bar{2}0 \rangle$ directions, but slip will occur on other systems when slip on the (0001) plane is inhibited for some reason. In particular, it has been found that $\{10\bar{1}1\}$ or $\{10\bar{1}0\}$ slip occurs in highly stressed areas, for example grain boundary corners [134] and that slip occurs on the system $\{10\bar{1}1\} \langle 11\bar{2}0 \rangle$ at temperatures of 225°C and above with relative ease [135 - 137]. The critically resolved shear stresses for slip on (0001) $\langle 11\bar{2}0 \rangle$ and $\{10\bar{1}1\} \langle 11\bar{2}0 \rangle$ have been determined as 451 KN/m² and 510 KN/m² respectively at 25°C.

When dealing with wrought, polycrystalline magnesium, the material often has a strongly preferred orientation after recrystallisation, with basal planes lying in, or near, the plane of the sheet (or parallel to the axis of the rod). When such a material is loaded in tension the basal planes are parallel to the applied load and the system (0001) $\langle 11\bar{2}0 \rangle$ is far from being ideally orientated for easy slip. In such a situation it has been shown [136,137] that the system $\{10\bar{1}1\} \langle 11\bar{2}0 \rangle$ will operate at

temperatures lower than 225°C and Reed-Hill and Robertson [137] found this to be the predominant mode of deformation at 150°C .

The results obtained from the tensile and creep tests in the present work can be explained in terms of the predominant mechanisms operative at the respective test temperatures, and by the interaction of the dislocations with precipitate particles. It is seen from Figure 7.1 that the binary Mg-Nd alloy is stronger than the ternary Mg-Nd-Zn alloy aged at both 200°C and 250°C when tested at room temperature. The phases present in the binary Mg-Nd system aged at these temperatures are β'' and β' , which form as plates on the $\{11\bar{2}0\}$ and $\{10\bar{1}0\}$ Mg planes respectively. These plates thus form extremely effective barriers to dislocation movement on the (0001) plane, which, as explained earlier, is expected to be the prominent deformation mode at this temperature. The Mg-Nd-Zn system, however, containing γ'' phase as plates on the (0001) plane, are in the least favourable orientation for blocking slip, as dislocations can climb or cross slip around these particles with relative ease.

Over-ageing these alloys at 250°C causes precipitation of the γ phase in the ternary alloy and coarsening of the β' plates and transformation to β in the binary alloy. The β phase forms as an irregular shaped precipitate with no unique morphology. The γ phase forms as rods on the

(0001)Mg with $\langle 11\bar{2}0 \rangle$ and $\langle 10\bar{1}0 \rangle$ growth directions and is very much coarser than the γ'' phase. These phases thus confer far less strengthening to the alloy and, as can be seen from Figure 7.1, the properties fall off rapidly as these phases are formed.

In the creep tests at 200°C and 250°C, the predominant mode of deformation would be expected to be $\{10\bar{1}1\}$ $\langle 11\bar{2}0 \rangle$ slip. The γ'' plates, being extremely fine and lying at an angle of 62° to the $\{10\bar{1}1\}$ planes, are a far more efficient barrier to dislocation movement on the $\{10\bar{1}1\}$ planes than the β' phase, which is much coarser and makes an angle of 63° and 28° to the $\{10\bar{1}1\}$ planes. The improvement in creep properties can be seen from Figure 7.4 to occur in the alloys containing 0.7% and 1.3% zinc in which the γ'' is precipitating. The alloy with an addition of only 0.3% zinc showed little or no improvement in creep properties over the binary alloy, and electron microscopy showed that this alloy precipitated only those phases found in the binary system.

This strengthening effect by precipitate plates on the basal planes of magnesium has also been observed in the system Mg-Th-Mn, where a precipitate similar to γ'' has been observed [127,62]. The temperature range of stability of this phase, however, is greater than that of γ'' and therefore the useful working range of the alloy is extended to 350°C. From the present data it is expected

that the range of application of the Mg-Nd-Zn alloy (or Mg-RE-Zn where the rare earth addition is mainly neodymium) would be temperatures preferably not exceeding 200°C as at temperatures in excess of this the γ'' transforms to γ , which is not such an efficient barrier to dislocation movement.

These results are contrary to some work that has been carried out in Russia [121], where it was claimed that optimum creep properties at 250°C occur in an alloy containing 0.5% zinc; additions beyond this were detrimental to the high temperature creep properties. However, the results of this work are not directly comparable to those in the present study as the alloys used contained zirconium and were tested in the cast condition. Also the heat treatment cycle used by the Russian workers (535°C for eight hours, air cool, eighteen hours at 210°C) produced a structure with a pronounced grain boundary film, a microstructure that is completely different to the homogenised alloy studied in the present work.

Figure 7.1(a) Proof stress vs ageing time at 200°C

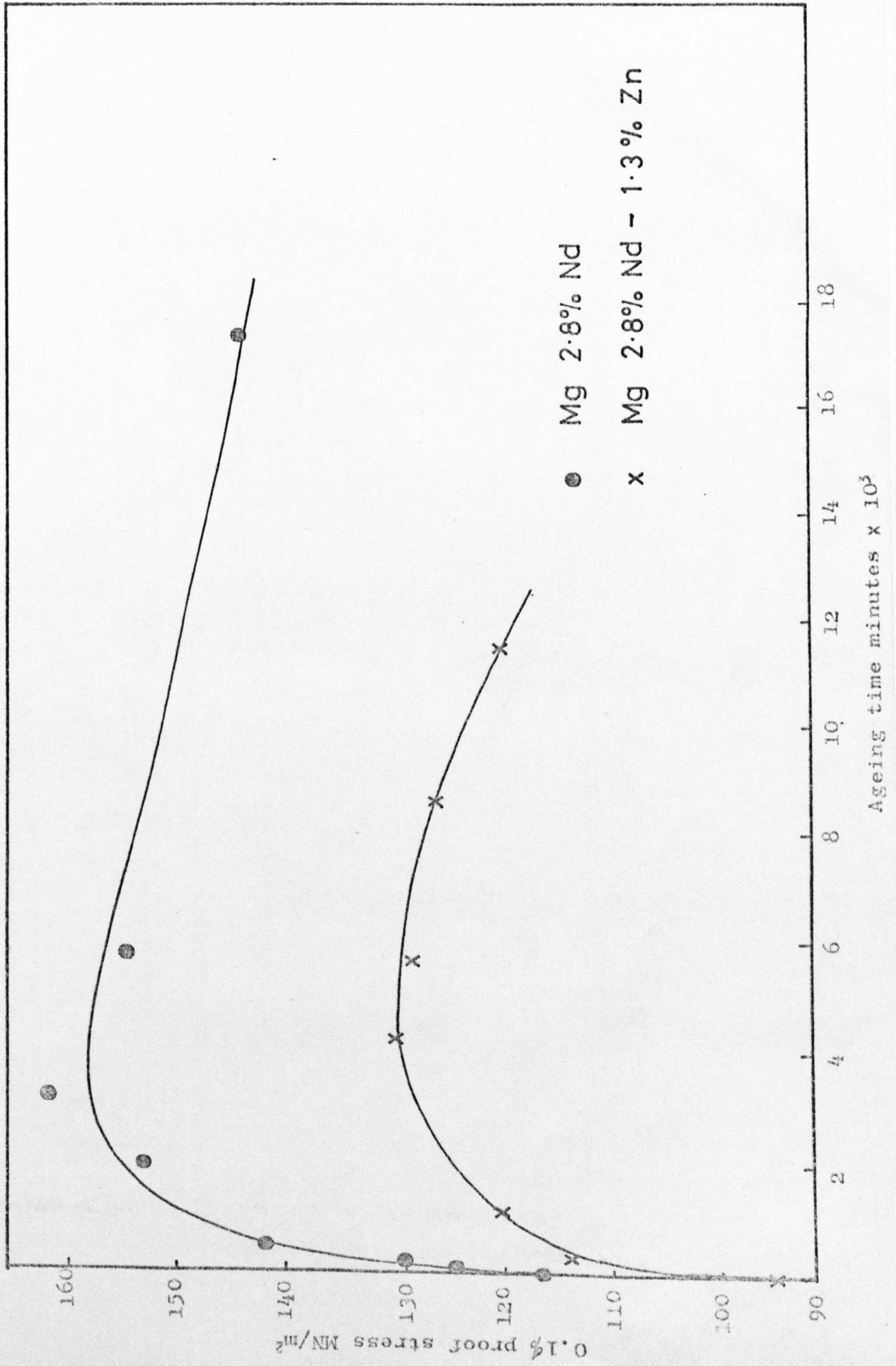


Figure 7.1(b) Proof stress vs ageing time at 250°C

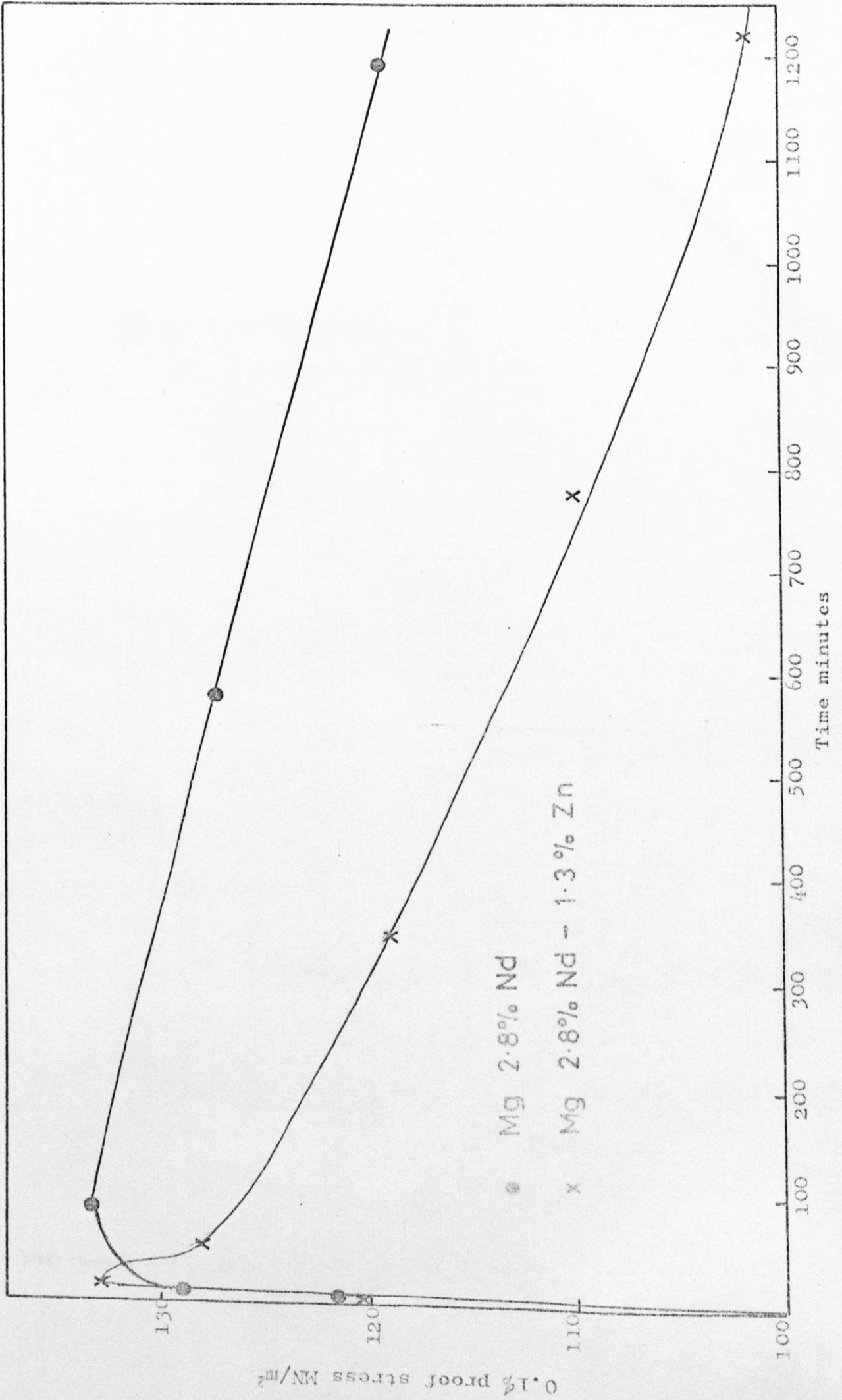


Figure 7.2 Typical creep curves
Tested at 200°C 12 Kg/mm²

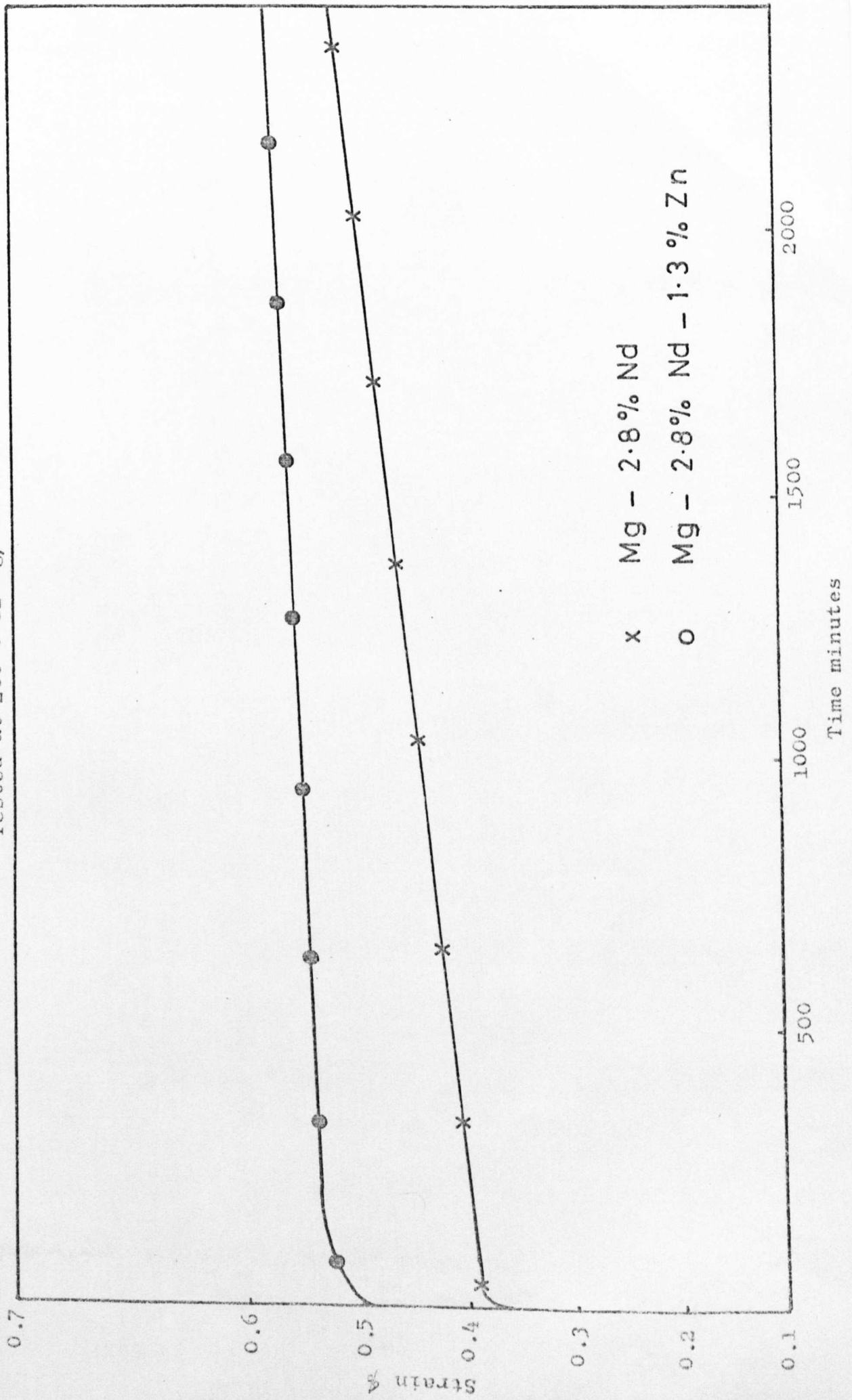


Figure 7.3 Variation of 0.1% P.S. with neodymium content at room temperature

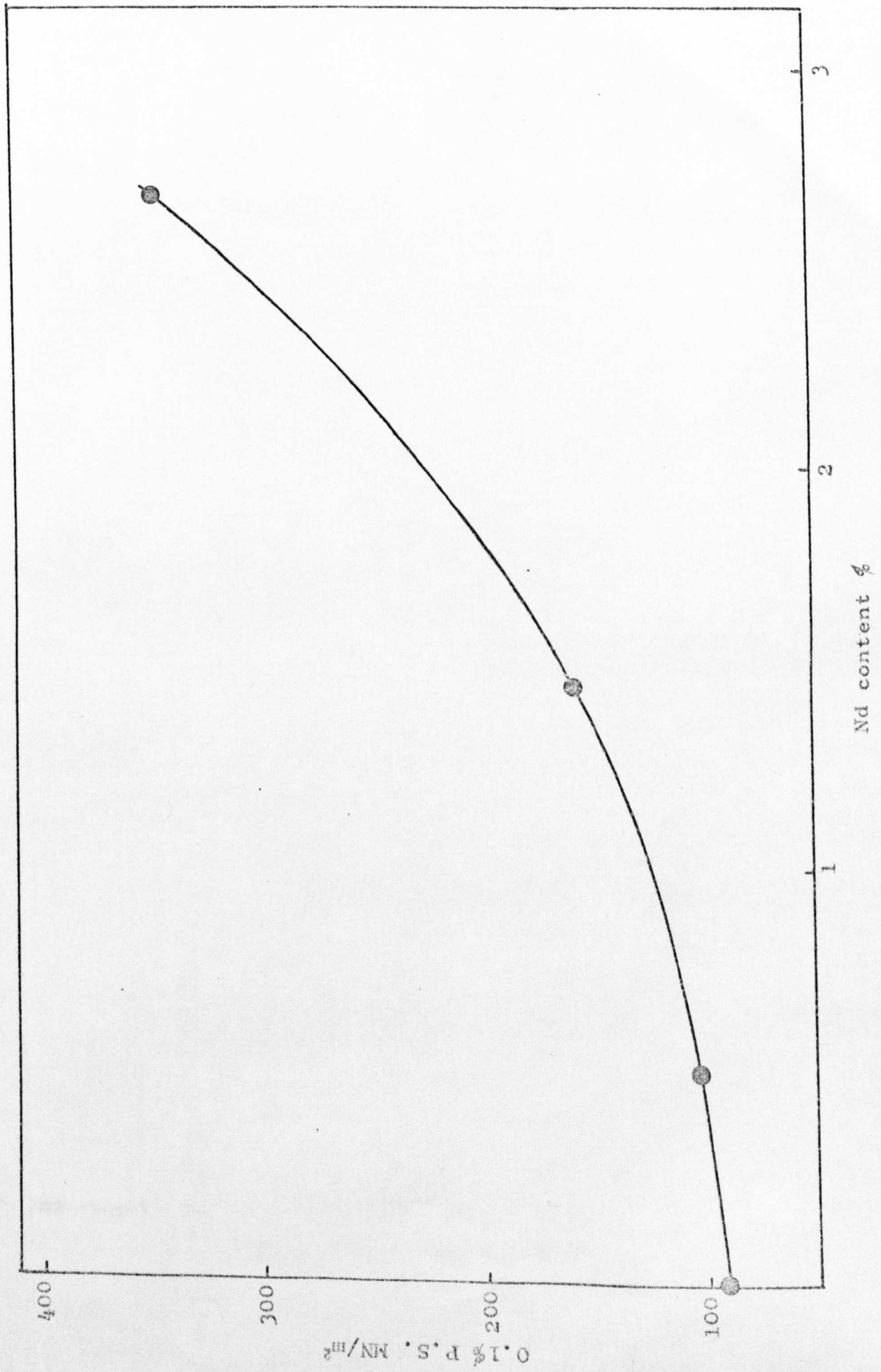


Figure 7.4 Effect of zinc content on secondary creep rate

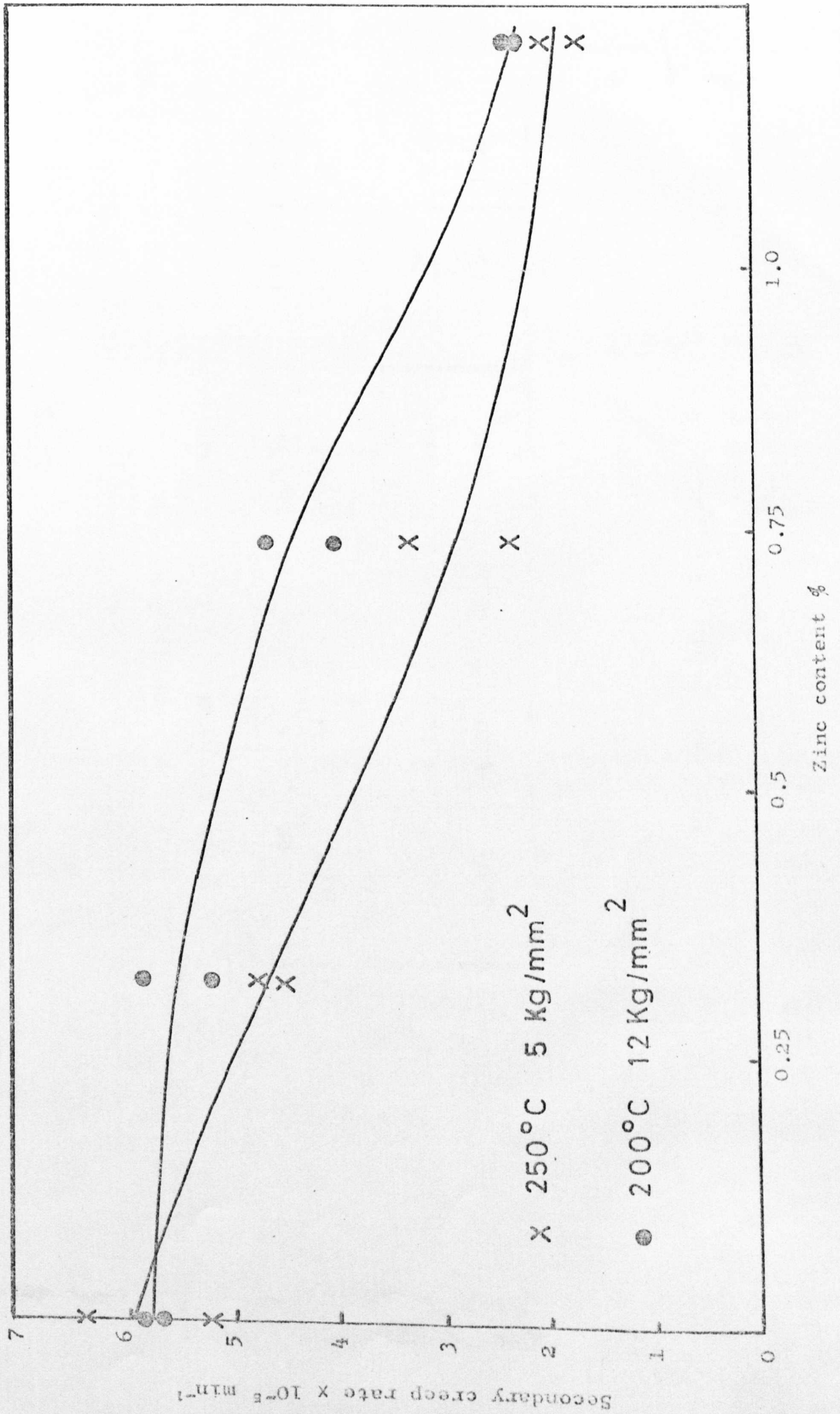


Table 6.1
Steady state creep rates $\dot{\epsilon} \times 10^{-5} / \text{min}$

2.8% Nd		2.8% Nd 0.3% Zn *		2.8% Nd 0.7% Zn		2.8% Nd 1.3% Zn	
200°C	250°C	200°C	250°C	200°C	250°C	200°C	250°C
12 Kg/mm ²	5 Kg/mm ²						
5.88	6.45	5.87	4.74	4.03	2.33	2.37	2.02
5.67	5.2?	4.76	4.50	4.69	3.31	2.24	1.62

* Corrected value (see text)

Figure 7.5 Effect of applied stress on creep rate
 Binary Mg 2.8% Nd alloy aged 4 days at 200°C, tested at 200°C

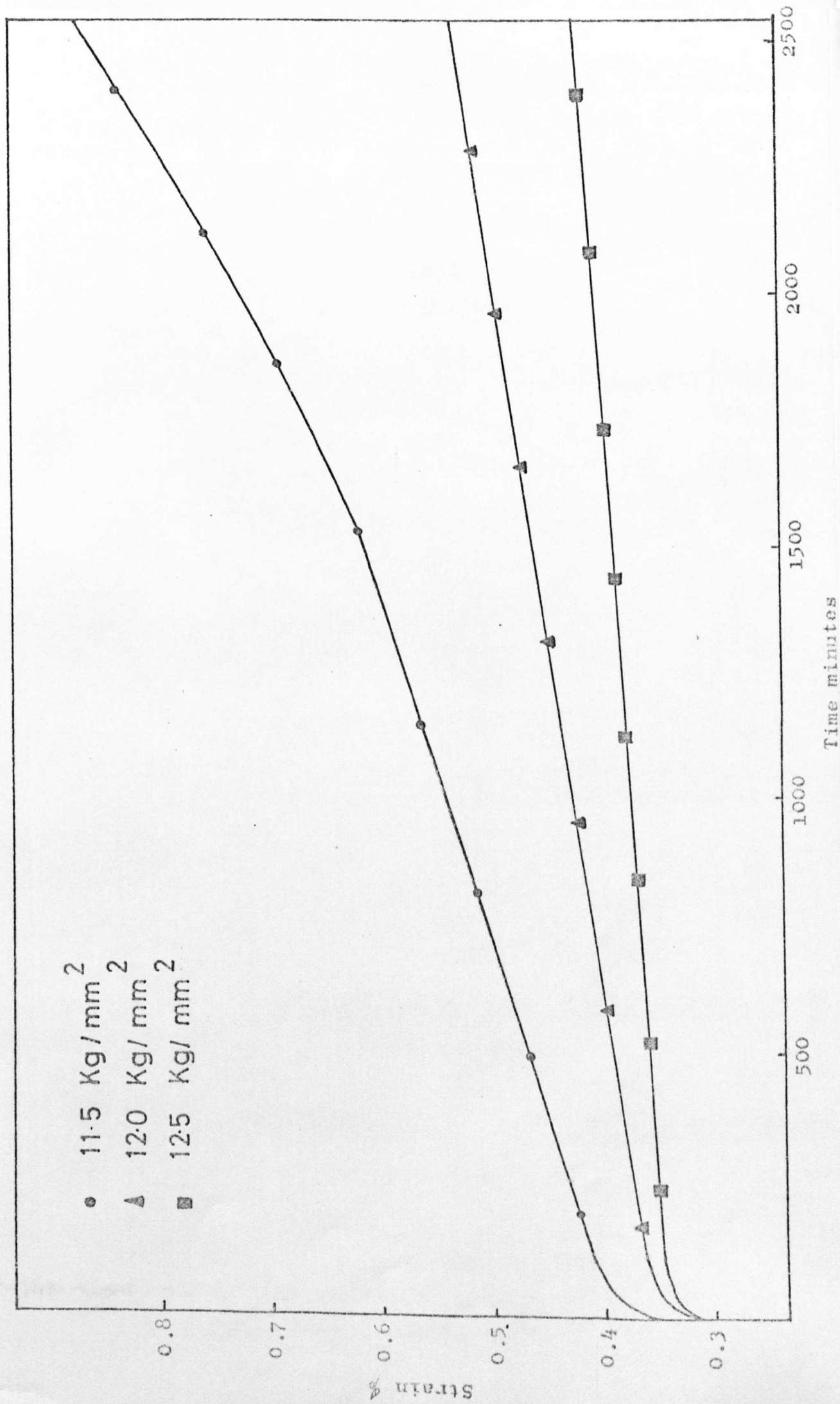
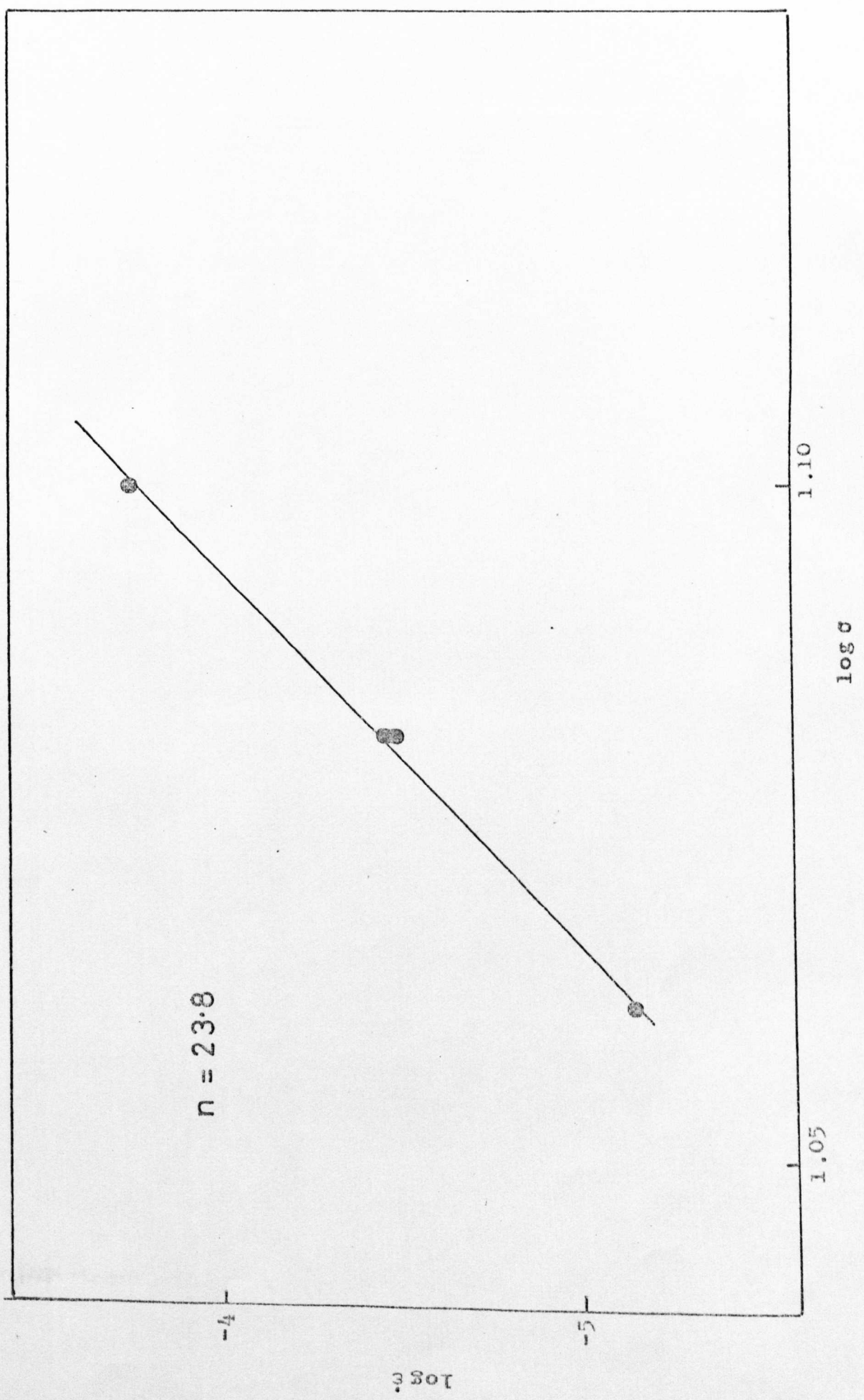
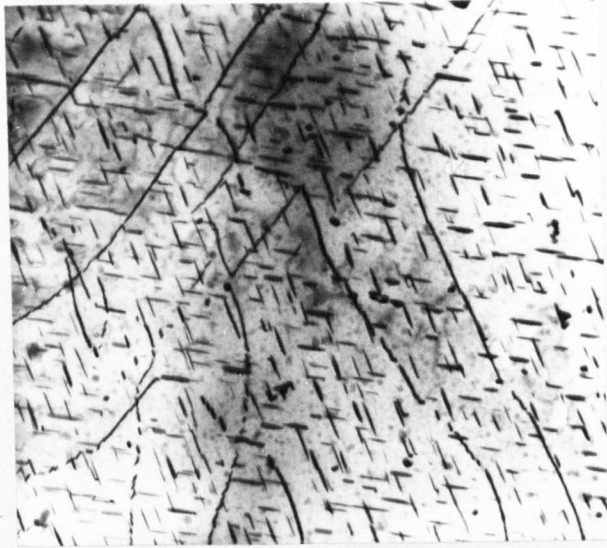


Figure 7.6 $\log \epsilon$ vs $\log \sigma$





(a)

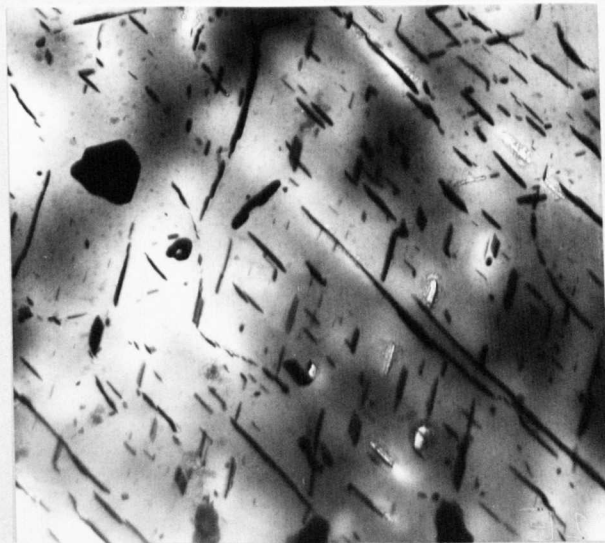
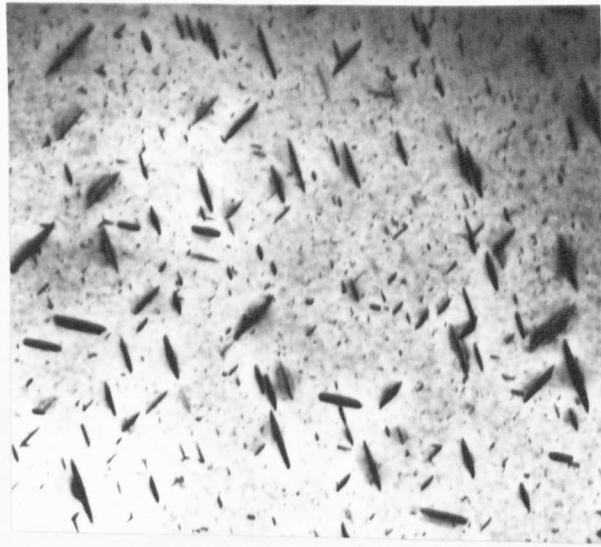


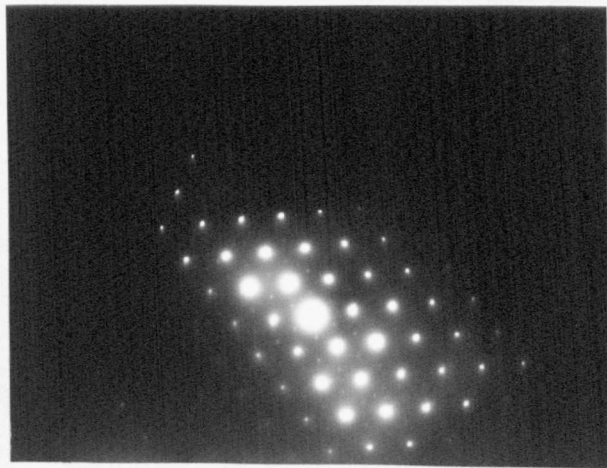
Figure 7.7 Mg 2.8% Nd

(a) Aged 200°C for 4 days. Mag 20,000 x

(b) Aged 200°C for 4 days + 2 days at 250°C . Mag 20,000 x



(a)

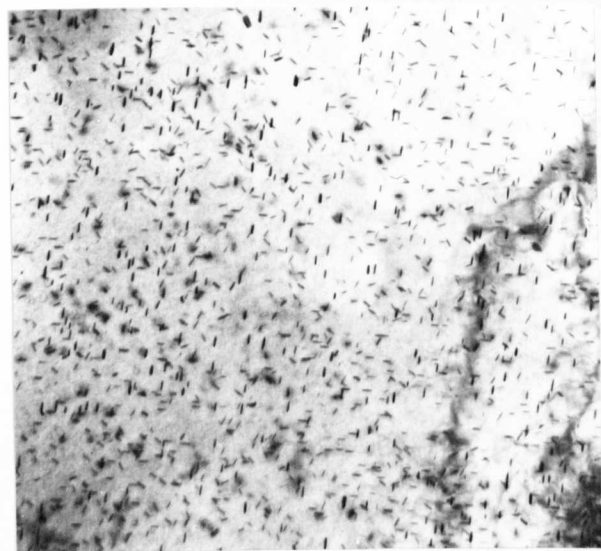


(b)

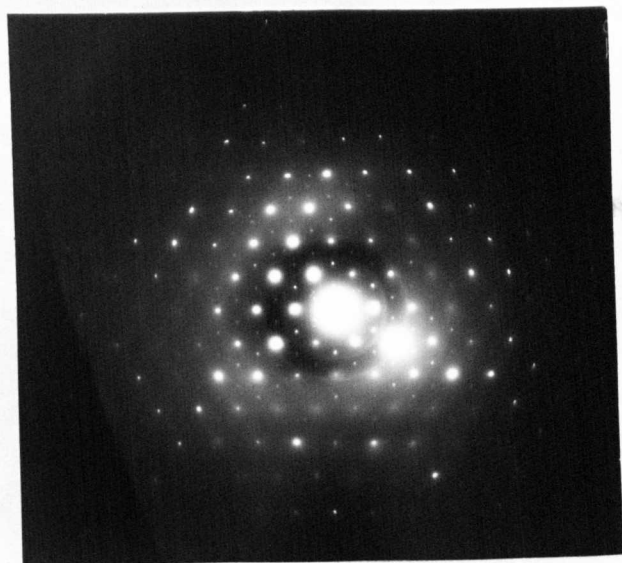
Figure 7.8 Mg 2.8% Nd 0.7% Zn

(a) Aged 200°C for 4 days. Mag 40,000 x

(b) Selected area diffraction pattern of above



(a)



(b)



(c)

Figure 7.9 Mg 2.8% Nd 1.3% Zn

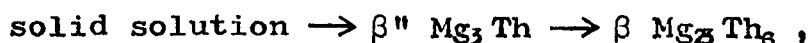
- (a) Aged 4 days at 200°C. Mag 40,000 x
- (b) Selected area diffraction of above
- (c) Aged 4 days at 200°C + 2 days at 210°C. Mag 40,000 x

CHAPTER 8

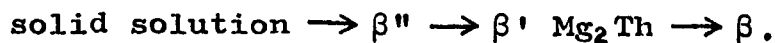
GENERAL SUMMARY AND CONCLUSIONS

This thesis has been concerned with the study of the ageing characteristics of the creep resistant alloys based on the systems Mg-Th and Mg-Nd. Both alloys are of high commercial importance, the Mg-Th system being creep resistant to temperatures of 350°C and the Mg-didymium (which contains a large concentration of neodymium) being usable up to temperatures of 250°C.

The precipitation sequences of the systems Mg-Th and Mg-Th-Zr have been investigated and the results of this and other studies have been shown to be consistent with a precipitation sequence for the binary alloy



and for the ternary alloy



In the ternary alloy the term β' is taken to include both polymorphs β' cubic and β' hex. The β' hex was found to precipitate extensively on dislocations and could be induced to precipitate in the binary alloy when a deformation of 10% was applied prior to ageing. The mode of formation of the β' cubic, however, is not clear.

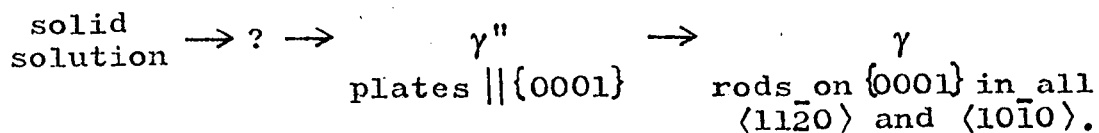
This phase has not been detected in the binary alloy, or in the ternary alloy in the solution treated condition, so from the available evidence it appears to be part of the precipitation sequence of the ternary alloy. Further work would be desirable on the factors promoting the formation of this precipitate and on the reasons why it is not found in the binary alloy, as it appears it is a binary compound and does not contain zirconium.

Trace additions of manganese and silver have very little effect on the precipitation characteristics of the Mg-Th system but a small (approximately 0.25%) zinc addition is sufficient to completely suppress β'' formation. The addition of approximately 2% manganese promotes the formation of a phase with lattice parameters $a = \sqrt{3}a_{\text{Mg}}$ and $c = 6c_{\text{Mg}}$. This phase, precipitating on the (0001) planes, is stable to temperatures in excess of 350°C and is therefore the reason for the good elevated temperature properties of this alloy.

The effect of zinc additions to the Mg-Nd system has been studied in some detail. The effect of a 1.3% zinc addition to the Mg-Nd system is to change the precipitation sequence completely from



in the binary alloy to



The low temperature reaction appears to be vacancy assisted and is similar to the low temperature reaction that takes place in Mg-Th. No evidence of any G.P. zone formation has been found in either alloy but careful study by X-ray technique is desirable to elucidate the nature of these low temperature processes.

The effect of the change in precipitation sequence caused by the addition of zinc to the Mg-Nd alloys has a marked effect on the mechanical properties. In the alloy containing 1.3% zinc the room temperature strength has been found to be inferior to the binary alloy but the elevated temperature creep properties have been shown to be superior. A reduction in the steady state creep rate of approximately 60% occurs when an addition of 1.3% zinc is made to the binary alloy. This reduction in creep rate has been explained in terms of γ'' , as very fine plates on the (0001)Mg, acting as a barrier to $\{10\bar{1}1\} \langle 11\bar{2}0 \rangle$ slip, which is the expected mode of deformation at this temperature.

A preliminary survey, not mentioned in the text, has also been made of the effect of silver additions to the Mg-Nd system. Considerable interest has been

shown in alloys of this type since the discovery by Payne and Bailey [138] that the properties of the Mg-RE-Zr alloys could be considerably improved by the addition of silver. The properties have been shown to be further increased by the use of didymium mischmetal which is richer in neodymium than cerium mischmetal, indicating the probability of strengthening from a ternary Mg-Nd-Ag compound. The preliminary work has shown a highly ordered transition precipitate with a greater temperature range of stability than γ'' in Mg-Nd-Zn. It is felt that further study on this alloy would be desirable as the commercial use of the alloy, in spite of the cost of silver, indicates that it has considerable potential.

APPENDIX ICRYSTALLOGRAPHY OF THE HEXAGONAL CLOSE-PACKED SYSTEM

Planes and directions in c.p.h. crystals are usually assigned indices based on either the 3 or 4 axis notation, known as the Miller and Miller-Bravais systems respectively. The method of derivation of these indices is shown in Figure A.1.

The 3 axis system is based on the three vectors a_1 , a_2 and c , which define the unit cell. A plane is defined by:

$$(HKL) = \frac{a_1}{H} + \frac{a_2}{K} + \frac{c}{L}$$

and a direction:

$$(UVW) = a_1 U + a_2 V + cW.$$

This system, however, has the disadvantage that equivalent directions do not have the same mathematical form. For example, the close packed directions on the basal plane have indices $[100]$ $[110]$ and $[010]$ (Figure A.1).

The 4 axis system is based on the vectors a_1 , a_2 , a_3 and c ; a_3 is redundant since $-(a_1 + a_2) = a_3$.

A plane is defined as:

$$(hkil) = \frac{a_1}{h} + \frac{a_2}{k} + \frac{a_3}{i} + \frac{c}{l}$$

and a direction

$$[uvtw] = a_1 u + a_2 v + a_3 t + cw.$$

All the close packed directions on the basal plane can be described by indices of the type $[11\bar{2}0]$. As stated, a condition of the Miller-Bravais system is that $-(h+k) = i$ and this has led to the use of the 4 axis three index method where planes are defined as (hkl) . Transformation of indices from the Miller to Miller-Bravais system is carried out as follows:

- (i) Planes $(HKL) = (hkl)$ and $i = -(h+k)$
 (ii) Directions $U = u - t, V = v - t, W = w$

or

$$u = \frac{1}{3}(2U-V), v = \frac{1}{3}(2V-U), w = W, t = -(U+V).$$

In general the indices of the directions perpendicular to a plane are not the same as the plane itself. Important exceptions occur with Miller-Bravais indices, where planes with $\{hki0\}$ are normal to directions $\langle hki0 \rangle$ and (0001) is normal to $[0001]$. In table A.1 some low-index planes and directions are listed in terms of both Miller and Miller-Bravais indices. The directions include the zone axes frequently encountered in electron diffraction.

The zone law applies to Miller-Bravais indices but the redundant index must be retained, i.e.

$$hu + kv + it + lw = 0.$$

The zone law is expressed as

$$[UVW] = \left[\left| \frac{K_1 L_1}{K_2 L_2} \right|, \left| \frac{L_1 H_1}{L_2 H_2} \right|, \left| \frac{H_1 K_1}{H_2 K_2} \right| \right]$$

$$[uvw] = \left[\left| \begin{array}{ccc} \bar{l}_1 & k_1 & i_1 \\ \bar{l}_2 & k_2 & i_2 \\ 0 & 1 & 1 \end{array} \right|, \left| \begin{array}{ccc} h_1 & \bar{l}_1 & i_1 \\ h_2 & \bar{l}_2 & i_2 \\ 1 & 0 & 1 \end{array} \right|, \left| \begin{array}{ccc} h_1 & k_1 & \bar{l}_1 \\ h_2 & k_2 & \bar{l}_2 \\ 1 & 1 & 0 \end{array} \right|, \left| \begin{array}{ccc} h_1 & k_1 & i_1 \\ h_2 & k_2 & i_2 \\ 1 & 1 & 1 \end{array} \right| \right]$$

where (UVW) and (uvw) are the zone axes of planes with indices (HKL) and (hkil).

The Miller-Bravais system has been used throughout the present work and below are quoted several of the more important relationships in the system:

$$d_{(hkil)} = a \left[\frac{4}{3}(h^2 + hk + k^2) + \frac{1}{(c/a)^2} \right]^{-\frac{1}{2}}$$

The angle between two directions $[u_1 v_1 t_1 w_1]$ and $[u_2 v_2 t_2 w_2]$ is given by

$$\phi = \cos^{-1} \left[\frac{u_1 u_2 + v_1 v_2 + t_1 t_2 + \lambda^2 w_1 w_2}{(u_1^2 + v_1^2 + t_1^2 + \lambda^2 w_1^2)^{\frac{1}{2}} (u_2^2 + v_2^2 + t_2^2 + \lambda^2 w_2^2)^{\frac{1}{2}}} \right]$$

where $\lambda^2 = \frac{2}{3} \left(\frac{c}{a} \right)^2$.

Similarly the angle between lattice planes is

$$\theta = \cos^{-1} \left[\frac{h_1 h_2 + k_1 k_2 + i_1 i_2 + \lambda^{-2} l_1 l_2}{(h_1^2 + k_1^2 + i_1^2 + \lambda^{-2} l_1^2)^{\frac{1}{2}} (h_2^2 + k_2^2 + i_2^2 + \lambda^{-2} l_2^2)^{\frac{1}{2}}} \right].$$

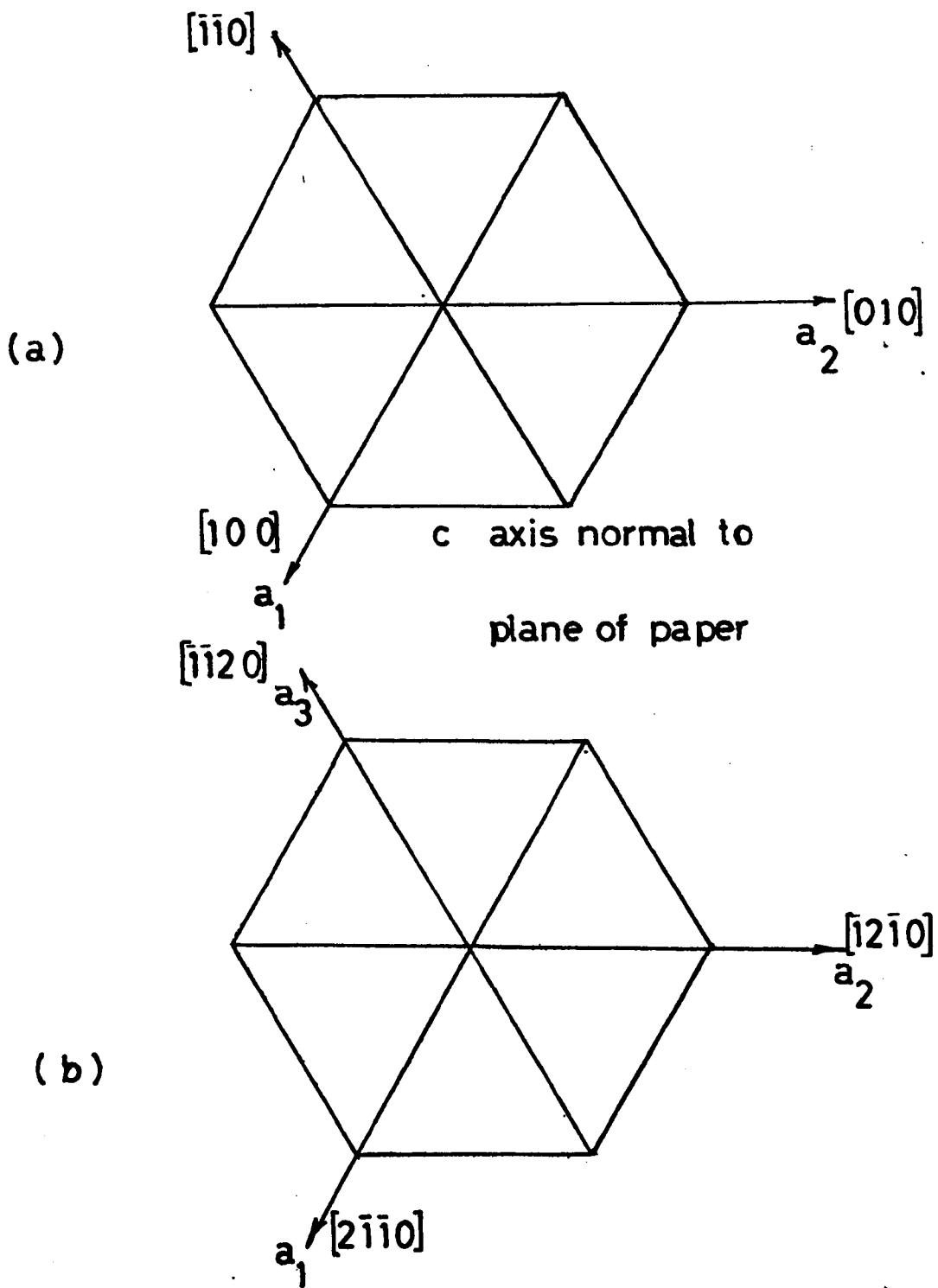


FIG A.1 Indices of directions in (a) Miller and (b) Miller-Bravais notation

TABLE 1. Indices of directions and planes

Directions			
Miller indices 3 axes	Miller-Bravais indices 4-axes		Indices (<i>hkl</i>) of plane normal to [<i>uvw</i>]
[<i>UVW</i>]	4 index [<i>uvw</i>]	3 index [<i>uv.w</i>]	
001	0001	001	0001
110	1120	110	1120
010	1210	120	1210
100	2110	210	2110
031	1211	121	121 n 2 > n > 1
012	1216	126	121 n $n \sim 8$
011	1213	123	121 n 6 > n > 4
021	2423	243	121 n 3 > n > 2
210	1010	100	1010
120	0110	010	0110
110	1100	110	1100
211	1011	101	101 n 2 > n > 1
121	0111	011	011 n 2 > n > 1
111	1101	111	110 n 2 > n > 1
212	1012	102	101 n 4 > n > 3
122	0112	012	011 n 4 > n > 3
112	1102	112	110 n 4 > n > 3
450	1230	120	1230
310	5140	510	5140
210	5410	540	5410
311	5143	513	—
211	5413	543	—
411	7253	723	\sim 3122

(<i>hkl</i>) Miller-Bravais indices	(<i>HKL</i>) Miller indices
Planes	

APPENDIX IIALLOY COMPOSITIONS

The following is a list of the compositions of alloys used in the creep experiments. Other alloys used in the investigation have been analysed and the compositions in most cases were confirmed to within $\pm 0.1\%$.

Composition

Atom %	Weight %
Mg - 0.49 Nd	Mg - 2.64 Nd
Mg - 0.42 Nd - 0.12 Zn	Mg - 2.42 Nd - 0.32 Zn
Mg - 0.48 Nd - 0.27 Zn	Mg - 2.75 Nd - 0.72 Zn
Mg - 0.48 Nd - 0.47 Zn	Mg - 2.74 Nd - 1.22 Zn

ACKNOWLEDGEMENTS

I would like to express my sincere thanks to my supervisor Dr. B. Noble for his help and encouragement throughout the course of this work and also to my colleagues in the department, especially Dr. T.J. Pike, for many helpful discussions.

I am also grateful to Mr. D.F. Wheatly and his technical staff, especially Mr. M. Brown and Mr. F. Garlick, for help with the experimental work and chemical analysis. The work has been supported by a maintenance grant from the Science Research Council for the period 1970-3.

Finally I would like to thank my wife for her painstaking care in typing this thesis and whose help, both moral and financial, has been invaluable throughout the work.

REFERENCES

- [1] Kelly A. and Nicholson R.B., Prog. Mat. Sci. 1963 10 149
- [2] Nabarro F.R.N., Proc. Phys. Soc. 1940 52 90
- [3] Nicholson, R.B., Kelly A. and Nutting J., J. Inst Met. 1958-9 87 429
- [4] Jagodzinski H. and Laves F., Z. Metallkunde 1949 40 296
- [5] Federighi T. Acta Met. 1958 6 379
- [6] Zener C., Proc. of Int. Conf. on Physics of Metals Amsterdam 1948 p.117
- [7] Turnbull D., Impurities and imperfections, A.S.M. 1955 p.121
- [8] Turnbull D., Defects in crystalline solids, Physical Soc. 1955 p.203
- [9] Turnbull D., Solid state physics, Academic Press 1956 3 p.226
- [10] Turnbull D. and Cormia R.L., Acta Met. 1960 8 747
- [11] Hart E.W., Acta Met. 1958 6 553
- [12] Federighi T. and Thomas G., Phil. Mag. 1962 8 127
- [13] Girifalco L.A. and Herman H., Acta Met. 1965 13 583
- [14] Ipohoriski M. and Bonfiglioli A.F., Acta Met. 1970 18 281
- [15] Berry B.S., Acta Met. 1959 7 741
- [16] Lutts A., Acta Met. 1961 9 577
- [17] Turnbull D. and Servi I.S., Acta Met 1966 14 161
- [18] Phillips V.A., Acta Met. 1966 14 1533
- [19] Noble B. and Thompson G.E., Met. Sci. Journal 1971 5 114

- [20] Russell K.C., Phase transformations, A.S.M. Cleveland 1970
- [21] Nicholson R.B., Phase transformations, A.S.M. Cleveland 1970
- [22] Turnbull D., Rosenbaum H.S. and Treafitis H.N., Acta Met. 1960 8 277
- [23] Lorimer G.W., Ph.D. thesis, University of Cambridge 1967
- [24] Embury J.D. and Nicholson R.B., Acta Met. 1965 13 403
- [25] Lorimer G.W. and Nicholson R.B., Acta Met. 1966 14 1009
- [26] Lorimer G.W. and Nicholson R.B., Conference on phase transformations in crystalline solids (Inst. of Metals) 1968 36
- [27] Pashley D.W., Rhodes J.W. and Sendorek A., J. Inst Met. 1966 94 41
- [28] Pashley D.W., Jacobs M.H. and Vietz J.T., Phil. Mag 1967 16 51
- [29] Pashley D.W. and Jacobs M.H., Conference on phase transformations in crystalline solids (Inst. of Metals) 1968 43
- [30] Koster V., Mat. Sci. Eng. 1969-70 5 174
- [31] Rosenbaum H.S. and Turnbull D., Acta Met. 1959 7 664
- [32] Unwin P.N.T. and Nicholson R.B., Acta Met. 1964 12 687
- [33] Wilson R.N. and Partridge P.G., Acta Met. 1965 13 1321
- [34] Hornbogen E., Acta Met. 1962 10 525
- [35] Clark J.B., Acta Met. 1965 13 1281
- [36] Cahn J.W., Acta Met. 1957 5 169
- [37] Pickering F.B., Relations between structures and mechanical properties of metals, N.P.L. Symposium no. 15 H.M.S.O. London 1963 p.131
- [38] Silcock J.M., J. Iron and Steel Inst. 1963 201 409
- [39] Honeycombe R.W.K., Van Aswegen J.S.T. and Warrington D.H., N.P.L. Symposium no. 15 H.M.S.O. London 1963 p.379

- [40] Silcock J M. and Tunstall W.J., Phil. Mag. 1964
10 361
- [41] Suzuki H., Sci. Rep. Res. Inst. Tohoku University
1949 A1 183
- [42] Nicholson R.B. and Nutting J., Acta Met. 1970 18 253
- [43] Nemoto M. and Koda S., J. Inst. Met. 1964-5 93 164
- [44] Boswell F.C.W. and Ruddle G.E., Can. J. Phys. 1965
43 2096
- [45] Noble B and Thompson G.E., Met. Sci. Journal 1972
6 167
- [46] Baker R.G and Nutting J, Acta Met. 1961 9 332
- [47] Silcock J.M., Heal T.J. and Hardy H.K., J. Inst. Met.
1955-6 84 23
- [48] Silcock J.M., Phil. Mag. 1959 4 1187
- [49] Kimura H. and Hasiguti R.R., Acta Met. 1961 9 1076
- [50] Noble B., Acta Met. 1968 16 393
- [51] Noble B., Met. Sci. Journal 1968 2 117
- [52] Auld J.H., Vietz J.T. and Polmear I.J., Nature 1966
209 703
- [53] Leontis T.E., Trans. A.I.M.E. 1952 194
- [54] Leontis T.E., Trans. A.I.M.E. 1952 206
- [55] Sturkey L., Trans. A.I.M.E. 1960 218 466
- [56] Yamamoto A.S. and Rostoker W., Trans. A.S.M. 1958
50 1095
- [57] Kent R.G. and Kelly A., J. Inst. Metals 1964-5 93 536
- [58] Murikami Y., Kawano O. and Tamura H., Mem. Fac. Eng.
Kyoto University 1962 24 411
- [59] Mushovic J.N. and Stoloff N.S., Trans. A.I.M.E. 1969
245 1449
- [60] Mushovic J.N. and Stoloff N.S., Supplement to Trans
Jap. Inst. Met 1968 9 360

- [61] Noble B. and Crook A., J. Inst. Metals 1970 98 375
- [62] Stratford D.J. and Beckley L., Met. Sci. Journal 1972 6 83
- [63] Stratford D.J., J. Inst. Metals 1971 99 201
- [64] Peterson D.T., Diljak P.F. and Vold C.L., Acta Cryst. 1956 9 1036
- [65] Pike T.J., Ph.D. Thesis, University of Nottingham 1971
- [66] Noble B., Pike T.J. and Crook A., Phil. Mag. 1971 183 23 543
- [67] Leontis T.E., Trans. A.I.M.E. 1949 185 968
- [68] Tikhoa N.M. and Afanas'eva L.A., Metallov i Obrabotka Metallov 1958 3 38
- [69] Beletzki M.S. and Gal'perin L.Y., Phys. Met. Metallog. 1961 1 80
- [70] Drits M.E., Padezhnova Y.M. and Bochvar N.R., Russian Met. 1966 1 86
- [71] Padezhnova Y.M., Russian Met. 1969 3 150
- [72] Evdokimento V.I. and Kripyakevich P.I., Soviet Phys. Cryst. 1963 8 135
- [73] Lashko N.F. and Morozova G.I., Sov. Phys. Cryst. 1964 2 209
- [74] Lashko N.F. and Morozova G.I., Ind. Lab. 1964 30 1470
- [75] Pike T.J. and Noble B., J. Less Common Metals 1973 30 63
- [76] Mellor G.A. and Ridley R.W., J. Inst. Met. 1952-3 81 245
- [77] Payne R.J.M. and Bailey N., J. Inst. Met. 1959-60 68 417
- [78] Sturkey L. and Clark J.B. J. Inst. Metals 1959-60 85 177
- [79] Clark J.B., Acta Met. 1965 13 1281
- [80] Chun J.S. and Byrne J.G., J. Met. Sci 1969 4 801

- [81] Murikami Y., Kawano O. and Tamura H., Mem. Fac. Eng. Kyoto University 1962 24 411
- [82] Mima G. and Tanaka Y., Trans. Jap. Inst Met. 1971 12 71
- [83] Mima G. and Tanaka Y., Trans. Jap. Inst. Met. 1971 12 77
- [84] Mima G. and Tanaka Y., Trans. Jap. Inst. Met. 1971 12 317
- [85] Mima G. and Tanaka Y., Trans. Jap. Inst. Met. 1971 12 323
- [86] Vydyanth H.R., Sastry D.H. and Vasu K.I., Phys. Stat. Sol. 1968 29 K 137
- [87] Gallot J., Lal K. Graf R. and Guinier A., Comptes Rendu 1964 258B 2818
- [88] Gallot J. and Graf R., Comptes Rendu 1965 261B 728
- [89] Gallot J. and Graf R., Comptes Rendu 1966 262B 1219
- [90] Gallot J., Bernote M. and Graf R., J. Microscopie 1965 4 787
- [91] Hall E.O., J. Inst. Met. 1968 96 21
- [92] Clark J.B., Acta Met. 1968 16 141
- [93] Clark J.B., Supplement to Trans. Jap. Inst. Met. 1968 2 354
- [94] Gjønnes J. and Østmo T., Z. Metallkunde 1970 61 604
- [95] Nagashima S., J. Jap. Inst. Met. 1959 23 381
- [96] Nagashima S., J. Jap. Inst. Met. 1959 23 460
- [97] Nagashima S., Trans. Jap. Inst. Met. 1960 1 58
- [98] Nagashima S. and Nishiyama Z., Osaka University Mem. Inst. Sci. Ind. Res. 1954 11 135
- [99] Walker E.A. and Fisher P.A., J. Nuc. Mats. 1963 8 179
- [100] Kent R.P. and Wells T.C., J. Nuc. Mats. 1963 8 198
- [101] Smith C.C., Taylor A.M. and Greenfield P., J. Nuc. Mats. 1964 12 198

- [102] Day J.H., J. Nuc. Mats. 1964 11 249
- [103] Harris J.E., Partridge P.G., Eeles W.T. and Rickards G.K., J. Nuc. Mats. 1963 9 339
- [104] Harris J.E. and Partridge P.G., J. Inst. Met. 1964-5 93 15
- [105] DeLuca R. and Byrne J.G., Acta Met. 1965 13 1187
- [106] DeLuca R. and Byrne J.G., Trans. Jap. Inst. Met. 1968 9 Supplement 514
- [107] Henes S. and Gerold V., Z. Metallkde 1962 53 703
- [108] Henes S. and Gerold V., Z. Metallkde 1962 53 743
- [109] Hirano K., Maniwa H. and Tagagi Y., J. Phy. Soc. Japan 10 3 193
- [110] Van der Planken J., J. Mat. Sci. 1964 4 927
- [111] Van der Planken J. and Deruyttere A., Acta Met. 1969 17 451
- [112] Abe H., Ito K. and Suzuki T., Acta Met. 1970 18 991
- [113] Abe H., Ito K. and Suzuki T., Trans. Jap. Inst. Met. 1970 11 368
- [114] Andrews K.W., Dyson D.J. and Keown S.R., 'Interpretation of electron diffraction patterns', 1967 London (Hilger and Watts)
- [115] Crook, A., Ph.D. Thesis University of Nottingham 1969
- [116] Stratford D.J., J. Inst. Metals 1972 100 381
- [117] Hales R., Dobson P.S. and Smallman R.E., Metal Sci. J. 1968 2 224
- [118] Ball C.J.P., Jessup A.C., Fisher P.A., Whitehead D.J and Wilson J.B., Trans A.I.M.E. 1953 197 924
- [119] Whitehead D.J., Trans A.F.S. 1961 69 442
- [120] Yamamoto A.S., Klimek E.J. and Rostoker W., W.A.D.C. Technical report 56-411 Armour Research Foundation, Illinois College of Tech. 1957

- [121] Tikhova N.M. and Blokhina V.A., 'Russian Castings Production'
- [122] Burke J., 'Kinetics of phase transformations in metals' 1965 Pergamon p.55
- [123] Beevers C.J., Acta Met. 1963 11 1029
- [124] Fine M.E. and Chiou C., Acta Met. 1958 212 553
- [125] Christian J.W., 'Theory of transformations in metals and alloys', Pergamon p.489
- [126] Mason J.T. and Chiotti P., Metallurgical Transactions 1972 3 2851
- [127] Emley E.F., 'Principles of magnesium technology', 1966 Pergamon
- [128] Norton F.H., 'The creep of steel', 1971 New York
- [129] Jones R.B. and Harris J.E., Joint Int. Conf. on Creep, Inst. Mech. Eng. Proc. 1963-4 178
- [130] Tegart W.G., Acta Met. 1961 9 614
- [131] Milicka K., Cadek J. and Rys P., Acta Met. 1970 18 1071
- [132] Roberts C.S., Trans. A.I.M.E. 1953 197 1121
- [133] Chadhuri A.R., Chang H.C. and Grant N.J., Trans. A.I.M.E. 1955 203 682
- [134] Roberts C.S., 'Magnesium and its alloys', 1960 Wiley
- [135] Schmid E. and Wasserman G., Handbuch der Physikalisches 1931 4 319
- [136] Burke E.C. and Hibbard W.R., Trans. A.I.M.E. 1952 295
- [137] Reed-Hill R.E. and Robertson W.D., Trans. A.I.M.E. 1957 496
- [138] Payne R.J.M. and Bailey N., J. Inst. Met. 1959-60 88 417